JAERI 1298

JAERI 1298

FEMAXI-III : A Computer Code for the Analysis of Thermal and Mechanical Behavior of Fuel Rods

December 1985

日 本 原 子 力 研 究 所

Japan Atomic Energy Research Institute

JAERIレポートは，日本原子力研究所が研究成果編集委員会の審査を経て不定期に公刊している研究報告書です。

入手の問合わせは，日本原子力研究所技術情報部情報資料課（〒319-11茨城県那珂郡東海村）あて，お申しこしください。なお，このほかに財団法人原子力弘済会資料センター（〒319-11 茨城県那珂郡東海村日本原子力研究所内）で複写による実費頒布をおこなっております。

JAERI reports are reviewed by the Board of Editors and issued irregularly.

Inquiries about availability of the reports should be addressed to Information Division Department of Technical Information, Japan Atomic Energy Research Institute, Tokai-mura, Naka-gun, Ibaraki-ken 319-11, Japan.

編集兼発行　日本原子力研究所
印　　刷　いばらき印刷㈱

FEMAXI-III : A Computer Code for the Analysis of Thermal and Mechanical Behavior of Fuel Rods

Tetsuo NAKAJIMA, Michio ICHIKAWA, Yoshihiko IWANO*1, Kenichi ITO*1, Hiroaki SAITO*2, Koichi KASHIMA*3, Motoyasu KINOSHITA*3 and Tadatsune OKUBO*4

Department of Fuel Safety Research,
Tokai Research Establishment,
Japan Atomic Energy Research Institute
Tokai-mura, Naka-gun, Ibaraki-ken

Received May 27, 1985

Abstract

FEMAXI-III is a computer code to predict the thermal and mechanical behavior of a light water fuel rod during its irradiation life. It can analyze the integral behavior of a whole fuel rod throughout its life, as well as the localized behavior of a small part of fuel rod. The localized mechanical behavior such as the cladding ridge deformation is analyzed by the two-dimensional axisymmetric finite element method.

FEMAXI-III calculates, in particular, the temperature distribution, the radial deformation, the fission gas release, and the inner gas pressure as a function of irradiation time and axial position, and the stresses and strains in the fuel and cladding at a small part of fuel rod as a function of irradiation time.

For this purpose, Elasto-plasticity, creep, thermal expansion, fuel cracking and crack healing, relocation, densification, swelling, hot pressing, heat generation distribution, fission gas release, and fuel-cladding mechanical interaction are modelled and their interconnected effects are considered in the code.

Efforts have been made to improve the accuracy and stability of finite element solution and to minimize the computer memory and running time.

This report describes the outline of the code and the basic models involved, and also includes the application of the code and its input manual.

Keywords: FEMAXI-III, Computer Code, Fuel Rods, Thermal Behavior, Mechanical Behavior, Fission Gas Release, Cladding Ridge Deformation, Fuel-Cladding Mechanical Interaction, Finite Element Method, Stresses, LWR, Temperature, Input Manual

*1 : Nippon Nuclear Fuel Development Co. Ltd.,
*2 : Century Research Center Corp.,
*3 : Central Research Institute of Electric Power Industries,
*4 : Sophia University

FEMAXI-Ⅲ：燃料棒の熱的及び力学的なふるまい解析コード

日本原子力研究所東海研究所燃料安全工学部

中島　鐵雄・市川　達生・岩野　義彦[*1]
伊東　賢一[*1]・斎藤　裕明[*2]・鹿島　光一[*3]
木下　幹康[*3]・大久保忠恒[*4]

（1985年5月27日受理）

要　　旨

FEMAXⅠ－Ⅲは軽水炉燃料棒の照射中における熱的及び力学的なふるまいを解析する計算コードである．FEMAXⅠ－Ⅲは燃料棒全長の総合的なふるまいを全照射期間を通して解析する機能と同時に，燃料棒の一部分の局所的なふるまいを解析する機能とを併せ持っている．被覆管のリッジ変形のような局所的な力学的ふるまいは二次元軸対称有限要素法により解析される．

FEMAXⅠ－Ⅲは特に，温度分布，半径方向変位，FPガス放出及び燃料棒内ガス圧力を時間と軸方向位置の関数として計算すると共に燃料棒の一部分における燃料と被覆管内の応力とひずみを時間の関数として計算する．

このため計算コードでは，弾塑性クリープ，熱膨脹，燃料の割れとゆ着，リロケーション，焼きしまり，スウェリング，ホットプレッシング，発熱分布，FPガス放出，燃料と被覆管の力学的相互作用などの諸現象及びそれらの重畳効果が考慮されている．

有限要素解の精度と安定性を向上させることと計算機記憶容量及び計算時間を最小に抑えることに注意を払った．

本報告書ではFEMAXⅠ－Ⅲコードの概要と基本的なモデルを記述すると共に，適用例と入力の説明を記した．

*1　日本核燃料開発株式会社
*2　センチュリリサーチセンタ株式会社
*3　電力中央研究所
*4　上智大学

CONTENTS

目　次

This is a blank page.

List of Figures and Tables

1. Introduction

A fuel rod for light water reactors consists of a cylindrical cladding tube containing sintered uranium dioxide fuel pellets. The cladding tube is the first barrier against the release of radioactive fission products to the surrounding coolant. The cladding integrity during steady-state and transient power conditions is the most important criterion in the design of fuel rods. The cladding local deformation due to the fuel-cladding mechanical interaction is considered the principal cause of cladding failure.

The mechanical interaction between the fuel and cladding depends on a great number of thermal and mechanical processes which are highly complex and interconnected, as for examples, the temperature distribution, the thermal expansion, the fuel cracking and healing, the fuel relocation, densification, and swelling, the elasto-plasticity and creep deformation, the fission gas release, and the fuel-cladding contact forces, etc.

This complicated problem can be analyzed only by a computer code. In a code, a number of thermal and mechanical processes must be modelled. Furthermore, the fuel-cladding time dependent response to the steady-state and transient power histories must be considered.

The computer codes are usually classified into two groups, the integral fuel rod behavior code and the local fuel rod behavior code. The integral fuel rod codes, such as CYGRO[1], COMETHE[2], LIFE[3], URANUS[4], treat the entire fuel rod and analyze the integral behavior of fuel rod. The localized phenomena, such as the cladding bambooridge formed by the expansion of fuel pellets, is not treated in these codes except COMETHE.

The local fuel rod codes deal with the localized phenomena and concentrate on the evaluation of local stresses and strains in the cladding due to the fuel-cladding mechanical interaction. The finite element method is quite suitable for such a detailed analysis of stress and strain under complex mechanical interaction. A detailed stress analysis by finite element method, modelling creep, plasticity, fuel cracking, fuel-cladding mechanical interaction, requires a large computer memory and running time. Hence a detailed analysis of the localized phenomena by finite element method is limited to a small part of fuel rod.

The finite element computer codes for analyzing the localized behavior of fuel rod were developed by Visser[5], Swanson[6], Levy[7], Rashid[8], et al. Co-authors also developed the similar finite element computer codes, FEMAXI[9,10], FEAST[11], and MIPAC[12], respectively. However these finite element computer codes required so a large computer memory and running time that these codes were not available for analyzing a problem of long irradiation history including power ramps within acceptable running time.

The FEMAXI-III code[13,14] is an extension of the three finite element computer codes, FEMAXI, FEAST, and MIPAC. Its principal purpose is the determination of local stresses and strains in the cladding due to the fuel-cladding mechanical interaction. The localized phenomena is analized by the two-dimensional axisymmetric finite element method. In the development of FEMAXI-III, efforts have been made to minimize the computer memory and running time and to improve the accuracy and stability of finite element solution, so that the code can obtain the accurate and stable solution for a long irradiation problem including power ramps within reasonable running time. In order to minimize the computer memory and running time, the number of finite elements was decreased by adopting a quadratic element instead of a linear element and the finite element analysis is applied only to the region of half-pellet height. The accuracy and numerical stability were improved by employing an

implicit algorithm to the finite element solution via the Newton-Raphson iterative procedure. Furthermore in FEMAXI-III, the capability to analyze the integral fuel rod behavior was added, and hence FEMAXI-III can analyze the integral behavior of a whole fuel rod throughout its life, as well as the localized mechanical behavior at a small part of fuel rod.

The capability of the FEMAXI-III code has been extensively tested with a number of experimental results obtained in the international fuel irradiation programs, such as the OECD Halden Reactor Project and the Studsvik Inter-Ramp and Over-Ramp Projects[15,16,17]. The agreement between calculations and measurements was quite satisfactory.

This report provides a general description of the code and of the various models involved. Some results of applications and input manual for the code are also included.

2. Code Abstract

2.1 Code Capabilities

FEMAXI-III is a FORTRAN-IV computer code to predict the in-pile thermal and mechanical behavior of light water reactor fuel rods as a function of the reactor operating history. The code can not treat the fuel rod behavior during fast transient conditions. The steady-state thermal calculations are used at each time step with an iterative procedure. The code assumes an axisymmetry.

The code consists of two major calculation parts, the thermal analysis part and the mechanical analysis part. In the thermal analysis part, the integral behavior of a whole fuel rod is analyzed and the temperature distribution, the dimensional changes of fuel and cladding, the fission gas release, and the associated inner gas pressure are determined. Then, the results of temperature distribution and inner gas pressure are transfered to the mechanical analysis part where the localized mechanical behavior is analyzed by the two-dimensional axisymmetric

Table 1 Thermal and mechanical processes considered in FEMAXI-III

Analysis Part		Thermal Analysis Part	Mechanical Analysis Part
Fuel Mechanics	Thermal expansion	○	○
	Elasticity	–	○
	Plasticity	–	○
	Creep	–	○
	Cracking and healing	–	○
	Initial reloction	○	○
	Densification	○	○
	Swelling	○	○
	Hot pressing	–	○
Fuel-Cladding Mechanical Interaction	Radial contact pressure	○	○
	Axial contact pressure	–	○
	Axial force	–	○
	Inner gas pressure	–	○
Cladding Mechanics	Thermal expansion	○	○
	Elasticity	○	○
	Plasticity	–	○
	Creep	○	○
	Anisotropy	–	○
	Radiation hardening	–	○
Thermal Processes	Heat transfer between coolant and cladding	○	–
	Temperature distribution in cladding	○	–
	Heat transfer between fuel and cladding	○	–
	Heat generation distribution in fuel	○	–
	Temperature distribution in fuel	○	–
	Fission gas felease	○	–
	Inner gas pressure	○	–
Ridging Treatment		–	○

Caption ○ : yes
– : no

finite element method. The finite element method (FEM) analysis is applied to a small part of fuel rod which is expected to have the most severe mechanical interaction. The results from the mechanical analysis part is not fedback to the thermal analysis part, hence the mechanical analysis part is regarded as a subcode for the analysis of localized behavior.

As a function of irradiation time and axial position, the thermal analysis part calculates the following:

- the temperature distribution in the fuel and cladding;
- the radial deformation of the fuel due to thermal expansion, swelling, densification, and relocation;
- the radial deformation of the cladding due to thermoelastic and creep;
- the gap or the contact pressure between fuel and cladding;
- the fission gas release and inner gas pressure.

As a function of irradiation time, the FEM mechanical analysis part calculates the following:

- stress and strain distributions in the fuel and cladding considering elasto-plasticity, creep, thermal expansion, fuel cracking and healing, relocation, hourglassing, densification, swelling, hot pressing, fuel-cladding mechanical interaction, inner gas pressure, and coolant pressure.

The thermal and mechanical processes considered in the two analysis parts are summarized in **Table 1**.

2.2 Code Input

The basic fuel rod geometry handled in the code consists of fuel in the form of a stack of sintered fuel pellets and a cylindrical Zircaloy cladding tube, closed at each end, with the upper plenum (**Fig. 1**). The fuel consists of uranium deoxide in the form of pellets. The fuel pellets may be solid or annular and may or may not be dished, or be chamfered.

The filling gas is considered as any composition, at any pressure, of the following four gases: helium, nitrogen, krypton, and xenon.

The design and characterization data of fuel and cladding such as geometry, density, grain size, filling gas composition and pressure, and cladding type are given as input data.

The fuel rod is supposed to be cooled by pressurized or boiling water. The coolant temperature and pressure are given as input data as a function of time and are assumed to constant in axial direction. The power and flux distribution in axial direction is given as input data as a function of time.

2.3 Method of Solution

2.3.1 Geometrical Models

The thermal analysis part treats the entire fuel rod. The geometrical model for thermal analysis is shown in **Fig. 2**. A fuel rod is divided into a number of axial segments (up to 12) to account for axial variations in the power, flux, and fuel geometry. The averaged values of all variables over the height of these segments are used in the calculations.

The fuel region in each axial segment is, in turn, divided into the 10 concentric rings (**Fig. 2**). The cladding is assumed as one ring. The values of the thermal and mechanical properties are averaged over the width of each of these rings.

The FEM mechanical analysis is applied to a small region of a fuel rod as shown in **Fig. 3**, which also illustrates how the region is modeled by finite elements. The region of half-pellet

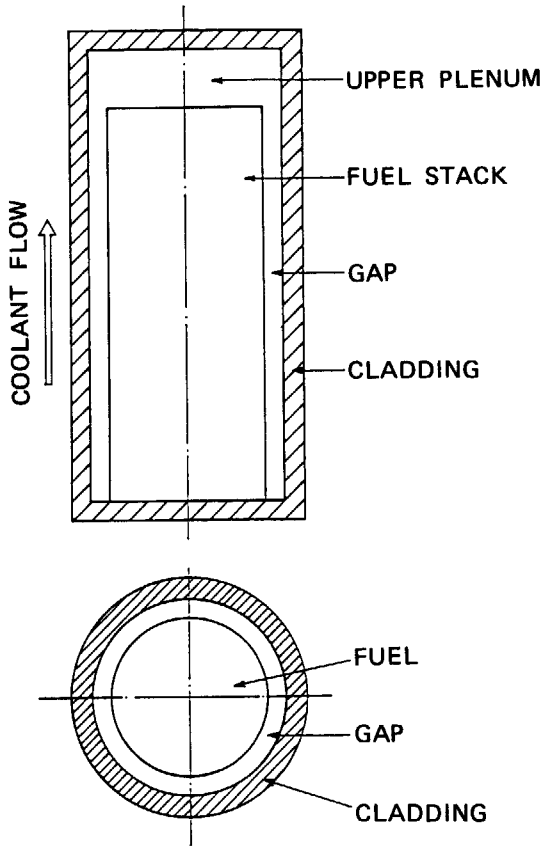

Fig. 1 Fuel Rod Geometry.

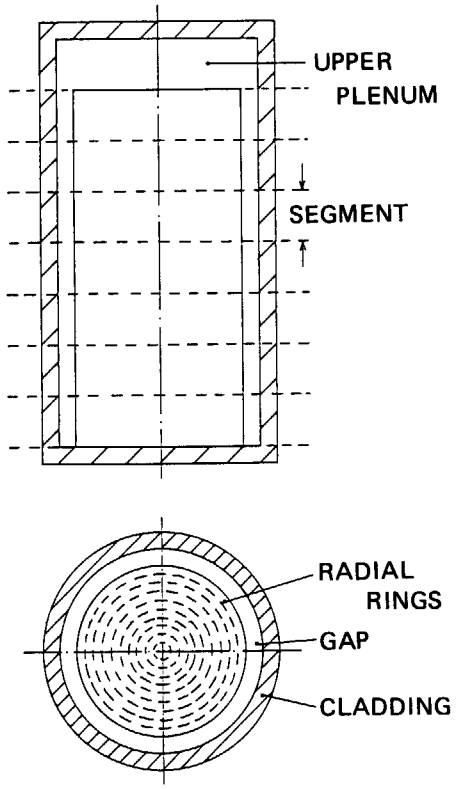

Fig. 2 Geometrical Model for Thermal Analysis.

height is analyzed assuming an axisymmetry and a plane-symmetry at the mid-plane of a pellet.

The geometrical model for the FEM mechanical analysis is shown in **Fig. 4**, together with an axisymmetric ring element. The boundary condition of the top of fuel and cladding is discussed in Chapter 4. The both fuel and cladding are divided into concentric ring elements which are linked by continuity laws of force and displacement. An 8-noded quadratic isoparametric ring element (**Fig. 4**) is used to built up the element stiffness equation. This element is used in preference to a linear element for the reason that a more accurate analysis is obtained with fewer elements than that are required when linear elements are used[7,18]. The element uses an isoparametric approach, so that the element ring can have 8 arbitrarily positioned nodes[7,18]. As the deformation of the fuel rod is described by a quadratic variation in the element, the code can takes highly accurate account of it. The stress, strain, and material properties are described by a linear variation in the element.

2.3.2 Calculation Procedure

A flow-chart of FEMAXI-III is shown in **Fig. 5**. The upper half of the flow-chart describes the thermal analysis part, and the lower half describes the FEM mechanical analysis part.

After operating conditions for a time step are determined, the radial temperature distribution in the fuel and cladding is obtained by a one-dimensional modelling, and the temperature is calculated at the boundaries of ten rings in the fuel and for three radial nodes in the cladding. At the first time step, the initial relocation is considered.

After the temperature distribution is determined, the thermal expansion, swelling, densification, and fission gas release are evaluated for each of fuel rings with the average temperature of each ring. The thermal expansion and flux-enhanced creep are calculated in a ring of cladding with the average temperature of the ring.

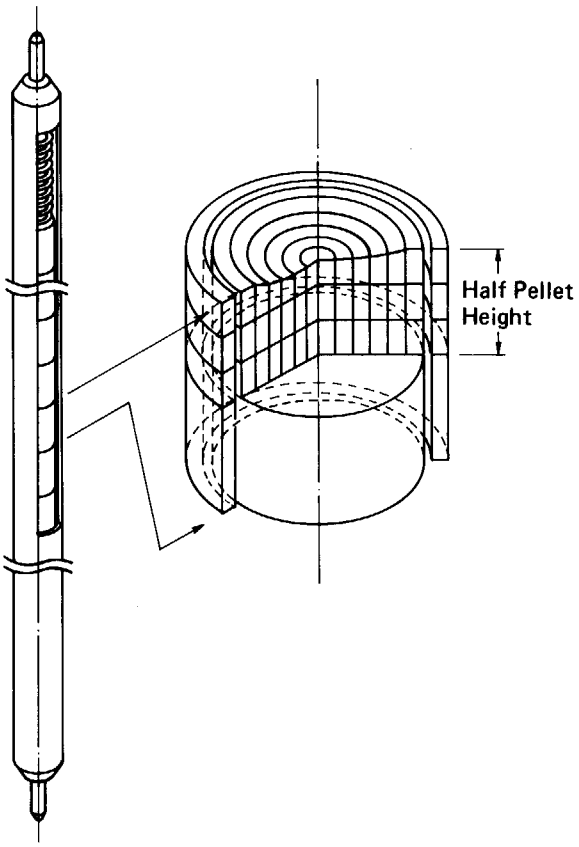

Fig. 3 Finite Element Idealization of Fuel Rod.

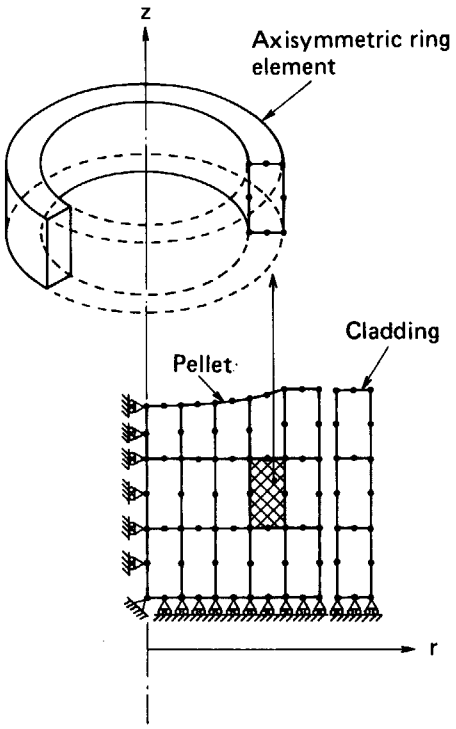

Fig. 4 Finite Element Geometrical Model.

These calculations are repeated for all axial segments, subsequently the total amount of fission gas released to the gap and plenum during a time step is calculated and added to that already released. The associated inner gas pressure and gas composition are then calculated. The code assumes instantaneous mixing of released fission gas and filler gas.

The preceding calculations are completed, the gap or contact pressure, and associated gap conductance are updated. Then the preceding calculations are repeated until the given convergence criterion is reached.

After completion of the thermal analysis, the temperature distribution and inner gas pressure are transfered to the FEM mechanical analysis part, where a two-dimensional analysis is performed at the axial segment of interest.

At the beginning of the FEM mechanical analysis, the change in free strains occured at each Gaussian integration point during the time step is calculated. If the time step is divided into the small sub-step, these values are linearly interporated to a point at which the time step is controlled.

An initial assumption for the boundary conditions at each interface node during the time step is made, based on the conditions in the previous step. Under this assumption, the preliminary calculations are made and first approximations of stresses and strains in the fuel and cladding are obtained. These first approximations for the creep strains are incorporated into the constitutive equations, which are then combined with the equations of equilibrium relations and solved with the same boundary conditions. This solution yields a second approximation for the change in stresses and strains in each integration point, which is then compared with the initial approximation. If agreement is not obtained, within specified limits, iteration continues. This is the Newton-Raphson iterative procedure, which is one of the techniques to solve the non-linear equations.

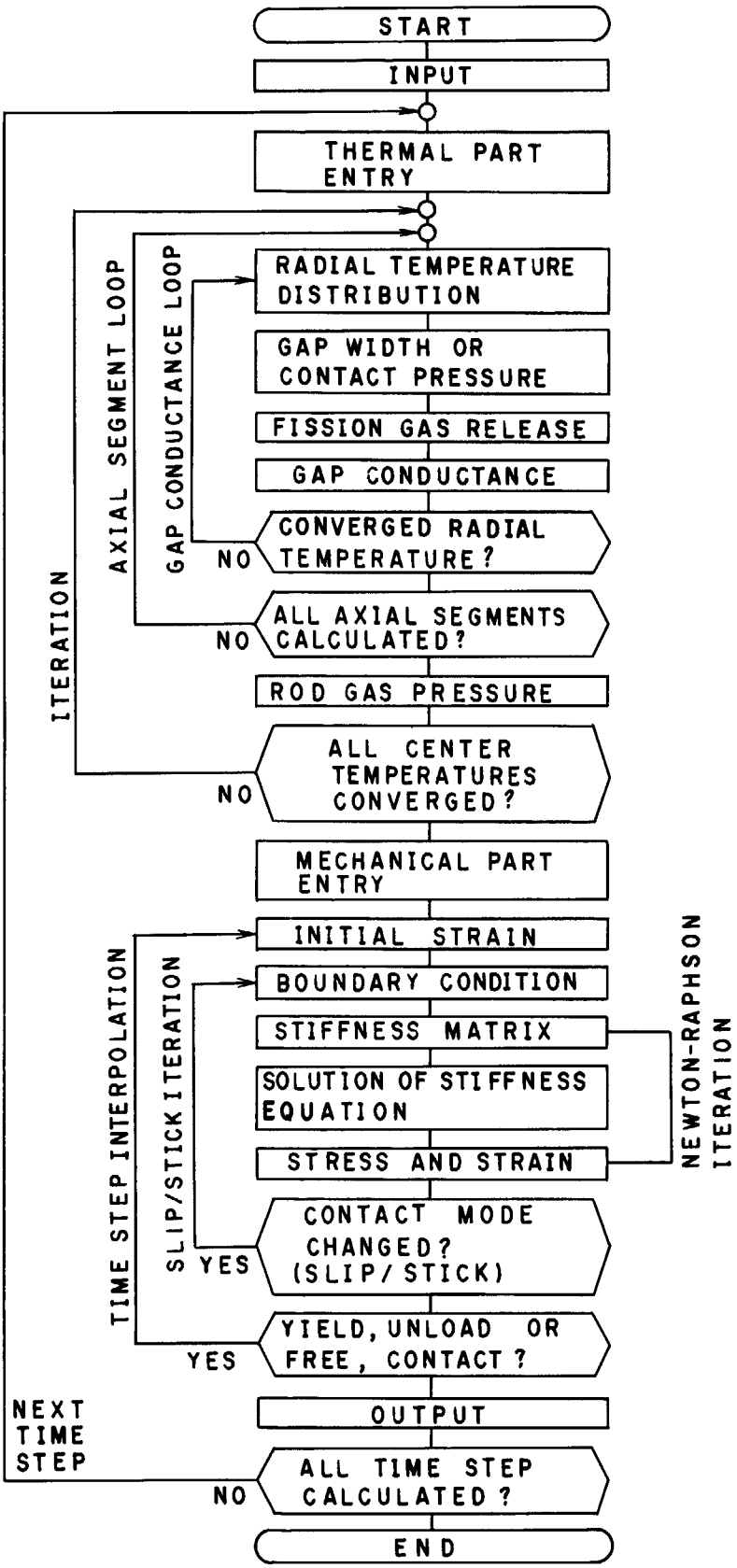

Fig. 5 FEMAXI-III Flow Chart.

After the convergence is achieved, the boundary condition is updated and compared with the first assumption. If agreement is not obtained, iteration continues and the Newton-Raphson iteration is repeated again. This is the another iteration loop to determine the contact condition in each interface node couple, whether in full bonding or in sliding.

After completion of these iterations, if the calculated results show that the material state changes from elastic to yielding or yielding to unloading, or that the contact condition changes from open to contact or from contact to open, the calculated results are linearly interpolated to a point of time at which the earliest change appears. Then the mechanical calculation is continued for the residual time step until the results at the end of time step are obtained.

After completion of the FEM mechanical analysis for a present time step, the calculation for a next time step starts.

2.4 Major Characteristics

The major characteristics of FEMAXI-III are the following:

- FEMAXI-III can analyze the integral behavior of a whole fuel rod throughout its life, as well as the localized mechanical behavior at a small part of a fuel rod;
- Localized behavior is analyzed in detail by the two-dimensional axisymmetric finite element method;
- Elasto-plasticity, creep, thermal expansion, fuel cracking and crack healing, relocation, densification, swelling, hot pressing, heat generation distribution, fission gas release, and fuel-cladding mechanical interaction are modelled;
- A quadratic isoparametric element is used to obtain a more accurate finite element solution with fewer elements than that are required when linear elements are used[18];
- Contact problem between fuel and cladding is exactly treated, where the contact condition, is determined by iterative procedure;
- An implicit algorithm, which necessitate use of iteration, is applied to obtain a accurate and stable solution for non-linear problems;
- Fuel is assumed as a no-tension material. Crack healing under compression is treated as recovering its stiffness gradually to nominal value. The recovery of fuel stiffness is related to initial relocation;
- Finite element analysis is applied only to a region of half-pellet height to save the computer memory and running time;
- An efficient sparse matrix storage scheme, which is called the skyline method[19,20], is used for solution of global stiffness equation to save the computer memory;
- The code can treat a problem of long irradiation history including power ramps with reasonable running time.

3. Thermal Analysis

3.1 Main Assumptions

The assumptions made in the thermal analysis are the following:

- thermal analysis neglects the circumferential and the axial heat conductions;
- steady-state thermal calculations are performed at each time step with an iterative procedure;
- instantaneous gas mixing of released gas with initial filler gas is assumed;
- coolant temperature is assumed to constant in the axial direction;
- empirical models are used to the relocation, densification, swelling, and fission gas release;
- burnup and power cycle effects to the relocation is not considered;
- fuel and cladding creep effects are not considered in the evaluation of fuel-cladding contact pressure.

3.2 Heat Transfer Models

3.2.1 Heat Transfer between Coolant and Cladding

The cladding outer temperature is given by

$$T_{co}=T_w+\frac{q'}{2\pi r_{co}h_c}, \tag{1}$$

where T_{co} : temperature of the outside of the cladding [K],
T_w : coolant temperature [K]
q' : linear heat rate [W/cm],
r_{co} : outer radius of the cladding [cm],
h_c : heat transfer coefficient between the coolant and the cladding [W/(cm^2·K)].

The coolant condition, nucleate boiling or forced convection, is selected by input at the first stage of calculation. The heat transfer coefficient for the nucleate boiling condition is calculated using the Jens-Lottes correlation [21], and given by

$$h_{c,NB}=0.1263\exp\left(\frac{P_w}{6.201\times10^6}\right)\cdot q''^{0.75}, \tag{2}$$

with

$$q''=\frac{q'}{2\pi r_{co}},$$

where $h_{c,NB}$: heat transfer coefficient between the coolant and the cladding for the nucleate boiling condition [W/(cm^2·K)],
P_w : coolant pressure [Pa],
q'' : heat flux [W/cm^2].

The heat transfer coefficient for the forced convection condition is calculated using the Dittus-Boelter correlation[22],

$$h_{c,FC}=0.023\frac{k_w}{D_e}\left(\frac{D_e v\rho}{\mu}\right)^{0.8}\cdot(Pr)^{0.4}, \tag{3}$$

where $h_{c,FC}$: heat transfer coefficient between the coolant and the cladding for the forced convection condition [Btu/(hr·ft^2·°F)],
k_w : coolant thermal conductivity [Btu/(hr·ft·°F)],
D_e : equivalent hydraulic diameter [in],

v : coolant velocity [ft/s],
ρ : coolant density [lb/ft^3],
μ : viscosity of coolant water [lb/(ft·s)],
Pr : Prandtl number, $Pr=c_p \cdot \mu / k$,
c_p : specific heat [Btu/(lb·°F)].

3.2.2 Temperature Distribution in the Cladding

Across the cladding the one-dimensional heat-conduction equation is integrated:

$$\int_{T_{co}}^{T} k_c dT = \frac{q'}{2\pi} \ln\left(\frac{r_{co}}{r}\right), \tag{4}$$

where T : cladding temperature at radius r [K],
k_c : thermal conductivity of the cladding [W/(cm·K)],
r : radial coordinate [cm].

The temperature at the radius r is calculated by solving Eq. (4).

The thermal conductivity of Zircaloy is given by [23]:

$$k_c = 7.51 + 2.09 \times 10^{-2} T - 1.45 \times 10^{-5} T^2 + 7.67 \times 10^{-9} T^3, \tag{5}$$

where k_c : thermal conductivity of Zircaloy [W/(m·K)],
T : temperature [K].

3.2.3 Fuel-Cladding Heat Transfer

The heat transfer coefficient between fuel and cladding is calculated by the modified Ross and Stoute model[24]. It is given by the sum of three components:

$$h_{gap} = h_g + h_s + h_r, \tag{6}$$

where h_{gap} : heat transfer coefficient between fuel and cladding [W/(cm^2·K)],
h_g : heat transfer coefficient through gap gas [W/(cm^2·K)],
h_s : heat transfer coefficient through solid to solid contact spots [W/(cm^2·K)],
h_r : heat transfer coefficient by radiation [W/(cm^2·K)].

Each component is explained in the following.

(a) Heat Transfer Coefficient through Gap Gas

The heat transfer coefficient h_g is given by

$$h_g = \frac{k_{gas}}{C(R_{eff} + R_2) + (g_1 + g_2) + \delta}, \tag{7}$$

where k_{gas} : thermal conductivity of gas mixture in the gap [W/(cm·K)],
C : a constant,
R_{eff} : effective surface roughness of the fuel [cm],
R_2 : surface roughness of the cladding [cm],
g_1 : average temperature-jump distance for a gas at the fuel surface [cm],
g_2 : average temperature-jump distance for a gas at the cladding surface [cm],
δ : radial gap [cm].

The thermal conductivity of gas mixture k_{gas} is calculated by the following equation according to the MATPRO-09 model[23]:

$$k_{gas} = \sum_{i=1}^{n} \left(\frac{k_i}{1 + \sum_{\substack{j=1 \\ j \neq i}}^{n} \psi_{ij} \frac{x_j}{x_i}} \right), \tag{8}$$

with

$$\psi_{ij}=\phi_{ij}\left[1+2.41\frac{(M_i-M_j)(M_i-0.142\,M_j)}{(M_i+M_j)^2}\right], \tag{9}$$

and

$$\phi_{ij}=\frac{\left[1+\left(\frac{k_i}{k_j}\right)^{\frac{1}{2}}\left(\frac{M_i}{M_j}\right)^{\frac{1}{4}}\right]^2}{2^{\frac{3}{2}}\left(1+\frac{M_i}{M_j}\right)^{\frac{1}{2}}}, \tag{10}$$

where n : number of components in gas mixture,
i & j : gas species,
M_i : molecular weight of gas species i,
x_i : mole fraction of gas species i,
k_i : thermal conductivity of gas species i [W/(cm·K)].

The four species of gas, helium, xenon, krypton, and nitrogen, are considered for the components in the gas mixture. The thermal conductivity equations for the individual rare gases are given by

$$k_{He}=3.366\times10^{-5}T^{0.668}, \tag{11}$$

$$k_{Xe}=4.0288\times10^{-7}T^{0.872}, \tag{12}$$

$$k_{Kr}=4.726\times10^{-7}T^{0.923}, \tag{13}$$

$$k_{N_2}=2.091\times10^{-6}T^{0.846}, \tag{14}$$

where k : thermal conductivity [W/(cm·K)],
T : temperature [K].

A constant C, which appears in Eq. (7), is given by

$$C=2.77-2.55\times10^{-8}\cdot P_c, \tag{15}$$

where P_c : contact pressure [Pa].

The minimum value of C is assumed to be unity.

The empirical parameter R_{eff} is used for the effective fuel surface roughness instead of the fuel surface roughness R_1 in the original model. This modification was made with the view of explaining in-pile gap conductance inferred from fuel center temperature measurements. The value of R_{eff} was estimated as 4×10^{-4} cm by fitting the model to the fuel center temperature data. This value is greater than the normal fuel surface roughness of about 1×10^{-4} cm. This implies that the fuel-cladding interface is actually more mismatched compared to the value given by the original Ross and Stoute model.

The value of (g_1+g_2) is given by the sum of values of $(g_1+g_2)_i$ for each gas species of i, as follows:

$$g_1+g_2=\sum_{i=1}^{n}(g_1+g_2)_i\cdot x_i\cdot\frac{10^5}{P_{gas}}, \tag{16}$$

where $(g_1+g_2)_i$: temperature-jump distance for gas species i [cm],
x_i : mole fraction of gas species i,
P_{gas} : inner gas pressure [Pa].

For a gas pressure of 76 cm Hg, mean values of $(g_1+g_2)_i$ for each gas species are

10×10^{-4} cm in helium,
1×10^{-4} cm in xenon,
1×10^{-4} cm in krypton,
5×10^{-4} cm in nitrogen.

(b) Heat Transfer Coefficient through Solid to Solid Contact Spots

$$h_s = \frac{k_m \cdot P_c}{0.5 \cdot R^{\frac{1}{2}} \cdot H} , \tag{17}$$

and

$$H = \exp\left(2.6034 \times 10 - 2.6394 \times 10^{-2} T_{ci} + 4.3502 \times 10^{-5} T_{ci}^2 + 2.5621 \times 10^{-8} T_{ci}^3\right) ,$$

where k_m : mean of fuel and cladding thermal conductivities [W/(cm·K)],
R : square mean of the fuel and cladding roughness [cm],
H : Mayer hardness of the cladding [Pa],
T_{ci} : temperature of the inside of the cladding [K].

The values of k_m and R are defined by the following equations:

$$k_m = \frac{2(k_1 \cdot k_2)}{(k_1 + k_2)} , \tag{18}$$

$$R = \left(\frac{R_{eff}^2 + R_2^2}{2}\right)^{\frac{1}{2}} , \tag{19}$$

where k_1 : thermal conductivity of the fuel [W/(cm·K)],
k_2 : thermal conductivity of the cladding [W/(cm·K)].

(c) Heat Transfer Coefficient by Radiation

The heat transfer coefficient by radiation h_r is given by

$$h_r = \frac{\sigma}{\frac{1}{e_1} + \frac{1}{e_2} - 1} \cdot \frac{T_1^4 - T_2^4}{T_1 - T_2} , \tag{20}$$

where e_1 : emissivity of the outer fuel surface,
e_2 : emissivity of the inner cladding surface,
σ : Stephan-Boltzman constant = 5.67×10^{-12} [W/(cm^2·K^4)],
T_1 : temperature of the outer fuel surface [K],
T_2 : temperature of the inner cladding surface [K].

The emissivity of the fuel is defined according to[23], as follows:

$$\left.\begin{array}{l} T_1 < 1000\,K, \quad e_1 = 0.8707 , \\ 1000\,K \leq T_1 \leq 2050\,K, \quad e_1 = 1.311 - 4.404 \times 10^{-4} \cdot T_1 , \\ T_1 > 2050\,K, \quad e_1 = 0.4083. \end{array}\right\} \tag{21}$$

The emissivity of the cladding surface for the zirconium oxide layer is given by[23]:

$$e_2 = 0.74 . \tag{22}$$

3.2.4 Heat Generation Rate in the Fuel

The neutron flux depression is expressed by Robertson[25] as follows:

$$\psi(r) = \psi_0 \left(I_0(\kappa \cdot r) + \frac{I_1(\kappa \cdot r_{fi})}{K_1(\kappa \cdot r_{fi})} \cdot K_0(\kappa \cdot r)\right) , \tag{23}$$

where ψ : thermal neutron flux [n/(sec·cm^2)],
r : radial coordinate [cm],
I_0, K_0 : modified Bessell functions of zero order,
I_1, K_1 : modified Bessell functions of first order,
κ : inverse diffusion length for neutrons in the fuel [cm^{-1}],
r_{fi} : inner radius of the fuel [cm].

The inverse diffusion length κ is given by

$$\kappa = 0.328(e \cdot f_d)^{0.8} + \left(0.54\frac{0.5}{r_{fo}}\right)^{0.82} \cdot (e \cdot f_d)^{0.19} \quad , \tag{24}$$

where e : enrichment of U^{235} [%],
f_d : fraction of theoretical density,
r_{fo} : outer radius of the fuel [cm].

The neutron flux depression given by Eq. (23) is fitted by the following parabolic form

$$\psi(r) = \psi_0 \left[\frac{(b+2)(1-\bar{r}_1^2)\{(1-a)\bar{r}^b + (a-\bar{r}_1^b)\}}{b(1-\bar{r}_1^2)(a-\bar{r}_1^b) + 2(1-\bar{r}_1^b)(1-a \cdot \bar{r}_1^2)}\right], \tag{25}$$

where a : fraction of inner and outer surface heat generation rate,
b : degree of heat generation distribution function = 2,
$\bar{r}_1$: normalized radius of fuel inner surface = r_{fi}/r_{fo} ,
$\bar{r}$: normalized radius of the fuel = r/r_{fo} .

The value of parameter a, which is defined as a fraction of inner and outer surface heat generation rate, is given by the following using Eq. (23):

$$a = \frac{\psi(r_{fi})}{\psi(r_{fo})} \ . \tag{26}$$

Since the rate of heat generation is proportional to the neutron flux, it is given by

$$q'''(r) = q_0 \left[\frac{(b+2)(1-\bar{r}_1^2)\{(1-a)\bar{r}^b + (a-\bar{r}_1^b)\}}{b(1-\bar{r}_1^2)(a-\bar{r}_1^b) + 2(1-r_1^b)(1-a \cdot \bar{r}_1^2)}\right], \tag{27}$$

with

$$q_0 = \frac{q'}{\pi(r_{fo}^2 - r_{fi}^2)} \ , \tag{28}$$

where q''' : heat generation rate per unit volume of fuel [W/cm^3].

3.2.5 Temperature Distribution in the Fuel

The temperature drop across the fuel-cladding gap is given by

$$T_{fo} = T_{ci} + \frac{q'}{2\pi r_{fo} h_{gap}} \tag{29}$$

where T_{fo} : temperature of the outside of the fuel [K],
T_{ci} : temperature of the inside of the cladding [K],
q' : linear heat rate [W/cm],
r_{fo} : outer radius of the fuel [cm],
h_{gap} : gap heat-transfer coefficient [W/(cm^2·K)].

Across the fuel the one-dimensional heat conduction equation is integrated

$$\int_{T_{fo}}^{T} k_f \mathrm{d}T = \int_{r}^{r_{fo}} \frac{1}{r}\left[\int_{r_{fi}}^{r} r \cdot q'''(r)\mathrm{d}r\right]\mathrm{d}r \ , \tag{30}$$

where T : temperature of the fuel at the radius r [K],
k_f : thermal conductivity of the fuel [W/(cm·K)],
r : radial coordinate [cm],
q''' : heat generation rate per unit volume of fuel [W/cm^3].

Substituting Eq. (27) into Eq. (30), we have

$$\int_{T_{fo}}^{T} k_f \mathrm{d}T = \frac{q'}{4\pi} \cdot F(\bar{r}) \ , \tag{31}$$

where

$$F(\bar{r})=\left\{\frac{4(1-a)(1-\bar{r}^{b+2})}{(b+2)^2}+(a-\bar{r}_1^{\,b})(1-\bar{r}^2)+4\left(\frac{1-a}{b+2}\bar{r}_1^{\,b+2}+\frac{a-\bar{r}_1^{\,b}}{2}\cdot\bar{r}_1^{\,2}\right)\ln\bar{r}\right\}$$

$$\Bigg/\left\{\frac{b+2}{b(1-\bar{r}_1^{\,2})(a-\bar{r}_1^{\,b})+2(1-\bar{r}_1^{\,b})(1-a\cdot\bar{r}_1^{\,2})}\right\}, \tag{32}$$

and $\bar{r}$: normalized radius $= r/r_{fo}$,

$\bar{r}_1$: normalized raidus of inner fuel surface $= r_{fi}/r_{fo}$.

The temperature at the boundaries of rings is calculated solving Eq. (31) from the outer ring.

The thermal conductivity of UO_2 is expressed as a function of temperature and porosity according to[23].

For 0 °C $< T \leq$ 1,650 °C;

$$k_f=\frac{[1-\beta(1-f_d)]}{[1-\beta(1-0.95)]}\left[\frac{K_1}{K_2+T}+K_3\exp(K_4T)\right], \tag{33}$$

For 1,650 °C $\leq T <$ 2,840 °C;

$$k_f=\frac{[1-\beta(1-f_d)]}{[1-\beta(1-0.95)]}[K_5+K_3\exp(K_4T)], \tag{34}$$

where k_f : thermal conductivity of UO_2 fuel [W/(cm·K)],

f_d : fraction of theoretical density,

β : porosity coefficient $= 2.58 - 0.58 \times 10^{-3}\,T$,

T : fuel temperature [°C].

The values of constants K_1 through K_5 are given by

$$\left.\begin{aligned} K_1&=40.4\ ,\\ K_2&=464\ ,\\ K_3&=1.216\times10^{-4}\ ,\\ K_4&=1.867\times10^{3}\ ,\\ K_5&=0.0191\ . \end{aligned}\right\} \tag{35}$$

3.3 Gap Closure Models

The gap closure is the most complex mechanism in the fuel, which depends on the following phenomena:

- fuel thermal expansion;
- fuel relocation;
- fuel densification;
- fuel swelling;
- cladding thermal expansion;
- cladding elastic and creep deformations.

The radial displacement of the fuel and of the cladding is calculated independently in the thermal analysis part from the FEM mechanical analysis part. The gap or contact pressure between the fuel and cladding is calculated more simply in the thermal analysis part to deal with the entire fuel rod.

3.3.1 Main Assumptions

The radial displacement of the fuel and of the cladding including fuel-cladding mechnaical interaction is calculated according to the following assumptions:

- fuel radial displacement due to thermal expansion, relocation, densification, and gaseous and

solid swelling is calculated by a free ring expansion model;
- fuel expands isotoropically;
- cladding radial displacement due to thermal expansion and creep is calculated by a thin wall cylinder model;
- elastic deformation of the cladding due to inner and outer pressures is claculated using elastic theory of thick wall cylinder;
- full bonding is assumed if gap closed. No sliding occurs between fuel and cladding;
- fuel behaves as a rigid body after contact. Fuel plasticity and creep are not considered;
- fission gas bubble swelling does not contoribute to the development of contact pressure;
- cladding deforms elastically after contact by the excess of fuel expansion. Plastic and creep deformations from stresses induced by fuel-cladding interaction are not considered.

3.3.2 Fuel Relocation Model

At the start-up the fuel cracking occurs due to the thermal expansion differences across the fuel caused by high temperature gradient in the fuel. The fragments of cracked fuel relocate outward to reduce a certain fraction of the gap. The radial displacement of the fuel due to relocation is given by

$$u^{\mathrm{rel}} = \alpha \delta_0 \ , \tag{36}$$

where u^{rel} : radial displacement of the fuel by relocation [cm],
α : relocation parameter,
δ_0 : as-fabricated radial gap [cm].

The relocation parameter α is assumed to constant during the whole irradiation period, and the burnup dependency or power cycle effect to the fuel relocation is not considered.

The value of empirical parameter α was determined by fitting the model to the in-pile fuel center temperature data. The best estimated value of α was 0.3.

This value is not applied to the FEM mechanical analysis part for the reason that the radial displacement of fuel and of cladding is calculated independently in the FEM mechanical analysis part from the thermal analysis part by using two-dimensional models. Therefore the relocation parameter for the FEM mechanical analysis was separately determined by fitting the model to the in-pile fuel diameter measurement data. The value of relocation parameter α for the FEM mechanical analysis was estimated to be 0.5.

3.3.3 Fuel Densification Model

The in-pile fuel shrinkage, which is called fuel densification, is attributed to the irradiation induced sintering of the initial fuel porosity. This phenomenon occurs even at low temperature and results in an asymptotic increase of the fuel density. An empirical expression for the volume change of porosity as a function of burnup is given by

$$\left(\frac{\Delta V}{V_0}\right)^d = \frac{\Delta V_{\max}}{V_0}\left[1-\exp\left(-2.3025\,\frac{BU}{SBU}\right)\right] \ , \tag{37}$$

where $\left(\frac{\Delta V}{V_0}\right)^d$: volume change by densification,
V_0 : initial free volume,
$\Delta V_{\max}$: maximum volume change of porosity,
BU : burnup [MWd/tUO_2],
SBU : burnup constant for densification.

$\Delta V_{\max}$ and SBU are given as input values determined on the basis of resintering tests on the fuel. SBU defines the slope of densification.

3.3.4 Fuel Swelling Model

The fuel swelling associated with retension of gaseous and solid fission products inside the fuel lattice is correlated to the fission numbers for uranium dioxide fuel. The swelling rate due to solid fission product is given by[23]

$$\left(\frac{\Delta V}{V_0}\right)^{ss} \text{ per } 10^{20} \text{ fissions/cm}^3 = 0.0025, \tag{38}$$

where $\left(\frac{\Delta V}{V_0}\right)^{ss}$: volume change by solid fission product swelling.

The swelling rate due to the retension of gaseous fission product is correlated to the fuel temperature and fission numbers according to[26] and[27], and it is given by

$$\left(\frac{\Delta V}{V}\right)^{gs} \text{ per } 10^{20} \text{ fissions/cm}^3 = 4.396\times10^2 \exp\left(-\frac{1.645\times10^4}{T_s}\right), \tag{39}$$

with

$$T_s = T - 100,$$

where $\left(\frac{\Delta V}{V_0}\right)^{gs}$: volume change by gaseous fission product swelling,

T : temperature [K].

3.3.5 Fuel Thermal Expansion

The fuel thermal expansion is given as a function of temperature[23]

$$\left(\frac{\Delta l}{l_0}\right)_f^{th} = -4.972\times10^{-4} + 7.107\times10^{-6}T + 2.581\times10^{-9}T^2 + 1.140\times10^{-13}T^3, \tag{40}$$

where $\left(\frac{\Delta l}{l_0}\right)_f^{th}$: linear thermal expansion of the fuel,

l_0 : initial length,

T : temperature [°C].

3.3.6 Fuel Radial Displacement

The fuel radial displacement due to thermal expansion, relocation, densification, and gaseous and solid swelling is given by integrating the radial displacement at each concentric ring as follows:

$$u_f = u^{rel} + \sum_{i=1}^{m}\left[\left(\frac{\Delta l}{l_0}\right)_{f,i}^{th} + \frac{1}{3}\left\{\left(\frac{\Delta V}{V_0}\right)_i^{d} + \left(\frac{\Delta V}{V_0}\right)_i^{ss} + \left(\frac{\Delta V}{V_0}\right)_i^{gs}\right\}\right]\Delta r_i, \tag{41}$$

where u_f : fuel radial displacement [cm],

u^{rel} : radial displacement of the fuel by relocation [cm],

m : number of concentric ring,

$\left(\frac{\Delta l}{l_0}\right)_{f,i}^{th}$: thermal expansion of ith concentric ring,

$\left(\frac{\Delta V}{V_0}\right)_i^{d}$: volumetric strain by densification of ith concentric ring,

$\left(\frac{\Delta V}{V_0}\right)_i^{ss}$: volumetric strain by solid fission product swelling of ith concentric ring,

$\left(\frac{\Delta V}{V_0}\right)_i^{gs}$: volumetric strain by gaseous fission product swelling of ith concentric ring,

Δr_i : width of ith concentric ring [cm].

3.3.7 Cladding Thermal Expansion

The cladding axial thermal expansion is expressed as a function of temperature[23]

$$\left(\frac{\Delta l}{l_0}\right)_c^{th} = -2.506\times10^{-5} + 4.441\times10^{-6}T \ , \tag{42}$$

where $\left(\frac{\Delta l}{l_0}\right)_c^{th}$: cladding axial thermal expansion,

T : temperature [°C].

The cladding diametral thermal expansion is given as a function of temperature[23)]

$$\left(\frac{\Delta D}{D_0}\right)_c^{th} = -2.373\times10^{-4} + 6.721\times10^{-6}T \ , \tag{43}$$

for 27 °C < T < 800 °C,

where $\left(\frac{\Delta D}{D_0}\right)_c^{th}$: cladding diametral thermal expansion,

D_0 : initial diameter,

T : temperature [°C].

3.3.8 Cladding Creep

The radial creep deformation of the cladding due to the inner and outer pressures is calculated very simply in the thermal analysis part using the empirical model, which is determined by fitting the model to the in-pile creep data.

The radial displacement of the cladding by creep is given as a function of burnup

$$u_c^{creep} = \frac{C\times10^{-10}}{3.0513}\cdot\frac{r_{co}(P_w - P_{gas})}{(r_{co}-r_{ci})}\sqrt{BU\times10^{-3}}\cdot\left(\frac{r_{co}+r_{ci}}{2}\right) \ , \tag{44}$$

with

C = 0.50 for recrystallized cladding tube,

or

C = 0.75 for stress-relieved cladding tube,

where u_c^{creep} : radial displacement of the cladding by creep [cm],

r_{co} : outer radius of the cladding [cm],

r_{ci} : inner radius of the cladding [cm],

P_w : coolant pressure [Pa],

P_{gas} : inner gas pressure [Pa],

BU : burnup [MWd/tUO_2].

3.3.9 Cladding Radial Displacement

The cladding radial displacement due to thermal expansion and elastic and creep deformations is calculated by

$$u_c = \frac{r_{ci}}{E_c}\left[\frac{P_{gas}(r_{ci}^2+r_{co}^2) - 2P_w r_{co}^2}{r_{co}^2 - r_{ci}^2} + \nu_c P_{gas}\right] + \left(\frac{\Delta D}{D_0}\right)_c^{th}\cdot\frac{r_{co}+r_{ci}}{2} + u_c^{creep} \ , \tag{45}$$

where u_c : cladding radial displacement [cm],

E_c : Young's modulus for cladding [Pa],

r_{ci} : inner radius of the cladding [cm],

r_{co} : outer radius of the cladding [cm],

P_{gas} : inner gas pressure [Pa],

P_w : coolant pressure [Pa],

ν_c : poisson's ratio for cladding,

$\left(\frac{\Delta D}{D_0}\right)_c^{th}$: diameteral thermal expansion of the cladding,

u_c^{creep} : cladding radial displacement by creep [cm].

3.3.10 Gap or Contact Pressure

The radial gap between fuel and cladding is given by

$$\delta = \delta_0 + u_c - u_f \quad , \tag{46}$$

where δ : radial gap between fuel and cladding [cm],
δ_0 : as-fabricated radial gap [cm],
u_c : cladding radial displacement [cm],
u_f : fuel radial displacement [cm].

If δ becomes minus, fuel/cladding contact occurs. After contact, the cladding radial displacement is calculated with the following assumptions:

- fuel behaves as a rigid body;
- cladding deforms elastically after contact by the excess of fuel expansion.

The cladding radial displacement after contact is given by

$$\delta_{fc} = -(\delta_0 + u_c - u_f) \quad , \tag{47}$$

where δ_{fc} : cladding radial displacement after contact [cm].

The contact pressure between fuel and cladding is calculated by

$$P_{fc} = \frac{\delta_{fc} \cdot E_c \cdot \Delta r_c}{r_{ci}^2} \quad , \tag{48}$$

where P_{fc} : contact pressure between fuel and cladding [Pa],
δ_{fc} : cladding radial displacement after contact [cm],
E_c : Young's modulus for cladding [Pa]
Δr_c : initial thickness of cladding [cm],
r_{ci} : inner radius of cladding [cm].

3.4 Fission Gas Release Model

3.4.1 Fission Gas Production

The fission gas production rate in the concentric ring i at the axial segment j is given by

$$\beta_{ij} = \frac{Y \cdot q'^{ij}}{E_f \cdot N_A} \quad , \tag{49}$$

with

$$q'^{ij} = 2\pi \int_{r_i - \Delta r_i/2}^{r_i + \Delta r_i/2} q'''(r)\, r\, dr \quad , \tag{50}$$

where i : concentric ring number,
j : axial segment number,
β : fission gas production rate per unit length [mole/(cm·sec)],
q' : heat generation rate per unit length [w/cm],
q''' : heat generation rate per unit volume of fuel described by Eq. (27) [W/cm^3],
Y : yielding ratio of $(K_r + X_e) = 0.3$,
E_f : fission energy = 200 MeV,
N_A : Avogadoro constant = 6.02×10^{23}.

3.4.2 Empirical Fission Gas Release Model

The Vitanza empirical model[28] is used in calculating the fission gas release rate. This model is based on the wide data base obtained from in-pile gas pressure measurements and post-irradiation gas analysis results. It assumes that the fission gas release from the fuel occurs when some burnup is accumulated. This incubation period depends on the fuel temperatures.

It lasts longer at lower temperatures.

The incubation period is given by

$$BU^* = 5.0 \exp(9800/T_{fc}) \ , \tag{51}$$

where BU^* : incubation burnup [MWd/tUO$_2$],
T_{fc} : fuel centerline temperature [°C].

If the burnup at the axial segment j exceeds the incubation burnup expressed by Eq. (51), the local release fraction in the ring i at the axial segment j is given by

$$f^{ij} = f(T^{ij})\left(1 - \frac{BU^{*j}}{BU^j}\right) \ , \tag{52}$$

with

$$f(T^{ij}) = \left(\frac{T^{ij}}{1800}\right)^5 \quad \text{if } T^{ij} \leq 1800℃,$$

and

$$f(T^{ij}) = 1 \quad \text{if } T^{ij} > 1800℃,$$

where f^{ij} : release fraction of fission gas in the concentric ring i at the axial segment j,
T^{ij} : fuel temperature in the concentric ring i at the axial segment j [°C],
BU^j : burnup at the axial segment j [MWd/tUO$_2$].

To take into account the fission gas release due to knock-out mechanism, the minimum release fraction of 0.005 is assumed through the whole irradiation period independent to fuel temperature.

3.4.3 Composition of Gas in the Fuel Rod

The total amount of released gas from the fuel up to the time t is given by

$$n_r = \sum_{j=1}^{m}\left[l^j \sum_{i=1}^{10}\left(\int_0^t f^{ij} \cdot \beta^{ij}\, dt\right)\right], \tag{53}$$

where n_r : number of released gas moles from the fuel up to the time t [mole],
m : number of axial segments considered,
i : concentric ring number,
j : axial segment number,
l : length of axial segment [cm],
t : irradiation time [s],
f : release fraction of fission gas,
β : fission gas production rate per unit length of fuel [mole/(cm·s)].

The assumptions made in the calculation of the composition of released gas are the following:

- the 87% of released gas is xenon and the residual gas is krypton;
- released gas mixes with initial filler gas completely at once;
- gas cmposition is uniform in the fuel rod.

The gas composition is calculated by the following equations:

$$\left.\begin{aligned} x_{He} &= n_0 \cdot x_{0,He}/n_t \ , \\ x_{Kr} &= (n_0 \cdot x_{0,Kr} + 0.13\, n_r)/n_t \ , \\ x_{Xe} &= (n_0 \cdot x_{0,Xe} + 0.87\, n_r)/n_t \ , \end{aligned}\right\} \tag{54}$$

where x_{He} : mole fraction of helium,
x_{Kr} : mole fraction of krypton,
x_{Xe} : mole fraction of xenon,

n_0 : number of gas moles initially in the fuel rod [mol],
n_r : number of released gas moles [mol],
n_t : total number of gas moles in the fuel rod = $n_0 + n_r$ [mole],
$x_{0,He}$: initial mole fraction of helium,
$x_{0,Kr}$: initial mole fraction of krypton,
$x_{0,Xe}$: initial mole fraction of xenon.

3.4.4 Fuel Rod Inner Gas Pressure

To determine the inner gas pressure, the temperature of gas in the plenum, gap, central hole, and internal void in the fuel are volume averaged for use in the perfect gas law

$$P_{gas} = \frac{n_t R T_{av}}{V_{pl} + \sum_{j=1}^{m} (V_{gap}^j + V_h^j + V_{int}^j)} , \tag{55}$$

with

$$T_{av} = \frac{V_{pl} + \sum_{j=1}^{m} (V_{gas}^j + V_h^j + V_{int}^j)}{\left[\frac{V_{pl}}{T_{pl}} + \sum_{j=1}^{m} \left(\frac{V_{gap}^j}{T_{gap}} + \frac{V_h^j}{T_{fi}} + \frac{V_{int}^j}{\overline{T}_f}\right)\right]} , \tag{56}$$

where P_{gas} : inner gas pressure [Pa],
T_{av} : volume average temperature of the gas [K],
n_t : total number of gas moles in the fuel rod [mol],
R : universal gas constant = 8.314 [J/(K·mol)],
V_{pl} : volume of the plenum [m^3],
m : number of axial segments considered,
j : axial segment number,
V_{gap} : volume of the gap between the fuel and cladding [m^3],
V_h : volume of the central hole [m^3],
V_{int} : volume of the internal void in the fuel [m^3],
T_{pl} : plenum temperature = $T_w + 25$ [K],
T_w : coolant temperature [K],
T_{fi} : inner temperature of the fuel [K],
T_{gap} : gap temperature between the fuel and cladding = $0.5(T_{fo}+T_{ci})$ [K],
T_{fo} : outer temperature of the fuel [K],
T_{ci} : inner temperature of the cladding [K],
$\overline{T}_f$: volume average temperature of the fuel [K].

The internal void in the fuel includes the dish volume, chamfer volume, and crack volume, etc.

4. Mechanical Analysis

4.1 Main Assumptions

The mechanical analysis is based on the following assumptions:

- FEM analysis is applied to the region of half-pellet height;
- axisymmetry is assumed;
- symmetrical plane is assumed to mid-plane of a pellet;
- cladding top-plane perpendicular to the axis remains plane;
- for a small time increment, the free expansion strain is assumed to change linearly;
- strain increments are related to stress increments by the Prandtl-Reuss equations[29] including thermal expansion, fuel growth, plasticity, and creep.

4.2 Finite Element Formulation

4.2.1 General Procedure for Solution of Non-Linear Problems

In the non-linear problems, such as creep and plasticity, the relationship between stress and strain is not linear and the strain is described by

$$\{\varepsilon\}=f(\{\sigma\}) \quad , \tag{57}$$

where $\{\varepsilon\}$: strain vector,
$\{\sigma\}$: stress vector.

Hence the explicit determination of $\{\sigma\}$ in terms of $\{\varepsilon\}$ is not possible in the non-linear problems.

As usual the rate of non-elastic strain is defined as some function of stresses, i.e.,

$$\{\dot{\varepsilon}^{\mathrm{ne}}\}=\frac{\{\Delta\varepsilon^{\mathrm{ne}}\}}{\Delta t}=\beta(\{\sigma\}) \quad , \tag{58}$$

where $\{\dot{\varepsilon}^{\mathrm{ne}}\}$: non-elastic strain rate vector,
$\{\Delta\varepsilon^{\mathrm{ne}}\}$: incremental non-elastic strain vector,
Δt : increment of time,
β : non-elastic strain rate vector.

If we consider an interval of time Δt_{n+1} at the beginning of which the state characterized by nodal displacements, stresses, and forces are known, we can write the equilibrium condition and the constitutive equation as follows:

$$\int_V B^T\{\sigma_{n+1}\}\,\mathrm{d}V-\{F_{n+1}\}=0 \quad , \tag{59}$$

and

$$\begin{aligned}\{\sigma_{n+1}\}-\{\sigma_n\}&=D\{\Delta\varepsilon_{n+1}\}-D\{\Delta\varepsilon^{\mathrm{ne}}_{n+1}\}\\&=DB(\{u_{n+1}\}-\{u_n\})-D\{\Delta\varepsilon^{\mathrm{ne}}_{n+1}\} \quad ,\end{aligned} \tag{60}$$

where B : strain-displacement matrix,
$\{\sigma_{n+1}\}$: stress vector at the time t_{n+1},
$\{F_{n+1}\}$: external force vector at the time t_{n+1},
D : stress-strain matrix,
$\{\Delta\varepsilon_{n+1}\}$: incremental total strain vector during the time interval Δt_{n+1},
$\{\Delta\varepsilon^{\mathrm{ne}}_{n+1}\}$: incremental non-elastic strain vector during the time interval Δt_{n+1},

$\{u_{n+1}\}$: nodal displacement vector at the time t_{n+1}.

From the system of Eqs. (59) and (60), $\{\sigma_{n+1}\}$ and $\{u_{n+1}\}$ are solved. To solve Eqs. (59) and (60), the approximate values for $\{\Delta\varepsilon^{ne}_{n+1}\}$ need to be determined. The explicit or implicit approach is used to compute $\{\Delta\varepsilon^{ne}_{n+1}\}$.

If an explicit approach is applied, the approximation to $\{\Delta\varepsilon^{ne}_{n+1}\}$ is simply computed by the stresses at the start of the time interval, i.e.,

$$\{\Delta\varepsilon^{ne}_{n+1}\}=\Delta t_{n+1}\,\beta\,(\{\sigma_n\}) \tag{61}$$

The advantages of this approach are that it is concise, simply coded and that the nonlinearities, which necessitate use of iterating, do not enter through β to the system of Eqs. (59) and (60). The disadvantage is that the numerical stability condition on the size of time step is rather severe than implicit approach.

If an implicit approach is applied, $\{\Delta\varepsilon^{ne}_{n+1}\}$ is computed by intermediate stresses between t_n and t_{n+1} as follows:

$$\{\Delta\varepsilon^{ne}_{n+1}\}=\Delta t_{n+1}\,\beta\,(\{\sigma_{n+\theta}\})\ , \tag{62}$$

where

$$\{\sigma_{n+\theta}\}=(1-\theta)\{\sigma_n\}+\theta\{\sigma_{n+1}\}\quad(0\leq\theta\leq1). \tag{63}$$

If $\theta = 0$ is taken, Eq. (62) is reduced to an explicit form of Eq. (61). In the implicit approach, nonlinearities, which need the use of iterating, enter through β to the system of Eqs. (59) and (60). To solve the non-linear equations, the Newton-Raphson iterative procedure is used. In the Newton-Raphson method, if an approximation of $\{\Delta\varepsilon^{ne}_{n+1}{}^{i}\}$ is obtained at i-th iteration to Eq. (60), we can write an improved approximation using a curtailed Taylor expression as

$$\begin{aligned}\{\Delta\varepsilon^{ne}_{n+1}{}^{i+1}\}&=\Delta t_{n+1}\,\beta\,(\{\sigma^{i+1}_{n+\theta}\})\\&=\Delta t_{n+1}\,\beta\,(\{\sigma^{i}_{n+\theta}\})+\Delta t_{n+1}\,\theta\,\beta'^{i}_{n+\theta}\{d\sigma^{i+1}_{n+1}\}\ ,\end{aligned} \tag{64}$$

and

$$\beta'=\left\{\frac{\partial\beta}{\partial\{\sigma\}}\right\}\ , \tag{65}$$

where i : iteration number within a time interval,

$\{d\sigma^{i+1}_{n+1}\}$: increments of stresses during the iteration i and $i+1$,

β' : Jacobian matrix formed by differentiating β with respect to the components of $\{\sigma\}$.

Updating $\beta'^{i}_{n+\theta}$ at each iteration, the convergence of solution to Eqs. (59) and (60) is accelerated. This implicit approach, which needs the iterative procedure, is more complex than the explicit approach. However, for appropriate values of the parameter θ, the implicit scheme is unconditionally stable[18]. Thus the time intervals can be employed which are much larger than those necessary for the stability of the explicit scheme. Furthermore in the implicit scheme, the solution is improved by the iterative procedure, hence larger time intervals can be employed to obtain the same accurate results of the explicit scheme. Therefore the implicit scheme was applied to obtain the approximate solutions to Eqs. (59) and (60).

The implicit algorithm to the solution via the Newton-Raphson method is described below.

Taking the first guess of $\{\sigma^0_{n+1}\}$ and $\{u^0_{n+1}\}$ as

$$\{\sigma^0_{n+1}\}=\{\sigma_n\}\quad\text{and}\quad\{u^0_{n+1}\}=\{u_n\}\ ,$$

we can write for Eq. (60) a set of successive iterations

$$\{\sigma_{n+1}^{i+1}\}-\{\sigma_n\}-DB(\{u_{n+1}^{i+1}\}-\{u_n\})+D\{\Delta\varepsilon_{n+1}^{\mathrm{ne},i+1}\}$$
$$=\{\sigma_{n+1}^{i}\}-\{\sigma_n\}-DB(\{u_{n+1}^{i}\}-\{u_n\})+D\{\Delta\varepsilon_{n+1}^{\mathrm{ne},i}\}+\{\mathrm{d}\,\sigma_{n+1}^{i+1}\}$$
$$-DB\{\mathrm{d}\,u_{n+1}^{i+1}\}+D\,\Delta t_{n+1}\,\theta\,\beta_{n+\theta}'^{i}\{\mathrm{d}\sigma_{n+1}^{i+1}\}$$
$$=0\quad, \tag{66}$$

where

$$\{\sigma_{n+1}^{i+1}\}=\{\sigma_{n+1}^{i}\}+\{\mathrm{d}\,\sigma_{n+1}^{i+1}\}\quad,$$
$$\{u_{n+1}^{i+1}\}=\{u_{n+1}^{i}\}+\{\mathrm{d}\,u_{n+1}^{i+1}\}\quad.$$

Similarly for Eq. (59), we ahve

$$\int_V B^{\mathrm{T}}\{\sigma_{n+1}^{i+1}\}\,\mathrm{d}\,V-\{F_{n+1}\}$$
$$=\int_V B^{\mathrm{T}}\{\sigma_{n+1}^{i}\}\mathrm{d}\,V-\{F_{n+1}\}+\int_V B^{\mathrm{T}}\{\mathrm{d}\,\sigma_{n+1}^{i+1}\}\mathrm{d}\,V=0. \tag{67}$$

It is convenient to rewrite Eq. (66) as

$$\{\mathrm{d}\,\sigma_{n+1}^{i+1}\}=-(\bar{D}^i D^{-1})\phi_{n+1}^{i}+\bar{D}^i B\{\mathrm{d}\,u_{n+1}^{i+1}\}\quad, \tag{68}$$

where

$$\bar{D}^i=[D^{-1}+\Delta t_{n+1}\,\theta\,\beta_{n+\theta}'^{i}]^{-1}\quad, \tag{69}$$

$$\phi_{n+1}^{i}=\{\sigma_{n+1}^{i}\}-\{\sigma_n\}-DB(\{u_{n+1}^{i}\}-\{u_n\})+D\{\Delta\varepsilon_{n+1}^{\mathrm{ne},i}\} \tag{70}$$

Substituting Eq. (68) into Eq. (67), we have an explicit algorithm for $\{\mathrm{d}u_{n+1}^{i+1}\}$ as follows:

$$\left(\int_V B^{\mathrm{T}}\bar{D}^i B\,\mathrm{d}\,V\right)\{\mathrm{d}\,u_{n+1}^{i+1}\}=\int_V(B^{\mathrm{T}}\bar{D}^i D^{-1}\phi_{n+1}^{i})\mathrm{d}\,V-\int_V B^{\mathrm{T}}\{\sigma_{n+1}^{i}\}\mathrm{d}\,V+\{F_{n+1}\}\,, \tag{71}$$

from which $\{\mathrm{d}u_{n+1}^{i+1}\}$ and hence $\{\mathrm{d}\sigma_{n+1}^{i+1}\}$ are obtained.

Updating the $\{\sigma_{n+1}^{i+1}\}$ and $\{u_{n+1}^{i+1}\}$ as

$$\{\sigma_{n+1}^{i+1}\}=\{\sigma_{n+1}^{i}\}+\{\mathrm{d}\,\sigma_{n+1}^{i+1}\}\quad\text{and}\quad\{u_{n+1}^{i+1}\}=\{u_{n+1}^{i}\}+\{\mathrm{d}\,u_{n+1}^{i+1}\}\quad,$$

the next iteration is repeated. This iteration is terminated when the error, i.e.,

$$\{e\}=\{u_{n+1}^{i+1}\}-\{u_{n+1}^{i}\}\,, \tag{72}$$

becomes sufficiently small.

4.2.2 Basic Equations

The stress-strain relations including non-linear material problems, such as creep and plasticity, are formulated by the standard finite element method[18]. Creep and plastic strains are expressed by non-linear forms in terms of stresses, hence nonlinearities, which necessitate use of iterating, enter through creep and plastic strain expressions. The implicit algorithm is employed obtaining the approximate solution to the non-linear problems via the Newton-Raphson iterative procedure.

As usual the equilibrium condition is written in the following form

$$\int_V B^{\mathrm{T}}\{\sigma\}\mathrm{d}\,V-\{F\}=0\quad, \tag{73}$$

where B : strain-displacement matrix,
$\{\sigma\}$: stress vector,
$\{F\}$: external force vector.

If we consider an interval of time Δt_{n+1} at the beginning of which the state characterized by nodal displacements, stresses, and forces is known, we can write a set of non-linear algebraic equations linking the final conditions with time. Thus we have

$$\psi_{n+1} = \int_V B^T\{\sigma_{n+1}\}\,dV - \{F_{n+1}\} = 0 \quad , \tag{74}$$

as the equilibrium condition.

The problems considered here includes the non-linear material behaviors, such as creep, plasticity, and fuel cracking and crack healing. Taking into account these non-linear problems, the constitutive relations are formulated by the incremental approach.

The incremental elastic strain during the time interval $\Delta t_{n+1}\ (=t_{n+1}-t_n)$ is related to the incremental stress by

$$\{\Delta\varepsilon^e_{n+1}\} = C_{n+\theta}\{\Delta\sigma_{n+1}\} \quad , \tag{75}$$

with

$$C_{n+\theta} = (1-\theta)C_n + \theta C_{n+1} \quad (0 \leq \theta \leq 1) \quad ,$$

where $\{\Delta\varepsilon^e_{n+1}\}$: incremental elastic strain vector during the time interval Δt_{n+1},
$C_{n+\theta}$: strain-stress matrix expressed as an intermediate between C_n and C_{n+1},
$\{\Delta\sigma_{n+1}\}$: incremental stress vector during the time interval Δt_{n+1},
n : time step number.

The intermediate matrix $C_{n+\theta}$ is used in Eq. (75) to take into account the change of elastic material properties due to fuel cracking and crack healing and temperature differences.

The incremental elastic strain is given by

$$\{\Delta\varepsilon^e_{n+1}\} = \{\Delta\varepsilon_{n+1}\} - \{\Delta\varepsilon^c_{n+1}\} - \{\Delta\varepsilon^p_{n+1}\} - \{\Delta\varepsilon^0_{n+1}\} \quad , \tag{76}$$

where $\{\Delta\varepsilon_{n+1}\}$: incremental total strain vector during the time interval Δt_{n+1},
$\{\Delta\varepsilon^c_{n+1}\}$: incremental creep strain vector during the time interval Δt_{n+1},
$\{\Delta\varepsilon^p_{n+1}\}$: incremental plastic strain vector during the time interval Δt_{n+1},
$\{\Delta\varepsilon^0_{n+1}\}$: incremental free expansion strain vector during the time interval Δt_{n+1}.

The free expansion strains $\{\Delta\varepsilon^0_{n+1}\}$ are due to thermal expansion, relocation, densification, and irradiation induced swelling.

The total strains are related to the nodal displacement by

$$\{\Delta\varepsilon_{n+1}\} = B\{\Delta u_{n+1}\} \quad , \tag{77}$$

where $\{\Delta u_{n+1}\}$: incremental nodal displacement vector during the time interval Δt_{n+1}.

Substituting Eq. (76) into Eq. (75) and using the relation of Eq. (77), we have

$$C_{n+\theta}(\{\sigma_{n+1}\} - \{\sigma_n\}) = B\{\Delta u_{n+1}\} - \{\Delta\varepsilon^c_{n+1}\} - \{\Delta\varepsilon^p_{n+1}\} - \{\Delta\varepsilon^0_{n+1}\} \tag{78}$$

Usually the rate of creep strain is defined as some function of stress and total creep strain, i.e. the creep strain is not determined explicitly. Thus from Eq. (78), we have another non-linear equation

$$\bar{\psi}_{n+1} = C_{n+\theta}(\{\sigma_{n+1}\} - \{\sigma_n\}) - B(\{u_{n+1}\} - \{u_n\}) + \{\Delta\varepsilon^c_{n+1}\} + \{\Delta\varepsilon^p_{n+1}\} + \{\Delta\varepsilon^0_{n+1}\} = 0 \ , \tag{79}$$

where $\bar{\psi}$: non-linear descrete equation operator.

The system of Eqs. (74) and (79) is a set of non-linear algebraic equations from which $\{\sigma_{n+1}\}$ and $\{u_{n+1}\}$ are solved. The implicit form is applied to the expressions of $\{\Delta\varepsilon^c_{n+1}\}$ and $\{\Delta\varepsilon^p_{n+1}\}$, hence the iterative procedure is necessary to obtain the solution to Eqs. (74) and (79).

Taking the first guess of $\{\sigma^0_{n+1}\}$ and $\{u^0_{n+1}\}$ as

$$\{\sigma^0_{n+1}\} = \{\sigma_n\} \quad \text{and} \quad \{u^0_{n+1}\} = \{u_n\} \ ,$$

we can write for Eq. (79) a set of successive iterations

$$\bar{\psi}_{n+1}^{i+1}=0=C_{n+\theta}^{i}(\{\sigma_{n+1}^{i}\}+\{\mathrm{d}\,\sigma_{n+1}^{i+1}\}-\{\sigma_n\})-B(\{u_{n+1}^{i}\}+\{\mathrm{d}\,u_{n+1}^{i+1}\}-\{u_n\})$$
$$+\{\Delta\varepsilon_{n+1}^{c,i+1}\}+\{\Delta\varepsilon_{n+1}^{p,i+1}\}+\{\Delta\varepsilon_{n+1}^{0}\}\ , \tag{80}$$

where i : iteration number.

Similarly for Eq. (74), we can write an improved solution as

$$\psi_{n+1}^{i+1}=0=\psi_{n+1}^{i}+\int_V B^{\mathrm{T}}\{\mathrm{d}\,\sigma_{n+1}^{i+1}\}\,\mathrm{d}\,V$$
$$=\int_V B^{\mathrm{T}}\{\sigma_{n+1}^{i}\}\,\mathrm{d}\,V-\{F_{n+1}\}+\int_V B^{\mathrm{T}}\{\mathrm{d}\,\sigma_{n+1}^{i+1}\}\,\mathrm{d}\,V\ . \tag{81}$$

Substituting Eq. (80) into Eq. (81) to eleminate $\{\mathrm{d}\sigma_{n+1}^{i+1}\}$ from Eq. (81), successive corrections for $\{\mathrm{d}u_{n+1}^{i+1}\}$ and hence for $\{\mathrm{d}\sigma_{n+1}^{i+1}\}$ can be determined giving

$$\left.\begin{aligned}\{\sigma_{n+1}^{i+1}\}&=\{\sigma_{n+1}^{i}\}+\{\mathrm{d}\,\sigma_{n+1}^{i+1}\}\ ,\\ \{u_{n+1}^{i+1}\}&=\{u_{n+1}^{i}\}+\{\mathrm{d}\,u_{n+1}^{i+1}\}\ .\end{aligned}\right\} \tag{82}$$

4.2.3 Creep

The uniaxial creep strain rate is usually defined as some function of stress, total creep strain, temperature, and fast neutron flux, i.e.,

$$\dot{\bar{\varepsilon}}^{\mathrm{c}}=\frac{\Delta\bar{\varepsilon}^{\mathrm{c}}}{\Delta t}=f(\bar{\sigma},\bar{\varepsilon}^{\mathrm{c}},T,\phi)\ , \tag{83}$$

where $\dot{\bar{\varepsilon}}^{\mathrm{c}}$: uniaxial creep strain rate,
f : creep function,
$\bar{\sigma}$: equivalent stress,
$\bar{\varepsilon}^{\mathrm{c}}$: total creep strain (equivalent creep strain),
T : temperature,
ϕ : fast neutron flux.

Using a creep flow rule as in plasticity theory, Eq. (83) can be extended into multiaxial state as follows

$$\{\dot{\varepsilon}^{\mathrm{c}}\}=\frac{3}{2}\frac{f}{\bar{\sigma}}\{\sigma'\}\ , \tag{84}$$

where $\{\dot{\varepsilon}^{\mathrm{c}}\}$: creep strain rate vector,
$\{\sigma'\}$: deviatoric stress vector.

Considering the anisotropic case and including the effect of hot pressing in the manner proposed by Rashid et al.[30], the equivalent stress $\bar{\sigma}$ is defined as

$$\bar{\sigma}=\left[\frac{3}{2(\mathrm{F+G+H})}\{H(\sigma_r-\sigma_\theta)^2+F(\sigma_\theta-\sigma_z)^2+G(\sigma_z-\sigma_r)^2+2N\tau_{rz}^2\}\right.$$
$$\left.+3\alpha(\sigma_r+\sigma_z+\sigma_\theta)^2\right]^{1/2}\ , \tag{85}$$

where F, G, H and N : anisotropic coefficients,
α : hot pressing parameter,
σ_r : radial stress,
σ_z : axial stress,
σ_θ : circumferential stress,
τ_{rz} : shear stress.

The deviatoric stresses are defined as

$$\{\sigma'\}=\frac{2}{3}\,\bar{\sigma}\left\{\frac{\partial\bar{\sigma}}{\partial\sigma}\right\}\ . \tag{86}$$

The incremental creep strain during the time interval $\Delta t_{n+1}(=t_{n+1}-t_n)$ is given approximately

$$\{\Delta\varepsilon^{c}_{n+1}\}=\Delta t_{n+1}\{\dot{\varepsilon}^{c}_{n+\theta}\} \quad , \tag{87}$$

where

$$\{\dot{\varepsilon}^{c}_{n+\theta}\}=\frac{3}{2}\frac{f(\bar{\sigma}_{n+\theta},\bar{\varepsilon}^{c}_{n+\theta},T_{n+\theta},\phi_{n+\theta})}{\bar{\sigma}_{n+\theta}}\{\sigma'_{n+\theta}\} \quad , \tag{88}$$

and

$$\bar{\sigma}_{n+\theta}=(1-\theta)\bar{\sigma}_n+\theta\bar{\sigma}_{n+1} \quad (0\leq\theta\leq1) \quad ,$$

$$\bar{\varepsilon}_{n+\theta}=(1-\theta)\bar{\varepsilon}^{c}_n+\theta\bar{\varepsilon}^{c}_{n+1} \quad ,$$

$$T_{n+\theta}=(1-\theta)T_n+\theta T_{n+1} \quad ,$$

$$\phi_{n+\theta}=(1-\theta)\phi_n+\theta\phi_{n+1} \quad .$$

The incremental creep strain is described by implicit form as seen in Eq. (87), hence the Newton-Raphson iterative procedure is made to obtain the approximate values of $\{\dot{\varepsilon}^{c}_{n+\theta}\}$. If the approximate values of $\{\dot{\varepsilon}^{c,i}_{n+\theta}\}$ and $\{\sigma^{i}_{n+1}\}$ are obtained to Eq. (88) at i-th iteration, we can write improved values using a curtailed Taylor expression about $\{\sigma\}$ and $\bar{\varepsilon}^{c}$ as follows

$$\{\dot{\varepsilon}^{c,i+1}_{n+\theta}\}=\{\dot{\varepsilon}^{c,i}_{n+\theta}\}+\frac{9}{4(\bar{\sigma}^{i}_{n+\theta})^2}\left(\left(\frac{\partial f}{\partial\sigma}\right)^{i}_{n+\theta}-\frac{f^{i}_{n+\theta}}{\bar{\sigma}^{i}_{n+\theta}}\right)[\sigma'_i\,\sigma'_j]^{i}_{n+\theta}\,\theta\{d\sigma^{i+1}_{n+1}\}$$
$$+\frac{3f^{i}_{n+\theta}}{2\bar{\sigma}_{n+\theta}}\left[\frac{\partial\sigma'}{\partial\sigma}\right]^{i}_{n+\theta}\theta\{d\sigma^{i+1}_{n+1}\}+\frac{3}{2\bar{\sigma}^{i}_{n+\theta}}\{\sigma'^{i}_{n+\theta}\}\left(\frac{\partial f}{\partial\bar{\varepsilon}^{c}}\right)^{i}_{n+\theta}\theta\,d\bar{\varepsilon}^{c,i+1}_{n+1}, \tag{89}$$

where $\{d\sigma^{i+1}_{n+1}\}=\{\sigma^{i+1}_{n+1}\}-\{\sigma^{i}_{n+1}\}$,

$d\bar{\varepsilon}^{c,i+1}_{n+1}=\bar{\varepsilon}^{c,i+1}_{n+1}-\bar{\varepsilon}^{c,i}_{n+1}$.

From Eq. (83) the incremental equivalent creep strain during the time interval Δt_{n+1} is given by

$$\Delta\bar{\varepsilon}^{c}_{n+1}=\Delta t_{n+1}f(\bar{\sigma}_{n+\theta},\bar{\varepsilon}^{c}_{n+\theta},T_{n+\theta},\phi_{n+\theta}) \quad . \tag{90}$$

Expanding Eq. (90) in a curtailed Taylor series about $\{\sigma\}$ and $\bar{\varepsilon}^{c}$, we can write for Eq. (90) a set of successive corrections

$$\Delta\bar{\varepsilon}^{c,i+1}_{n+1}=\Delta\bar{\varepsilon}^{c,i}_{n+1}+\theta\,\Delta t_{n+1}\left(\frac{\partial f}{\partial\bar{\sigma}}\right)^{i}_{n+\theta}\left\lfloor\frac{\partial\bar{\sigma}}{\partial\sigma}\right\rfloor^{i}_{n+\theta}\{d\sigma^{i+1}_{n+1}\}+\theta\,\Delta t_{n+1}\left(\frac{\partial f}{\partial\bar{\varepsilon}^{c}}\right)^{i}_{n+\theta}d\bar{\varepsilon}^{c,i+1}_{n+1} \quad , \tag{91}$$

where $\lfloor\ \rfloor$ denotes row vector.

From Eq. (91) and using the relation $d\bar{\varepsilon}^{c,i+1}_{n+1}=\Delta\bar{\varepsilon}^{c,i+1}_{n+1}-\Delta\bar{\varepsilon}^{c,i}_{n+1}$, we have

$$d\bar{\varepsilon}^{c,i+1}_{n+1}=\frac{\theta\,\Delta t_{n+1}\left(\frac{\partial f}{\partial\bar{\sigma}}\right)^{i}_{n+\theta}\left\lfloor\frac{\partial\bar{\sigma}}{\partial\sigma}\right\rfloor^{i}_{n+\theta}\{d\sigma^{i+1}_{n+1}\}}{1-\theta\,\Delta t_{n+1}\left(\frac{\partial f}{\partial\bar{\varepsilon}^{c}}\right)^{i}_{n+\theta}} \quad . \tag{92}$$

Eliminating $d\bar{\varepsilon}^{c,i+1}_{n+1}$ from Eq. (89) by using Eq. (92), we have

$$\{\dot{\varepsilon}^{c,i+1}_{n+\theta}\}=\{\dot{\varepsilon}^{c,i}_{n+\theta}\}+F_1\theta[\sigma'_i\,\sigma'_j]^{i}_{n+\theta}\{d\sigma^{i+1}_{n+1}\}+F_2\theta\left[\frac{\partial\sigma'}{\partial\sigma}\right]^{i}_{n+\theta}\{d\sigma^{i+1}_{n+1}\} \quad , \tag{93}$$

where

$$F_1=\frac{9}{4(\bar{\sigma}^{i}_{n+\theta})^2}\left(\left(\frac{\partial f}{\partial\bar{\sigma}}\right)^{i}_{n+\theta}-\frac{f^{i}_{n+\theta}}{\bar{\sigma}^{i}_{n+\theta}}+\frac{\left(\frac{\partial f}{\partial\bar{\varepsilon}^{c}}\right)^{i}_{n+\theta}\theta\,\Delta t_{n+1}\left(\frac{\partial f}{\partial\bar{\sigma}}\right)^{i}_{n+\theta}}{1-\theta\,\Delta t_{n+1}\left(\frac{\partial f}{\partial\bar{\varepsilon}^{c}}\right)^{i}_{n+\theta}}\right) \quad , \tag{94}$$

$$F_2 = \frac{3f^{i}_{n+\theta}}{2\bar{\sigma}^{i}_{n+\theta}} \quad . \tag{95}$$

From Eqs. (87) and (93) we have a set of successive corrections for incremental creep strain as

$$\{\Delta\varepsilon^{c,i+1}_{n+1}\} = \{\Delta\varepsilon^{c,i}_{n+1}\} + C^{c,i}_{n+\theta}\{d\sigma^{i+1}_{n+1}\} \quad , \tag{96}$$

where

$$C^{c,i}_{n+\theta} = \theta\,\Delta t_{n+1}\left(F_1[\sigma'_i\,\sigma'_j]^{i}_{n+\theta} + F_2\left[\frac{\partial\sigma'}{\partial\sigma}\right]^{i}_{n+\theta}\right) \quad . \tag{97}$$

Substituting this into Eq. (80) gives

$$\{d\sigma^{i+1}_{n+1}\} = \hat{D}^{i}_{n+\theta}(B\{\Delta u^{i+1}_{n+1}\} - C^{i}_{n+\theta}(\{\sigma^{i}_{n+1}\} - \{\sigma_n\}) - \{\Delta\varepsilon^{c,i}_{n+1}\} - \{\Delta\varepsilon^{p,i+1}_{n+1}\} - \{\Delta\varepsilon^{0}_{n+1}\}) \quad , \tag{98}$$

with

$$\hat{D}^{i}_{n+\theta} = (C^{i}_{n+\theta} + C^{c,i}_{n+\theta})^{-1} \quad , \tag{99}$$

where $\hat{D}^{i}_{n+\theta}$: elastic and creep matrix computed by intermediate values between t_n and t_{n+1} .

4.2.4 Plasticity

The general yield criterion is expressed as

$$h(\{\sigma\}) = Q(\bar{\varepsilon}^{p}, T) \quad , \tag{100}$$

where h : yield function,
Q : plastic potential function,
$\bar{\varepsilon}^{p}$: equivalent plastic strain.

Appling the classical theory of anisotropy[29] to the two-dimensional axisymmetric case and including the effect of hot pressing[30], the yield function is defined as

$$h = \left[\frac{3}{2(F+G+H)}\{H(\sigma_r-\sigma_\theta)^2 + F(\sigma_\theta-\sigma_z)^2 + G(\sigma_z-\sigma_r)^2 + 2N\tau_{rz}^2\} + 3\alpha(\sigma_r+\sigma_z+\sigma_\theta)^2\right]^{1/2} \quad , \tag{101}$$

where F, G, H, and N : anisotropic coefficients.

Using an associated Mises flow rule, the incremental plastic strains during the time interval Δt_{n+1} are derivable from the yield function of Eq. (101), in the form of the flow rule

$$\{\Delta\varepsilon^{p}_{n+1}\} = \Delta\lambda_{n+1}\left\{\frac{\partial h}{\partial\sigma}\right\}_{n+\theta} \quad , \tag{102}$$

where $\{\Delta\varepsilon^{p}_{n+1}\}$: incremental plastic strain vector during the time interval Δt_{n+1},
$\Delta\lambda_{n+1}$: proportionality constant during the time interval Δt_{n+1},
$n+\theta$: intermediate point between t_n and t_{n+1},

and $\Delta\lambda_{n+1}$ is defined as

$$\Delta\lambda_{n+1} = \Delta\bar{\varepsilon}^{p}_{n+1} \quad , \tag{103}$$

where $\Delta\bar{\varepsilon}^{p}$: equivalent plastic strain.

The incremental plastic strain, given by Eq. (102), is expressed using implicit form, hence the Newton-Raphson iterative procedure is made to obtain approximation of $\{\Delta\varepsilon^{p}_{n+1}\}$. If the approximate solution at i-th iteration is obtained, we can write improved values for Eqs. (100) and (102) as follows

$$h(\{\sigma_n\}+\{\Delta\sigma_{n+1}^{i+1}\})=Q(\bar{\varepsilon}_n^{\mathrm{p}}+\Delta\bar{\varepsilon}_{n+1}^{\mathrm{p},i+1},\ T_n+\Delta T_{n+1}) \quad , \tag{104}$$

$$\{\Delta\varepsilon_{n+1}^{\mathrm{p},i+1}\}=\Delta\bar{\varepsilon}_{n+1}^{\mathrm{p},i+1}\left\{\frac{\partial h}{\partial\sigma}\right\}_{n+\theta}^{i} \quad . \tag{105}$$

Expanding Eq. (104) in a curtailed Taylor series about $\{\sigma\}$, $\bar{\varepsilon}^{\mathrm{p}}$, and T gives

$$h(\{\sigma_n\})+\left\lfloor\frac{\partial h}{\partial\sigma}\right\rfloor_{n+\theta}^{i}\{\Delta\sigma_{n+1}^{i+1}\}$$
$$=Q(\bar{\varepsilon}_n^{\mathrm{p}},T_n)+\left(\frac{\partial Q}{\partial\bar{\varepsilon}^{\mathrm{p}}}\right)_{n+\theta}^{i}\Delta\bar{\varepsilon}_{n+1}^{\mathrm{p},i+1}+\left(\frac{\partial Q}{\partial T}\right)_{n+\theta}\Delta T_{n+1} \quad . \tag{106}$$

Using the relation

$$\{\Delta\sigma_{n+1}^{i+1}\}=\{\sigma_{n+1}^{i}\}+\{\mathrm{d}\sigma_{n+1}^{i+1}\}-\{\sigma_n\} \quad ,$$

we can rewrite Eq. (106) as

$$\Delta\bar{\varepsilon}_{n+1}^{\mathrm{p},i+1}=\frac{1}{H'^{i}_{n+\theta}}\left(\left\lfloor\frac{\partial h}{\partial\sigma}\right\rfloor_{n+\theta}^{i}(\{\sigma_{n+1}^{i}\}-\{\sigma_n\})+h(\{\sigma\})-Q(\bar{\varepsilon}_n^{\mathrm{p}},T_n)\right.$$
$$\left.-\left(\frac{\partial Q}{\partial T}\right)_{n+\theta}\Delta T_{n+1}+\left\lfloor\frac{\partial h}{\partial\sigma}\right\rfloor_{n+\theta}^{i}\{\mathrm{d}\sigma_{n+1}^{i+1}\}\right), \tag{107}$$

where

$$H'^{i}_{n+\theta}=\left(\frac{\partial Q}{\partial\bar{\varepsilon}^{\mathrm{p}}}\right)_{n+\theta}^{i} \quad . \tag{108}$$

Substituting Eq. (98) into Eq. (107) to eliminate $\{\mathrm{d}\sigma_{n+1}^{i+1}\}$, we have

$$\Delta\bar{\varepsilon}_{n+1}^{\mathrm{p},i+1}=\frac{\left\lfloor\frac{\partial h}{\partial\sigma}\right\rfloor_{n+\theta}^{i}\hat{D}_{n+\theta}^{i}(B\{\Delta u_{n+1}^{i+1}\}-C_{n+\theta}^{i}(\{\sigma_{n+1}^{i}\}-\{\sigma_n\})-\{\Delta\varepsilon_{n+1}^{\mathrm{c},i}\}-\{\Delta\varepsilon_{n+1}^{0}\})}{H'^{i}_{n+\theta}+\left\lfloor\frac{\partial h}{\partial\sigma}\right\rfloor_{n+\theta}^{i}\hat{D}_{n+\theta}^{i}\left\{\frac{\partial h}{\partial\sigma}\right\}_{n+\theta}^{i}}$$
$$+\frac{\left\lfloor\frac{\partial h}{\partial\sigma}\right\rfloor_{n+\theta}^{i}(\{\sigma_{n+1}^{i}\}-\{\sigma_n\})-\left(\frac{\partial Q}{\partial T}\right)_{n+\theta}\Delta T_{n+1}+h(\{\sigma_n\})-Q(\bar{\varepsilon}_n^{\mathrm{p}},T_n)}{H'^{i}_{n+\theta}+\left\lfloor\frac{\partial h}{\partial\sigma}\right\rfloor_{n+\theta}^{i}\hat{D}_{n+\theta}^{i}\left\{\frac{\partial h}{\partial\sigma}\right\}_{n+\theta}^{i}} \quad . \tag{109}$$

Substituting Eq. (105) with this into Eq. (98), we have

$$\{\mathrm{d}\sigma_{n+1}^{i+1}\}=\hat{D}_{n+\theta}^{\mathrm{p},i}(B\{\Delta u_{n+1}^{i+1}\}-C_{n+\theta}^{i}(\{\sigma_{n+1}^{i}\}-\{\sigma_n\})-\{\Delta\varepsilon_{n+1}^{\mathrm{c},i}\}-\{\Delta\varepsilon_{n+1}^{0}\})$$
$$+\{S_{n+\theta}^{i}\}\Delta T_{n+1}-\{Z_1^{i}\}-\{Z_2^{i}\} \quad , \tag{110}$$

with

$$\hat{D}_{n+\theta}^{\mathrm{p},i}=\hat{D}_{n+\theta}^{i}-\frac{\hat{D}_{n+\theta}^{i}\left\{\frac{\partial h}{\partial\sigma}\right\}_{n+\theta}^{i}\left\lfloor\frac{\partial h}{\partial\sigma}\right\rfloor_{n+\theta}^{i}\hat{D}_{n+\theta}^{i}}{H'^{i}_{n+\theta}+\left\lfloor\frac{\partial h}{\partial\sigma}\right\rfloor_{n+\theta}^{i}\hat{D}_{n+\theta}^{i}\left\{\frac{\partial h}{\partial\sigma}\right\}_{n+\theta}^{i}} \quad , \tag{111}$$

$$\{S_{n+\theta}^{i}\}=\frac{\hat{D}_{n+\theta}^{i}\left\{\frac{\partial h}{\partial\sigma}\right\}_{n+\theta}^{i}\left(\frac{\partial Q}{\partial T}\right)_{n+\theta}}{H'^{i}_{n+\theta}+\left\lfloor\frac{\partial h}{\partial\sigma}\right\rfloor_{n+\theta}^{i}\hat{D}_{n+\theta}^{i}\left\{\frac{\partial h}{\partial\sigma}\right\}_{n+\theta}^{i}} \quad , \tag{112}$$

$$\{Z_1^{i}\}=\frac{\hat{D}_{n+\theta}^{i}\left\{\frac{\partial h}{\partial\sigma}\right\}_{n+\theta}^{i}\left\lfloor\frac{\partial h}{\partial\sigma}\right\rfloor_{n+\theta}^{i}(\{\sigma_{n+1}^{i}\}-\{\sigma_n\})}{H'^{i}_{n+\theta}+\left\lfloor\frac{\partial h}{\partial\sigma}\right\rfloor_{n+\theta}^{i}\hat{D}_{n+\theta}^{i}\left\{\frac{\partial h}{\partial\sigma}\right\}_{n+\theta}^{i}} \quad , \tag{113}$$

$$\{Z_2^i\}=\frac{\hat{D}_{n+\theta}^i\left\{\frac{\partial h}{\partial \sigma}\right\}_{n+\theta}^i(h(\{\sigma_n\})-Q(\bar{\varepsilon}_n^p, T_n))}{H'^i_{n+\theta}+\left[\frac{\partial h}{\partial \sigma}\right]_{n+\theta}^i\hat{D}_{n+\theta}^i\left\{\frac{\partial h}{\partial \sigma}\right\}_{n+\theta}^i}, \tag{114}$$

where $\hat{D}_{n+\theta}^{pi}$: elasto-plastic and creep matrix computed by intermediate values between t_n and t_{n+1}.

Eq. (110) is the constitutive equation which is used in the derivations of finite element stiffness and force matrices. Eliminating $\{d\sigma_{n+1}^{i+1}\}$ (Eq. (110)) from Eq. (81), we have an explicit algorithm for $\{\Delta u_{n+1}^{i+1}\}$.

4.2.5 Fuel Cracking

Fuel cracks are usually observed to occur on the principal planes, which are perpendicular to radial, axial, and circumferential direction, and are therefore associated with the principal stresses.

The assumptions made here are the following:

- the formation of a crack in one of the three principal direction occurs when the elastic strain in that direction becomes a tensile value;
- cracking is independently evaluated at each integration point in each element;
- if cracking occurs in one of the three principal direction, the elastic modulus in that direction is reduced from the nominal value E to a specified small value E_c. E_c is the very small value (e.g. 2×10^3 MPa);
- if the elastic strain changes to a compressive value, the crack then closes gradually. The crack does not heal immediately;
- if the fuel goes into compressive, the elastic modulus gradually recovers to nominal value;
- crack healing finishes when the compressive strain compensates the relocation strain;
- recovery of elastic modulus depends on the compressive strain.

The model for cracking and crack healing is schematically shown in **Fig. 6** where the relation between elastic modulus and elastic strain during cracking and crack healing is described.

The elastic strain-strees matrix C under condition of cracking is written as

$$C=\begin{bmatrix} \frac{1}{E_r} & -\frac{\nu}{E} & -\frac{\nu}{E} & 0 \\ & \frac{1}{E_z} & -\frac{\nu}{E} & 0 \\ & & \frac{1}{E_\theta} & 0 \\ \text{Sym.} & & & \frac{4(1+\nu)}{E_r+E_z} \end{bmatrix}, \tag{115}$$

where E_r, E_z, and E_θ : elastic moduluses during cracking in radial, axial, and circumferential directions respectively,

E : elastic modulus in uncracked condition,

ν : poisson's ratio.

The change of elastic modulus in the principal direction from uncracked to cracked condition in Eq. (115) is related to elastic strain. The elastic modulus for fuel under cracking and crack healing is given in **Table 2**.

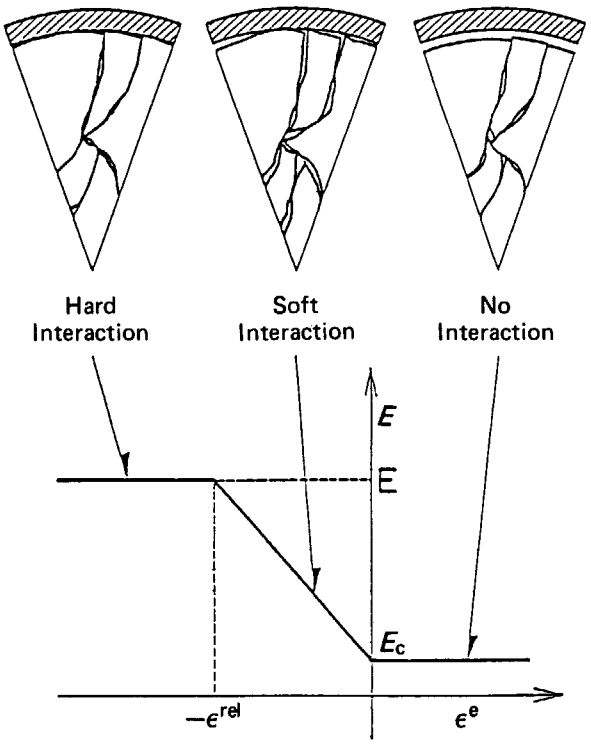

Fig. 6 Stiffness Model for Cracked Pellet.

Table 2 Elastic Modulus for Fuel under Cracking and Crack Healing

	Uncracked condition	Half cracked condition	Cracked condition
ε_j^e	$\varepsilon_j^e < -\varepsilon_j^{rel}$	$-\varepsilon_j^{rel} < \varepsilon_j^e < 0$	$\varepsilon_j^e \geq 0$
E_j	E	$-\dfrac{\varepsilon_j^e}{\varepsilon_j^{rel}}(E-E_c)+E_c$	E_c

E_c is the very small value (e.g. 2×10^3 MPa), j indicates the three principal direction, and ε_j^{rel} is the initial relocation strain in the j direction.

4.2.6 Hot Pressing

The general phenomenon of mechanical densification of fuel pellets, usually referred to as hot pressing, is characterized by plastic and creep volume change exhibited by the fuel during reactor operations. To take into account the plastic and creep volume changes, a new yield criterion and creep law which include the inelastic compressibility of the porous material is defined by Rashid et al.[30].

A new yield criterion for fuel is expressed from Eq. (101) assuming isotoropy as follows

$$h=\bar{\sigma}-\left[\frac{1}{2}\{(\sigma_r-\sigma_z)^2+(\sigma_z-\sigma_\theta)^2+(\sigma_\theta-\sigma_r)^2+6\tau_{rz}^2\}+3\alpha(\sigma_r+\sigma_z+\sigma_\theta)\right]^{1/2}. \quad (116)$$

Plastic flow rule is defined from Eq. (102) as

$$\{\Delta\varepsilon_{n+1}^p\}=\Delta\lambda_{n+1}\left\{\frac{\partial h}{\partial\sigma}\right\}_{n+\theta}. \quad (117)$$

Substituting Eq. (116) into Eq. (117) with the relation $\Delta\lambda_{n+1}=\Delta\bar{\varepsilon}_{n+1}^p$, we have

$$\{\Delta\varepsilon^{p}_{n+1}\}=\frac{\Delta\bar{\varepsilon}^{p}_{n+1}}{\bar{\sigma}_{n+\theta}}\begin{bmatrix} 1+3\alpha & -0.5+3\alpha & -0.5+3\alpha & 0 \\ & 1+3\alpha & -0.5+3\alpha & 0 \\ \text{Sym.} & & 1+3\alpha & 0 \\ & & & \frac{2}{3} \end{bmatrix}\{\sigma_{n+\theta}\} . \tag{118}$$

From this the increment of volumetric strain due to plastic hot pressing is given by

$$\Delta\varepsilon^{p}_{h,n+1}=\Delta\varepsilon^{p,r}_{n+1}+\Delta\varepsilon^{p,r}_{n+1}+\Delta\varepsilon^{p,z}_{n+1}+\Delta\varepsilon^{p,\theta}_{n+1}$$

$$=\frac{9\alpha\,\Delta\bar{\varepsilon}^{p}_{n+1}}{\bar{\sigma}}(\sigma_{r,n+\theta}+\sigma_{z,n+\theta}+\sigma_{\theta,n+\theta}) , \tag{119}$$

where $\Delta\varepsilon^{p}_{h,n+1}$: incremental volumetric strain due to plastic hot pressing during the time interval Δt_{n+1},

$\Delta\varepsilon^{p}_{r,n+1}$, $\Delta\varepsilon^{p}_{z,n+1}$, and $\Delta\varepsilon^{p}_{\theta,n+1}$: incremental plastic strain during the time interval Δt_{n+1} in radial, axial, and circumferential directions respectively,

$\sigma_{r,n+\theta}$, $\sigma_{z,n+\theta}$, and $\sigma_{\theta,n+\theta}$: radial, axial, and circumferential stresses respectively.

Similarly for creep, the incremental volumetric strain due to creep hot pressing is calculated from Eqs. (84), (85) and (86) assuming isotropy as follows

$$\Delta\varepsilon^{c}_{h,n+1}=\frac{9\alpha\,\Delta\bar{\varepsilon}^{c}_{n+1}}{\bar{\sigma}}(\sigma_{r,n+\theta}+\sigma_{z,n+\theta}+\sigma_{\theta,n+\theta}) , \tag{120}$$

where $\Delta\varepsilon^{c}_{h,n+1}$: incremental volumentric strain due to creep hot pressing during the time interval Δt_{n+1}.

Summing $\Delta\varepsilon^{p}_{h,n+1}$ and $\Delta\varepsilon^{c}_{h,n+1}$, the hot pressing due to plastic and creep volume change is given by

$$\Delta\varepsilon_{h,n+1}=\frac{9\alpha}{\bar{\sigma}}(\Delta\bar{\varepsilon}^{p}_{n+1}+\Delta\bar{\varepsilon}^{c}_{n+1})(\sigma_{r,n+\theta}+\sigma_{z,n+\theta}+\sigma_{\theta,n+\theta}) , \tag{121}$$

where $\Delta\varepsilon_{h,n+1}$: incremental volumetric strain due to plastic and creep hot pressing during the time interval Δt_{n+1}.

4.2.7 Stiffness Equation

Substituting Eq. (110) into Eq. (81) and remembering that the volume intergal has to be taken over the whole ring, we have the following stiffness equation to determine the successive correction $\{\Delta u^{i+1}_{n+1}\}$

$$K^{i}_{n+\theta}\{\Delta u^{i+1}_{n+1}\}=\{\Delta\bar{F}^{i}_{n+1}\} , \tag{122}$$

with

$$K^{i}_{n+\theta}=2\pi\iint B^{T}\hat{D}^{p,i}_{n+\theta}B\,r\,dr\,dz , \tag{123}$$

$$\{\Delta\bar{F}^{i}_{n+1}\}=2\pi\iint B^{T}\hat{D}^{p,i}_{n+\theta}[C^{i}_{n+\theta}(\{\sigma^{i}_{n+1}\}-\{\sigma\})+\{\Delta\varepsilon^{c,i}_{n+1}\}+\{\Delta\varepsilon^{0}_{n+1}\}]r\,dr\,dz$$

$$-2\pi\iint B^{T}(\{S^{i}_{n+\theta}\}\Delta T_{n+1}-\{Z^{i}_{1}\}-\{Z^{i}_{2}\})r\,dr\,dz+(\{F_{n+1}\}$$

$$-2\pi\iint B^{T}\{\sigma^{i}_{n+1}\}r\,dr\,dz) , \tag{124}$$

where $K^{i}_{n+\theta}$ and $\{\Delta\bar{F}^{i}_{n+1}\}$ are the finite element stiffness matrix and the force vectors, and the third term of Eq. (124) is referred to as unbalanced residual force.

Solving Eq. (122) for $\{\Delta u_{n+1}^{i+1}\}$, the improved estimate $\{u_{n+1}^{i+1}\}$ is obtained as

$$\{u_{n+1}^{i+1}\}=\{u_n\}+\{\Delta u_{n+1}^{i+1}\} \quad . \tag{125}$$

The successive iterations are repeated until covergence is obtained.

4.2.8 Isoparametric Element Characteristics

(1) Displacement Functions

Figure 7 shows a rectangular shape element with 8 arbitrary nodes. A set of normalized co-ordinates (ξ, η) is set in the element so that the values are either +1 or −1 on the faces of the rectangle. Nodes 1 to 8 are numbered in the order shown in **Fig. 7**.

The displacements of a node have two components

$$\{\delta_i\}=\begin{Bmatrix} u_i \\ v_i \end{Bmatrix} , \tag{126}$$

where $\{\delta_i\}$: displacement vector of node i ,
u_i : radial displacement of node i,
v_i : axial displacement of node i,

and the sixteen components of element displacements are listed as a vector

$$\{\delta\}^e=\begin{Bmatrix} \{\delta_1\} \\ \{\delta_2\} \\ \cdot \\ \cdot \\ \cdot \\ \cdot \\ \cdot \\ \{\delta_8\} \end{Bmatrix}=\begin{Bmatrix} u_1 \\ v_1 \\ u_2 \\ v_2 \\ \cdot \\ \cdot \\ \cdot \\ u_8 \\ v_8 \end{Bmatrix} , \tag{127}$$

where $\{\delta\}^e$: element nodal displacement vector.

The displacements at any point within the element are approximated by these sixteen values as a column vector

$$\{\delta\}=\begin{Bmatrix} u \\ v \end{Bmatrix}=N\{\delta\}^e , \tag{128}$$

with

$$N=[N_1 I \quad N_2 I \quad N_3 I \cdots\cdots N_8 I] , \tag{129}$$

where $\{\delta\}$: displacements at arbitrary point within the element,
N : displacement (shape) function,
I : 2 X 2 identity matrix.

The functions $N_1, N_2, \cdots\cdots, N_8$ are defined by quadratic members as follows

$$N_1=\frac{1}{4}(1-\xi)(1-\eta)(-\xi-\eta-1) ,$$

$$N_2=\frac{1}{4}(1+\xi)(1-\eta)(\xi-\eta-1) ,$$

$$N_3=\frac{1}{4}(1+\xi)(1+\eta)(\xi+\eta-1) ,$$

$$N_4=\frac{1}{4}(1-\xi)(1+\eta)(-\xi+\eta-1) , \tag{130}$$

$$N_5=\frac{1}{2}(1-\xi^2)(1-\eta)\ ,$$

$$N_6=\frac{1}{2}(1+\xi)(1-\eta^2)\ ,$$

$$N_7=\frac{1}{2}(1-\xi^2)(1+\eta)\ ,$$

$$N_8=\frac{1}{2}(1-\xi)(1-\eta^2)\ .$$

Thus each N function has a value of 1 at its corresponding node and zero at all other nodes. In addition, the N functions vary quadraticaly with ξ, η.

In the isoparametric element the relationship between the actual (r, z) co-ordinates and the normalized (ξ, η) co-ordinates is obtained by the N functions as follows

$$\left.\begin{aligned} r&=\sum_{i=1}^{8} N_i(\xi,\eta)\cdot r_i\ , \\ z&=\sum_{i=1}^{8} N_i(\xi,\eta)\cdot z_i\ , \end{aligned}\right\} \tag{131}$$

where r_i, z_i : co-ordinates of node i.

(2) Strain-Displacement Relations

The strain at any point within the element can be defined by its four components in the analysis of axisymmetric problem as follows

$$\{\varepsilon\}=\begin{Bmatrix}\varepsilon_r\\ \varepsilon_z\\ \varepsilon_\theta\\ \gamma_{rz}\end{Bmatrix}=\begin{Bmatrix}\dfrac{\partial u}{\partial r}\\ \dfrac{\partial v}{\partial z}\\ \dfrac{u}{r}\\ \left(\dfrac{\partial v}{\partial r}\right)+\left(\dfrac{\partial u}{\partial z}\right)\end{Bmatrix}, \tag{132}$$

where ε_r, ε_z, ε_θ, and γ_{rz} : radial, axial, circumferential, and shear strain respectively. Using the displacement functions defined by Eqs. (128) and (129) we have

$$\begin{aligned}\{\varepsilon\}&=B\{\delta\}^e\\ &=[B_2, B_2, \cdots\cdots, B_8]\begin{Bmatrix}\{\delta_1\}\\ \{\delta_2\}\\ \cdot\\ \cdot\\ \cdot\\ \cdot\\ \cdot\\ \cdot\\ \{\delta_8\}\end{Bmatrix},\end{aligned} \tag{133}$$

where

$$B_i = \begin{bmatrix} \frac{\partial N_i}{\partial r} & 0 \\ 0 & \frac{\partial N_i}{\partial z} \\ \frac{N_i}{r} & 0 \\ \frac{\partial N_i}{\partial z} & \frac{\partial N_i}{\partial r} \end{bmatrix} . \tag{134}$$

As N_i is defined in terms of local co-ordinates, it is necessary to provide the transformation from the global derivatives to the local derivatives.

The relation between them is given by

$$\begin{Bmatrix} \frac{\partial N_i}{\partial \xi} \\ \frac{\partial N_i}{\partial \eta} \end{Bmatrix} = J \begin{Bmatrix} \frac{\partial N_i}{\partial r} \\ \frac{\partial N_i}{\partial z} \end{Bmatrix} , \tag{135}$$

where J is the Jacobian matrix defined as

$$J = \begin{bmatrix} \frac{\partial r}{\partial \xi} & \frac{\partial z}{\partial \xi} \\ \frac{\partial r}{\partial \eta} & \frac{\partial z}{\partial \eta} \end{bmatrix}$$

$$= \begin{bmatrix} \sum_{i=1}^{8} \frac{\partial N_i}{\partial \xi} r_i & \sum_{i=1}^{8} \frac{\partial N_i}{\partial \xi} z_i \\ \sum_{i=1}^{8} \frac{\partial N_i}{\partial \eta} r_i & \sum_{i=1}^{8} \frac{\partial N_i}{\partial \eta} z_i \end{bmatrix} . \tag{136}$$

The global derivatives are given inverting J and we have

$$\begin{Bmatrix} \frac{\partial N_i}{\partial r} \\ \frac{\partial N_i}{\partial z} \end{Bmatrix} = J^{-1} \begin{Bmatrix} \frac{\partial N_i}{\partial \xi} \\ \frac{\partial N_i}{\partial \eta} \end{Bmatrix} . \tag{137}$$

Using this relation, B matrix is determined.

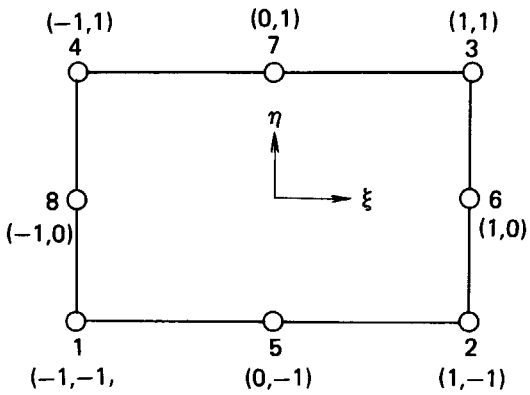

Fig. 7 Isoparametric Element with 8 Nodes.

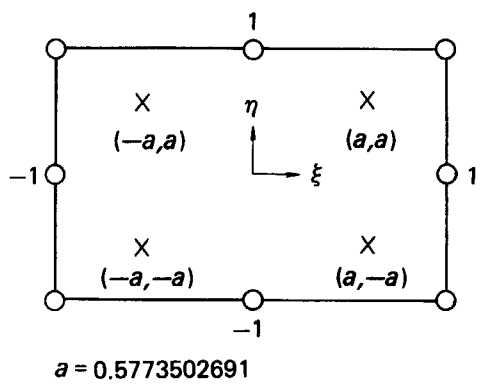

Fig. 8 Parabolic Isoparametric Element with 2 X 2 Integrating Points.

4.2.9 Numerical Integration

The element properties are defined in terms of local co-ordinates, hence the element of area over which the integration has to be carried out needs to be expressed in terms of the local co-ordinates with an appropriate change. Thus a area integral in the global co-ordinate system is related to the corresponding area integral in the local co-ordinate system by

$$\mathrm{d}r\ \mathrm{d}z = \det J\, \mathrm{d}\xi\ \mathrm{d}\eta\ . \tag{138}$$

Using the normalized co-ordinates, the stiffness matrix and force vectors defined by Eqs. (123) and (124) are expressed as

$$[K^i_{n+\theta}] = 2\pi \int_{-1}^{1}\int_{-1}^{1} B^{\mathrm{T}} \hat{D}^{\mathrm{p},i}_{n+\theta} B\left(\sum_{i=1}^{8} N_i r_i\right) \det J\, \mathrm{d}\xi\, \mathrm{d}\eta\ , \tag{139}$$

$$\begin{aligned}\{\Delta \bar{F}^i_{n+1}\} = {} & 2\pi \int_{-1}^{1}\int_{-1}^{1} B^{\mathrm{T}} \hat{D}^{\mathrm{p},i}_{n+1} (C^i_{n+\theta}(\{\sigma^i_{n+1}\} - \{\sigma_n\}) + \{\Delta\varepsilon^{\mathrm{c},i}_{n+1}\} + \{\Delta\varepsilon^{0}_{n+1}\}) \left(\sum_{i=1}^{8} N_i r_i\right) \det J\, \mathrm{d}\xi\, \mathrm{d}\eta \\ & - 2\pi \int_{-1}^{1}\int_{-1}^{1} B^{\mathrm{T}} (\{S^i_{n+\theta}\} \Delta T_{n+1} - \{Z^i_1\} - \{Z^i_2\}) \left(\sum_{i=1}^{8} N_i r_i\right) \det J\, \mathrm{d}\xi\, \mathrm{d}\eta \\ & + \{F_{n+1}\} - 2\pi \int_{-1}^{1}\int_{-1}^{1} B^{\mathrm{T}} \{\sigma^i_{n+1}\} \left(\sum_{i=1}^{8} N_i r_i\right) \det J\, \mathrm{d}\xi\, \mathrm{d}\eta\ .\end{aligned} \tag{140}$$

To obtain the integrals in the above equations, the Gaussian quadrature formula is used and it is written as

$$\int_{-1}^{1}\int_{-1}^{1} f(\xi, \eta)\, \mathrm{d}\xi\, \mathrm{d}\eta = \sum_{i=1}^{n} \sum_{j=1}^{m} H_i H_j f(\xi_j, \eta_i)\ , \tag{141}$$

where n : number of integrating points in the ξ direction,
m : number of integrating points in the η direction,
ξ_j and η_i : integrating positions,
H_i and H_j : quadrature weighting coefficients.

Taking integrating points $n = m = 2$ in a square region, the co-ordinates of integrating points shown in **Fig. 8** and weighting coefficients for Gaussian integration are defined as

$$\left.\begin{aligned} & (-a, -a),\ (a, -a),\ (-a, a),\ \text{and}\ (a, a), \\ & H_i = H_j = 1, \end{aligned}\right\} \tag{142}$$

where $a = 0.57735\ 02691$.

4.3 Boundary Conditions

4.3.1 Restraint Conditions

Figure 9 shows the geometrical model for finite element analysis. There is the eight boundary surfaces numbered from 1 to 8 as shown in **Fig. 9**.

Assuming an axisymmetry and a plane-symmetry at the mid-plane of a pellet, the mid-plane of fuel and cladding numbered 1 and 5 are not allowed to move axially and the inner surface of fuel of number 2 can not move radially over the z-axis.

The top-plane of cladding of number 8 is perpendicular to the axis and remains plane. The fuel top-plane can move freeley until fuel-cladding contact occurs. The boundary condition of fuel top-plane after contact is discussed later.

The restraint conditions for these boundary surfaces are summarized in **Table 3**.

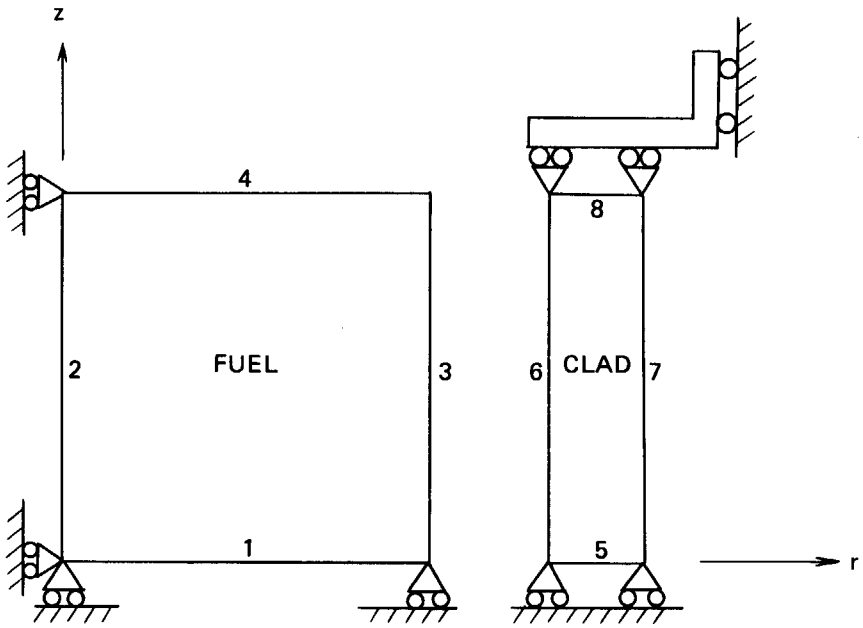

Fig. 9 Eight Boundaries of the Finite Element Geometrical Model.

Table 3 Restraint Conditions of the Nodes on the Boundary Surfaces

Boundary surface number		Degree of freedom of nodes on the boundary		Restraint conditions
		Radial	Axial	
1		0	1	$\{v\}^1=\{0\}$
2	Solid	1	0	$\{u\}^2=\{0\}$
	Annular	0	0	
3		0	0	
4		0	0	
5		0	1	$\{v\}^5=\{0\}$
6		0	0	
7		0	0	
8		0	1	$\{v\}^8=v_c\{I\}$

Caption 0 : free, 1 : restraint,
$\{v\}$: axial displacement vector,
$\{u\}$: radial displacement vector,
v_c : cladding axial displacement,
$\{I\}$: unit vector.

4.3.2 External Forces on Fuel and Cladding

Figure 10 shows the external force system on the fuel and cladding. For the fuel, the inner gas pressure P_{gas} acts on the inner surface of radius r_{fi}, on the outer surface of radius r_{fo} , and on the top surface of fuel. However these external forces due to inner gas pressure are not taken into account in the calculation, because the inner gas pressure also acts on the cracking faces in the fuel and these forces are canceled each other.

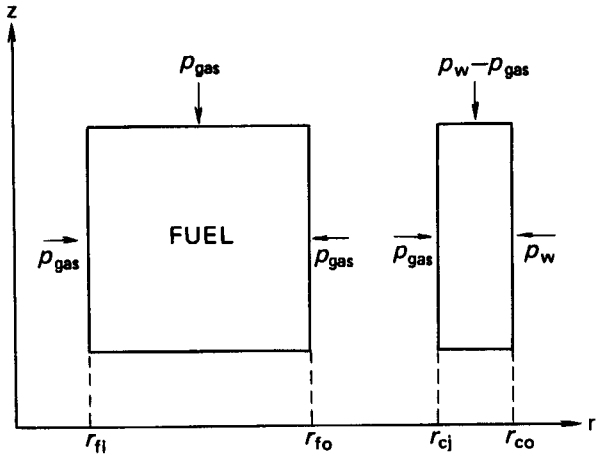

Fig. 10 External Force System on the Fuel and Cladding.

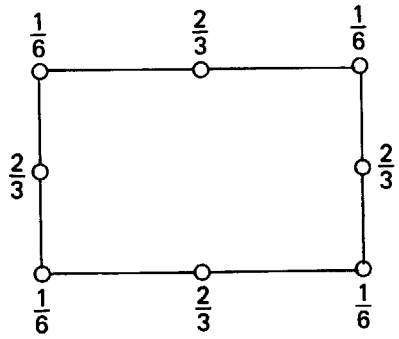

Fig. 11 Allocation of Uniform Pressure Loads to the Nodal Forces in the Quadratic Element.

For the cladding, the inner gas pressure P_{gas} acts on the inner surface of radius r_{ci}. The coolant pressure P_w acts on the outer surface of radius r_{co}. The pressure $(P_w - P_{gas})$ acts on the top surface of cladding.

These uniform pressure loads acting on the top of two-dimensional elements is allocated to nodal forces by the fraction shown in **Fig. 11**[18]. For the quadratic element, the intuitive allocation of uniform loads is no longer correct[18].

4.3.3 Contact Forces on Fuel and Cladding

If the fuel contacts with the cladding, the contact forces shown in **Fig. 12** act on the fuel and cladding.

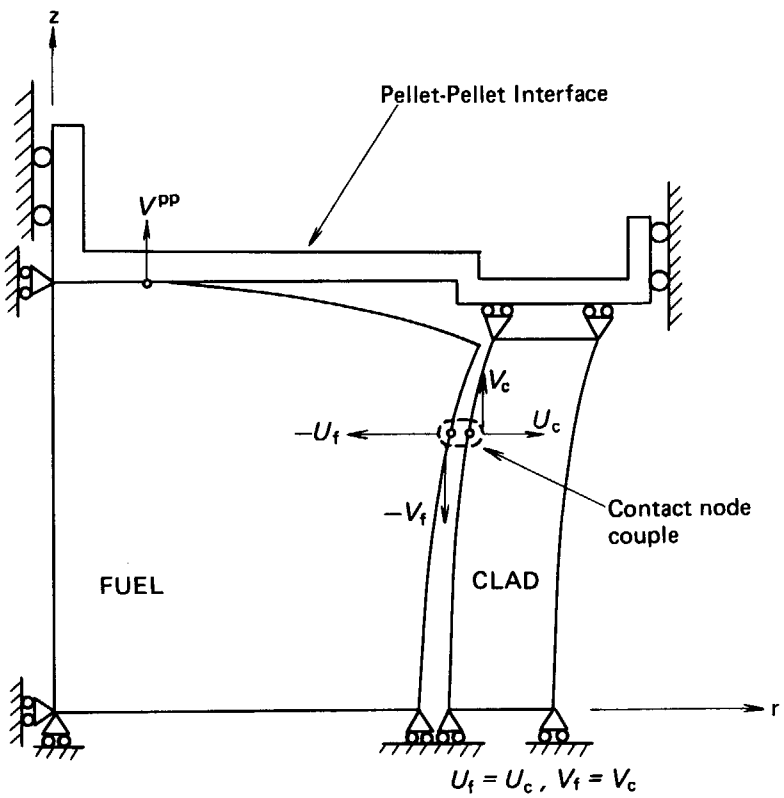

Fig. 12 Contact Force System on the Fuel and Cladding.

For the fuel (f) and cladding (c), the radial contact forces (U_f, U_c) and the axial contact forces (V_f, V_c) act on the contact node couples.

On the other hand, the additional pellet-pellet interface shown in **Fig. 12** is fixed at the highest node on the top of fuel to simulate the pellet-pellet interaction. This interface is assumed to be a plane perpendicular to the axis so that all nodes on the top of fuel can not exceeds the interface axial location. The axial displacement of the top of fuel, after contact starts, is assumed to same as that of the top of cladding. This boundary condition on the top of fuel suppresses the axial movement of fuel and hence the axial reaction force V^{pp} acts on the pellet-pellet interface.

4.3.4 Determination of Pellet-Cladding Contact Conditions

The pellet-cladding contact problem is exactly solved by the direct method with iterative procedure. The special element between fuel and cladding, such as spring element, is not used to solve the pellet-cladding contact problem. On the pellet-cladding interface, nodes on the fuel are connected to the corresponding nodes on the cladding as node couples shown in **Fig. 13**. Each node couple simulates the three kind of contact conditions, open gap, sliding, and full bonding. The contact condition of a node couple is determined with the iterative procedure.

If there is a radial gap between fuel and cladding, the radial contact forces U_f, U_c and axial contact forces V_f, V_c must become zero, so that the boundary conditions are as follows

$$\left.\begin{aligned} &\delta \geq 0, \\ &U_f = U_c = 0, \\ &V_f = V_c = 0, \end{aligned}\right\} \tag{143}$$

where δ : radial gap between fuel and cladding,
U_f and U_c : radial contact forces of fuel and cladding,
V_f and V_c : axial contact forces of fuel and cladding.

If δ_{n+1} becomes negative at the time step t_{n+1}, contact occurs between fuel and cladding and the time step t_{n+1} is divided at the intermediate time $t_{n+\alpha}$ at which the radial gap $\delta_{n+\alpha}$ becomes just zero. For a small time increment, the radial gap is assumed to change linearly and the intermediate time $t_{n+\alpha}$ is given by

$$t_{n+\alpha} = \frac{t_{n+1} - t_n}{\delta_n - \delta_{n+1}} \delta_n + t_n \quad , \tag{144}$$

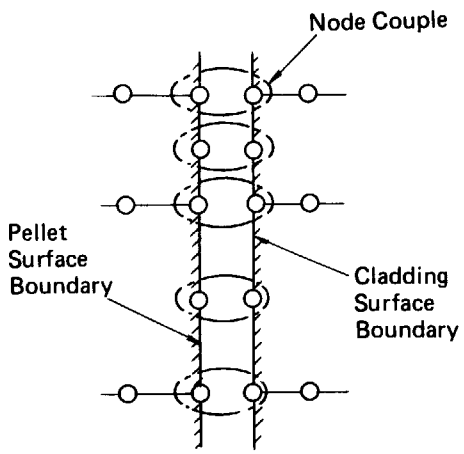

Fig. 13 Node Couples on the Pellet-Cladding Interface.

where n : time step number,
t : time,
δ : radial gap between fuel and cladding.

From the time $t_{n+\alpha}$ to t_{n+1}, the contact condition is corrected from open gap to full bonding.

The boundary conditions for full bonding are defined as

$$\left.\begin{aligned} \Delta u_f &= \Delta u_c \ , \\ \Delta v_f &= \Delta v_c \ , \\ U_f &= -U_c \ , \\ V_f &= -V_c \ , \end{aligned}\right\} \tag{145}$$

where $\Delta u_f, \Delta u_c$: increments of radial displacements of fuel and cladding respectively after contact,
$\Delta v_f, \Delta v_c$: increments of axial displacements of fuel and cladding respectively after contact.

If V_f becomes larger than μU_f, the sliding occurs between fuel and cladding. Then the contact condition is corrected from full bonding to sliding and the claculation is repeated using the following boundary conditions for sliding

$$\left.\begin{aligned} \Delta u_f &= \Delta u_c \ , \\ U_f &= -U_c \ , \\ V_f &= -V_c \ , \\ |V_f| &= \mu |U_f| \ , \end{aligned}\right\} \tag{146}$$

where μ : friction coefficient between fuel and cladding.

The contact condition, full bounding or sliding, holds as long as the radial contact force U_f does not become positive. When the $U_{f,n+1}$ at the time step t_{n+1} becomes positive, the time step t_{n+1} is cut to the intermediate time $t_{n+\alpha}$ at which the radial contact force $U_{f,n+\alpha}$ becomes just zero. For a time increment, the radial contact force is assumed to clange linearly and the intermediate time $t_{n+\alpha}$ is given by

$$t_{n+\alpha} = \frac{t_{n+1} - t_n}{U_{f,n} - U_{f,n+1}} U_{f,n} + t_n \ . \tag{147}$$

From the time $t_{n+\alpha}$ to t_{n+1}, the contact condition is corrected from full bonding or sliding to open gap and the boundary conditions defined by Eq. (143) are used for the residual time.

The judging criteria and boundary conditions to define the contact condition are shown in **Table 4.**

The contact condition of a contact node couple, whether full bounding or sliding, is determined through the following iterative procedure.

(1) Assume contact condition as full bonding or sliding for each contact node couple.
(2) Solve the global stiffness equation using the corresponding boundary conditions.
(3) Judge whether or not the solutions satisfy the assumed contact condition for each contact node couple.
(4) If the improved contact condition coincide with the assumed condition for each contact node couple, the iteration is over. If not, the wrong assumptions are corrected and the steps (2) to (4) are repeated until the convergence is achieved.

Table 4 The judging criteria and boundary conditions for a node couple on the pellet-cladding interface

Contact condition		Judging criteria	Boundary conditions
Before	After		
Open gap	Open gap	$\delta > 0$	$\delta > 0$, $U_f = U_c = 0$, $V_f = V_c = 0$
	Contact	$\delta \leq 0$	Same as full bonding or sliding conditions
Full bonding	Open gap	$U_f > 0$	$\delta > 0$, $U_f = U_c = 0$, $V_f = V_c = 0$
	Full bonding	$U_f < 0$, $\lvert V_f \rvert < \mu \lvert U_f \rvert$	$U_f = -U_c$, $V_f = -V_c$, $\Delta u_f = \Delta u_c$, $\Delta v_f = \Delta v_c$
	Sliding	$U_f < 0$, $\lvert V_f \rvert \geq \mu \lvert U_f \rvert$	$U_f = -U_c$, $V_f = -V_c$, $\lvert V_f \rvert \geq \mu \lvert U_f \rvert$, $\Delta u_f = \Delta u_c$
Sliding	Open gap	$U_f > 0$	Same as full bonding-open gap
	Full bonding	$U_f < 0$, $\lvert V_f \rvert < \mu \lvert U_f \rvert$	Same as full bonding-sliding
	Sliding	$U_f < 0$, $\lvert V_f \rvert \geq \mu \lvert U_f \rvert$	Same as full bonding-sliding

Δu_f, Δu_c : increments of raidal displacements,
Δv_f, Δv_c : increments of axial displacements,
U_f, U_c : radial contact forces,
V_f, V_c : axial contact forces,
f, c : suffices corresponding to fuel and cladding respectively,
μ : friction coefficient between fuel and cladding.

4.3.5 Determination of Pellet-Pellet Contact Conditions

If the fuel is in contact with the cladding, the additional pellet-pellet interface is fixed at the highest axial position on the top of fuel as shown in **Fig. 12** and the axial reaction force acts on this interface.

On the pellet-pellet interface, the two kind of contact conditions, open gap and full bonding, are treated to simulate the pellet-pellet interaction.

The pellet-pellet gap δ^{pp} is expressed as twice the axial distance between a node location and the interface location. If a node exceeds the interface axial location during the time interval Δt_{n+1}, the gap δ^{pp}_{n+1} is regarded negative and contact occurs between pellet and pellet. Then the time step t_{n+1} is cut to the intermediate time $t_{n+\alpha}$ at which the gap $\delta^{pp}_{n+\alpha}$ becomes just zero. For a small time increment, the gap is assumed to change linearly and the intermediate time $t_{n+\alpha}$ is given by

$$t_{n+\alpha} = \frac{t_{n+1} - t_n}{\delta^{pp}_n - \delta^{pp}_{n+1}} \delta^{pp}_n + t_n \quad , \tag{148}$$

where δ^{pp} : gap between pellet and pellet,
n : time step number,
$t_{n+\theta}$: intermediate time between t_n and t_{n+1}.

From the time $t_{n+\alpha}$ to t_{n+1}, the contact condition is corrected from open gap to full bonding.

The boundary conditions for full bonding is defined as

$$\{\Delta v\}^{pp} = \Delta\bar{v}^{pp}\{I\} \quad , \tag{149}$$

where $\{\Delta v\}^{pp}$: increments of axial displacement vector of all contact nodes on the pellet-pellet interface,

$\Delta\bar{v}^{pp}$: increment of axial displacement of contact nodes,

$\{I\}$: unit vector.

The contact condition of full bonding holds as long as the axial reaction force V^{pp} does not become positive. If the V^{pp}_{n+1} at the time t_{n+1} becomes positive, the time step is cut to the intermediate time $t_{n+\alpha}$ at which the axial reaction force $V^{pp}_{n+\alpha}$ becomes just zero. For a time increment, the axial reaction force is assumed to change linearly and the intermediate time $t_{n+\alpha}$ is given by

$$t_{n+\alpha} = \frac{t_{n+1} - t_n}{V^{pp}_n - V^{pp}_{n+1}} V^{pp}_n + t_n \quad , \tag{150}$$

where V^{pp} : axial reaction (contact)force between pellet and pellet.

From the time $t_{n+\alpha}$ to t_{n+1}, the contact condition is corrected from full bonding to open gap. The boundary conditions for open gap is given by

$$\left.\begin{aligned} \delta^{pp} &> 0 \quad , \\ V^{pp} &> 0 \quad . \end{aligned}\right\} \tag{151}$$

The judging criteria and boundary conditions to define the contact condition on the pellet-pellet interface are shown in **Table 5**.

4.3.6 Determination of Contact Forces

If we consider an interval of time Δt_{n+1} $(=t_{n+1}-t_n)$, we can write a global stiffness equation from Eq. (122) as follows

$$K_{n+\theta}\{\Delta u_{n+1}\} = \{\Delta\bar{F}_{n+1}\}, \tag{152}$$

where $K_{n+\theta}$: global stiffness matrix computed by intermediate values between t_n and t_{n+1},

$\{\Delta u_{n+1}\}$: incremental displacement vector during the time interval Δt_{n+1},

Table 5 The judging criteria and boundary conditions for a node on the pellet-pellet interface

Contact condition		Judging criteria	Boundary conditions
Before	After		
Open gap	Open gap	$\delta^{pp} > 0$	$\delta^{pp} > 0,\ V^{pp} > 0$
	Full bonding	$\delta^{pp} \leq 0$	Same as full bonding-full bonding
Full bonding	Open gap	$V^{pp} > 0$	Same as open gap-open gap
	Full bonding	$V^{pp} \leq 0$	$\{\Delta v\}^{pp} = \Delta\bar{v}\{I\}$

δ^{pp} : gap between pellet and pellet,

V^{pp} : axial reaction force between pellet and pellet,

$\Delta\bar{v}$: incremental axial displacement of contact nodes on the pellet-pellet interface.

$\{\varDelta\bar{F}_{n+1}\}$: incremental force vector defined by Eq. (124).

If one node couple is in full bounding and the other node couples are not in contact during the time interval $\varDelta t_{n+1}$, the global stiffness equation is expanded including the boundary conditions for full bonding defined by Eq. (145) as follows

$$
\begin{array}{c} \\ \\ \\ \\ \\ i \\ j \\ k \\ l \\ \\ \\ \\ \\ \\ \\ \\ \\ \end{array}
\left[\begin{array}{ccccccc}
 & & & & & 0 & 0 \\
 & & & & & \cdot & \cdot \\
 & & & & & \cdot & \cdot \\
 & & & & & \cdot & \cdot \\
 & & & & & 0 & 0 \\
 & & & & & -1 & 0 \\
 & & & & & 0 & -1 \\
 & & & & & 1 & 0 \\
 & & & & & 0 & 1 \\
 & & & & & 0 & 0 \\
 & & & & & \cdot & \cdot \\
 & & & & & \cdot & \cdot \\
 & & & & & \cdot & \cdot \\
 & & & & & 0 & 0 \\
\cdots & \cdots & \cdots & \cdots & \cdots & \cdots & \cdots \\
0 \cdots 0 & -1 & 0 & 1\,0\,0 & \cdots\cdots 0 & 0 & 0 \\
0 \cdots 0 & 0 & -1 & 0\,1\,0 & \cdots\cdots 0 & 0 & 0
\end{array}\right]
\left\{\begin{array}{c}
 \\ \\ \\ \\ \\
\varDelta u_{\mathrm{f},n+1} \\
\varDelta v_{\mathrm{f},n+1} \\
\varDelta u_{\mathrm{c},n+1} \\
\varDelta v_{\mathrm{c},n+1} \\
 \\ \\ \\ \\ \\
\cdots\cdots \\
U_{n+1} \\
V_{n+1}
\end{array}\right\}
=
\left\{\begin{array}{c}
 \\ \\ \\ \\ \\ \\ \\ \\
\varDelta\bar{F}_{n+1} \\
 \\ \\ \\ \\ \\
\cdots\cdots \\
0 \\
0
\end{array}\right\} , \qquad (153)
$$

where i, j : row positions in Eq. (153) corresponding to radial and axial components of fuel contact node respectively,

k, l : row positions in Eq. (153) corresponding to radial and axial components of cladding contact node respectively,

$\varDelta u_{\mathrm{f},n+1}$, $\varDelta v_{\mathrm{f},n+1}$: increments of radial and axial fuel displacements during the time interval $\varDelta t_{n+1}$,

$\varDelta u_{\mathrm{c},n+1}$, $\varDelta v_{\mathrm{c},n+1}$: increments of radial and axial cladding displacements during the time interval $\varDelta t_{n+1}$,

U_{n+1} : radial contact force between fuel and cladding at the time t_{n+1},

V_{n+1} : axial contact force between fuel and cladding at the time t_{n+1}.

The contact forces U_{n+1} and V_{n+1} are determined by solving the above global stiffness equation. This global stiffness equation satisfies the boundary conditions of full bonding for the contact node couple which are defined in Eq. (153) as follows

$$
\left.\begin{array}{l}
K_{n+\theta}^{(i)}\,\{\varDelta u_{n+1}\} = \varDelta\bar{F}_{n+1}^{(i)} + U_{n+1} \quad , \\
K_{n+\theta}^{(j)}\,\{\varDelta u_{n+1}\} = \varDelta\bar{F}_{n+1}^{(j)} + V_{n+1} \quad , \\
K_{n+\theta}^{(k)}\,\{\varDelta u_{n+1}\} = \varDelta\bar{F}_{n+1}^{(k)} - U_{n+1} \quad , \\
K_{n+\theta}^{(l)}\,\{\varDelta u_{n+1}\} = \varDelta\bar{F}_{n+1}^{(l)} - V_{n+1} \quad ,
\end{array}\right\} \qquad (154)
$$

$$
\left.\begin{array}{l}
-\varDelta u_{\mathrm{f},n+1} + \varDelta u_{\mathrm{c},n+1} = 0 \quad , \\
-\varDelta v_{\mathrm{f},n+1} + \varDelta v_{\mathrm{c},n+1} = 0 \quad ,
\end{array}\right\} \qquad (155)
$$

where $K_{n+\theta}^{(i)}$: ith row of matrix $K_{n+\theta}$,

$K_{n+\theta}^{(j)}$: jth row of matrix $K_{n+\theta}$,

$K_{n+\theta}^{(k)}$: kth row of matrix $K_{n+\theta}$,

$K_{n+\theta}^{(l)}$: lth row of matrix $K_{n+\theta}$,

$\Delta\bar{F}^{(i)}_{n+1}$: radial component of nodal forces of fuel contact node,
$\Delta\bar{F}^{(j)}_{n+1}$: axial component of nodal forces of fuel contact node,
$\Delta\bar{F}^{(k)}_{n+1}$: radial component of nodal forces of cladding contact node,
$\Delta\bar{F}^{(l)}_{n+1}$: axial component of nodal forces of cladding contact node.

during the time interval Δt_{n+1}, the global stiffness equation is expanded to include the boundary conditions of sliding defined in Eq. (146) as follows

$$\begin{array}{c} \\ \\ \\ \\ i \\ j \\ k \\ l \\ \\ \\ \\ \\ \\ \\ \end{array}
\left[\begin{array}{c:c} & 0 \\ & \cdot \\ & \cdot \\ & 0 \\ & -1 \\ & \mp\mu \\ & 1 \\ & \pm\mu \\ & 0 \\ & \cdot \\ & \cdot \\ & \cdot \\ & 0 \\ \hdashline 0\cdots 0\ \ -1\ \ 0\ \ 1\ \ 0\ \ 0\ \cdots\cdots\ 0 & 0 \end{array}\right]
\left\{\begin{array}{c} \\ \\ \\ \\ \Delta u_{\mathrm{f},n+1} \\ \Delta v_{\mathrm{f},n+1} \\ \Delta u_{\mathrm{c},n+1} \\ \Delta v_{\mathrm{c},n+1} \\ \\ \\ \\ \\ \\ \hdashline U_{n+1} \end{array}\right\}
=
\left\{\begin{array}{c} \\ \\ \\ \\ \\ \\ \\ \Delta\bar{F}_{n+1} \\ \\ \\ \\ \\ \\ \hdashline 0 \end{array}\right\}, \qquad (156)$$

where μ is the friction coefficient between fuel and cladding and the other symbols are same as that defined in Eq. (153).

The contact forces U_{n+1} and μU_{n+1} are determined by solving this. This equation satisfies the boundary conditions of sliding for the contact node couple which are defined in Eq. (156) as follows

$$\left.\begin{array}{ll} K^{(i)}_{n+\theta}\{\Delta u_{n+1}\} = \Delta\bar{F}^{(i)}_{n+1} + U_{n+1} & , \\ K^{(j)}_{n+\theta}\{\Delta u_{n+1}\} = \Delta\bar{F}^{(j)}_{n+1} \pm \mu U_{n+1} & , \\ K^{(k)}_{n+\theta}\{\Delta u_{n+1}\} = \Delta\bar{F}^{(k)}_{n+1} - U_{n+1} & , \\ K^{(l)}_{n+\theta}\{\Delta u_{n+1}\} = \Delta\bar{F}^{(l)}_{n+1} \mp \mu U_{n+1} & , \end{array}\right\} \qquad (157)$$

$$-\Delta u_{\mathrm{f},n+1} + \Delta u_{\mathrm{c},n+1} = 0 \ . \qquad (158)$$

4.3.7 Determination of Axial Displacements

If the fuel and cladding are in contact, the additional pellet-pellet interface is fixed at the highest axial position on the top of fuel as shown in **Fig. 12** and the axial displacement of the top of fuel, after contact starts, is assumed to same as that of the top of cladding.

If one node couple is in full bonding and the other node couples are not in contact during the time interval Δt_{n+1}, the axial displacements of top of fuel and cladding are calculated solving Eq. (153). Therefore Eq. (153) is modified to include the axial restraint conditions in the matrix equation as follows:

$$
\begin{array}{c}
 \\ \\ \\ \\ m \\ \\ \\ \\ \\ i \\ j \\ k \\ l \\ \\ \\ \\ \\ \\ n \\ \\ \\ \\ \\
\end{array}
\left[\begin{array}{cccc}
 & 0 & 0 & 0 \\
 & \cdot & \cdot & \cdot \\
 & \cdot & \cdot & \cdot \\
 & \cdot & 0 & 0 \\
 & 0 & 0 & -1 \\
 & \cdot & \cdot & \cdot \\
 & \cdot & \cdot & \cdot \\
 & \cdot & \cdot & \cdot \\
 & 0 & 0 & 0 \\
K_{n+\theta} & -1 & 0 & 0 \\
 & 0 & -1 & 0 \\
 & 1 & 0 & 0 \\
 & 0 & 1 & 0 \\
 & 0 & 0 & 0 \\
 & \cdot & \cdot & \cdot \\
 & \cdot & \cdot & \cdot \\
 & \cdot & \cdot & \cdot \\
 & 0 & 0 & 0 \\
 & 0 & 0 & 1 \\
\cdots\cdots\cdots\cdots\cdots\cdots & \cdots & \cdots & \cdots \\
0\cdots\cdots0\cdots0\ -1\quad 0\ 1\ 0\ 0\cdots\cdots0 & 0 & 0 & 0 \\
0\cdot\cdot0\quad 0\cdots0\quad 0\ -1\ 0\ 1\ 0\cdots\cdots0 & 0 & 0 & 0 \\
0\cdot\cdot0-1\cdots0\quad 0\quad 0\ 0\ 0\ 0\cdots\cdots1 & 0 & 0 & 0
\end{array}\right]
\left\{\begin{array}{c}
 \\ \\ \\ \\ \Delta\bar{v}_{\mathrm{f},n+1} \\ \\ \\ \\ \\ \Delta u_{\mathrm{f},n+1} \\ \Delta v_{\mathrm{f},n+1} \\ \Delta u_{\mathrm{c},n+1} \\ \Delta v_{\mathrm{c},n+1} \\ \\ \\ \\ \\ \\ \Delta\bar{v}_{\mathrm{c},n+1} \\ \cdots\cdots \\ U_{n+1} \\ V_{n+1} \\ \bar{V}
\end{array}\right\}
=
\left\{\begin{array}{c}
 \\ \\ \\ \\ \\ \\ \\ \\ \\ \\ \\ \Delta\bar{F}_{n+1} \\ \\ \\ \\ \\ \\ \\ \\ \cdots\cdots \\ 0 \\ 0 \\ 0
\end{array}\right\} , \tag{159}
$$

where $\Delta\bar{v}_{\mathrm{f},n+1}$: incremental axial displacement of contact nodes on the pellet-pellet interface,

$\Delta\bar{v}_{\mathrm{c},n+1}$: incremental axial displacement of nodes on the top of cladding,

$\bar{V}$: axial force induced by the axial restraint condition.

The axial components of contact nodes on the pellet-pellet interface are collected in the same row of m due to the restraint condition and also the axial components of nodes on the top of cladding are collected in the same row of n due to the restraint conditon of top of cladding. From Eq. (159) the stiffness equations of rows m and n are given by

$$
\left.\begin{array}{l}
K_{n+\theta}^{(m)}\{\Delta u_{n+1}\}=\Delta\bar{F}_{n+1}^{(m)}+\bar{V} , \\
K_{n+\theta}^{(n)}\{\Delta u_{n+1}\}=\Delta\bar{F}_{n+1}^{(n)}-\bar{V} ,
\end{array}\right\} \tag{160}
$$

where $K_{n+\theta}^{(m)}$: mth row vector of matrix $K_{n+\theta}$,

$K_{n+\theta}^{(n)}$: nth row vector of matrix $K_{n+\theta}$,

$\Delta\bar{F}_{n+1}^{(m)}$: axial compoment of nodal forces of contact nodes on the pellet-pellet interface,

$\Delta\bar{F}_{n+1}^{(n)}$: axial component of nodal forces of nodes on the top of cladding.

Eq. (159) satisfies the boundary condition for the axial displacements of the top of fuel and cladding as follows:

$$
-\Delta\bar{v}_{\mathrm{f},n+1}+\Delta\bar{v}_{\mathrm{c},n+1}=0 . \tag{161}
$$

If one node is in sliding condition and the other node couples are not in contact during the time interval Δt_{n+1} , the axial displacements of the top of fuel and cladding are calculated solving Eq. (153). Eq. (153) is modified to include the axial restraint conditions in the matrix equation as follows:

$$
\begin{array}{c}
\\ \\ \\ \\ m \\ \\ \\ \\ \\ i \\ j \\ k \\ l \\ \\ \\ \\ \\ \\ n \\ \\ \\
\end{array}
\left[\begin{array}{c:cc}
 & 0 & 0 \\
 & \cdot & \cdot \\
 & \cdot & \cdot \\
 & 0 & 0 \\
K_{n+\theta} & 0 & -1 \\
 & 0 & 0 \\
 & \cdot & \cdot \\
 & \cdot & \cdot \\
 & 0 & 0 \\
 & -1 & 0 \\
 & \mp\mu & 0 \\
 & 1 & 0 \\
 & \pm\mu & 0 \\
 & 0 & 0 \\
 & \cdot & \cdot \\
 & \cdot & \cdot \\
 & \cdot & \cdot \\
 & 0 & 0 \\
 & 0 & 1 \\
\hdashline
0\cdot\cdot0\quad 0\ 0\cdot\cdot0\ \ -1\ 0\ 1\ 0\ 0\cdots\cdots 0\ 0 & 0 & 0 \\
0\cdot\cdot0\ -1\ 0\cdot\cdot0\quad 0\ 0\ 0\ 0\ 0\cdots\cdots 0\ 1 & 0 & 0
\end{array}\right]
\left\{\begin{array}{c}
\\ \\ \\ \\ \Delta\bar{v}_{\mathrm{f},n+1} \\ \\ \\ \\ \\ \Delta u_{\mathrm{f},n+1} \\ \Delta v_{\mathrm{f},n+1} \\ \Delta u_{\mathrm{c},n+1} \\ \Delta v_{\mathrm{c},n+1} \\ \\ \\ \\ \\ \\ \Delta\bar{v}_{\mathrm{c},n+1} \\
\hdashline
U_{n+1} \\ \bar{V}
\end{array}\right\}
=
\left\{\begin{array}{c}
\\ \\ \\ \\ \\ \\ \\ \\ \\ \\ \Delta\bar{F}_{n+1} \\ \\ \\ \\ \\ \\ \\ \\ \\
\hdashline
0 \\ 0
\end{array}\right\} , \qquad (162)
$$

where the symbols are defined before..

From Eq. (162) the boundary condition for the axial displacements of the top of fuel and cladding is satisfied as follows:

$$-\Delta\bar{v}_{\mathrm{f},n+1}+\Delta\bar{v}_{\mathrm{c},n+1}=0\ . \qquad (163)$$

On the other hand, the reaction force V^{pp} to the axial force for each contact node on the pellet-pellet interface is calculated solving the element stiffness equation, that includes the corresponding contact node in it, as follows:

$$\{F_{n+1}\}^{\mathrm{e}}=\int_v B^{\mathrm{T}}\{\sigma_{n+1}\}^{\mathrm{e}}\mathrm{d}V\ , \qquad (164)$$

where $\{F_{n+1}\}^{\mathrm{e}}$: force vectors of element e at the time t_{n+1},

B : strain-displacement matrix,

$\{\sigma_{n+1}\}^{\mathrm{e}}$: stress vectors of element e at the time t_{n+1} .

5. Material Properties

5.1 Thermal Properties

(1) Heat Transfer Coefficient between Coolant and Cladding

See Eqs. (2) and (3).

(2) Heat Transfer Coefficient between Fuel and Cladding

See Eqs. (6), (7), (8), and (17).

(3) Thermal Conductivity of Cladding

See Eq. (5).

(4) Thermal Conductivity of Fuel

See Eqs. (33) and (34).

(5) Thermal Conductivities of Rare Gases

See Eqs. (11), (12), (13), and (14).

5.2 Mechanical Properties

(1) Young's Modulus for Fuel

Young's modulus is given as a function of temperature and density[23].

For $0 \leq T \leq 1300$ °C,

$$E_f = 2.26\times10^{11}(1-1.131\times10^{-4}T)[1-2.62(1-f_d)] \ ,$$

where E_f : Young's modulus for fuel [Pa],
T : temperature [°C],
f_d : fraction of theoretical density.

(2) Young's Modulus for Cladding

Young's modulus is given as a function of temperature[31],

$$E_c = [9.900\times10^5 - 566.9\times(T-273.15)]\times9.8067\times10^4 \ ,$$

where E_c : Young's modulus for cladding [Pa],
T : temperature [K].

(3) Poisson's Ratio for Fuel

Poisson's ratio for fuel is given by[23],

$$\nu_f = 0.316 \ ,$$

where ν_f : poisson's ratio for fuel.

(4) Poisson's Ratio for Cladding

Poisson's ratio for cladding is a function of temperature[31],

$$\nu_c = 0.3303 + 8.376\times10^{-5}\ (T-273.15) \ ,$$

where ν_c : poisson's ratio for cladding,
T : temperature [K].

(5) Plasticity for Fuel

Yield stress for fuel is expressed as a function of temperature[32],

for $T \leq 1800$ °C,

$$\sigma_Y = 1176.1 - 1.688\times T + 8.179\times10^{-4}\times T^2 - 1.293\times10^{-7}\times T^3 \ ,$$

for $T > 1800$ °C,

$$\sigma_Y = 33.62 \ ,$$

where σ_Y : yield stress [MPa],
T : temperature [°C].

(6) Plasticity for Cladding

Yield stress for cladding is given by[33],

$$\sigma_Y = K\left(\frac{\sigma_y}{E} + \varepsilon^p\right)^n \ ,$$

with

$$K = \sigma_{Y0}\left(\frac{\sigma_{Y0}}{E} + 0.002\right)^{-n} \ ,$$

where σ_Y : yield stress [kg/mm^2],
E : Young's modulus for cladding [kg/mm^2],
ε^p : plastic strain,
σ_{Y0} : 0.2% yield stress [kg/mm^2],
n : strain hardening exponent.

0.2% yield stress σ_{Y0} is expressed as

$$\sigma_{Y0} = \sigma_{Y0}^{t} + \Delta\sigma_{Y0}^{irr} \ ,$$

where σ_{Y0}^{t} : out-of-pile 0.2% yield stress [kg/mm^2],
$\Delta\sigma_{Y0}^{irr}$: increment of 0.2% yield stress due to irradiation induced hardening [kg/mm^2].

σ_{Y0}^{t} is given as a function of temperature for recrystallized cladding tube,

$$\sigma_{Y0}^{t} = 21.60 - 0.0213 \times T, \ 220℃ \leq T \leq 450℃,$$

for stress-relieved cladding tube,

$$\sigma_{Y0}^{t} = 31.32 - 0.0213 \times T, \ 220℃ \leq T \leq 450℃,$$

where T : temperature [°C].

$\Delta\sigma_{Y0}^{irr}$ is given as a function of fast neutron flux and irradiation time

$$\Delta\sigma_{Y0}^{irr} = 33.44\,[1 - \exp(-C\phi t)]^{1/2},$$

with

$$C = 2.92 \times 10^{-21} \exp(-1.6 \times 10^{-14}\phi) \ ,$$

where ϕ : fast neutron flux [n/(cm^2·s)],
t : time [s].

Strain hardening exponent n is given as a function of temperature

$$n = 0.0504 + 0.0001435 \times T \ ,$$

where T : temeprature [°C].

(7) Creep Law for Fuel

Creep law for the fuel is given by[23],

$$\dot{\varepsilon}^c = \frac{(A_1 + A_2\dot{F})\sigma e^{-Q_1/RT}}{(A_3 + f_d)G^2} + \frac{A_4\sigma^{4.5} e^{-Q_2/RT}}{(A_6 + f_d)} + A_7\sigma\dot{F}e^{-Q_3/RT} \ ,$$

with

$A_1 = 9.728 \times 10^6$, $Q_1 = 90{,}000$,
$A_2 = 3.240 \times 10^{-12}$, $Q_2 = 132{,}000$,
$A_3 = -87.7$, $Q_3 = 5{,}200$,
$A_4 = 1.376 \times 10^{-4}$,

$A_6 = -90.5$,

$A_7 = 9.24 \times 10^{-28}$,

where $\dot{\varepsilon}^c$: creep strain rate [hr^{-1}],

F : fission rate (= 8.4×10^{17} to 1.18×10^{20} [fissions/($m^3 \cdot s$)],

σ : stress [1,000 to 16,000 psi],

R : gas constant [cal/(mol·K)],

Q : activation energy for diffusion [cal/mol],

T : temperature [713 to 2,073 K],

f_d : fraction of theroretical density [0.92 to 0.98],

G : grain size [4 to 35 μm].

(8) Creep Law for Cladding

Creep law for the cladding is given by[23],

$$\dot{\varepsilon}^c = 2[5.129 \times 10^{-29} \phi\, e^{-\frac{10000}{RT}} \{\sigma + 7.252 \times 10^2 e^{4.967 \times 10^{-8} \sigma}\}]^2 \times \left(\frac{3600}{\varepsilon^c}\right),$$

where $\dot{\varepsilon}^c$: creep strain rate [sec^{-1}],

ε^c : total creep strain,

ϕ : fast neutron flux [n/($m^2 \cdot sec$)] E > 1.0 MeV,

σ : stress [Pa],

T : temperature [K],

R : gas constant = 1.987 [cal/(mol·K)].

(9) Fuel Thermal Expansion

See Eq. (40).

(10) Cladding Thermal Expansion

See Eqs. (42) and (43).

(11) Fuel Relocation

See Eq. (36).

(12) Fuel Densification

See Eq. (37).

(13) Fuel Swelling

See Eqs. (38) and (39).

(14) Fuel Cracking

See Eq. (115).

(15) Fuel Hot Pressing

See Eq. (121).

6. Assessment of the Code

The capability of the FEMAXI-III code has been tested with a large data base obtained in the international progroms such as the OECD Halden Reactor Project and the Studsvik Inter-Ramp and Over-Ramp Projects. These data consist of in-pile measurements of fuel center temperature, internal gas pressure, rod diameter, and axial elongation and post-irradiation examinations such as fission gas release fraction and residual cladding deformations. Some comparisons between calculations and these data have been published[15-17]. Typical examples of these comparisons are described below.

6.1 Fuel Temperature Calculations

To assess the thermal models incorporated in the code, FEMAXI-III calculations have been compared with the data of fuel center temperature during the first power operation. The data were obtained from a variety of fuel rods covering a wide range of initial gap from 60 μm to 400 μm.

For this assessment, mainly the fuel relocation model was checked through the comparisons. The burnup dependent models, such as fission gas release and swelling etc., are not assessed here because these are not essential at the beginning of irradiation.

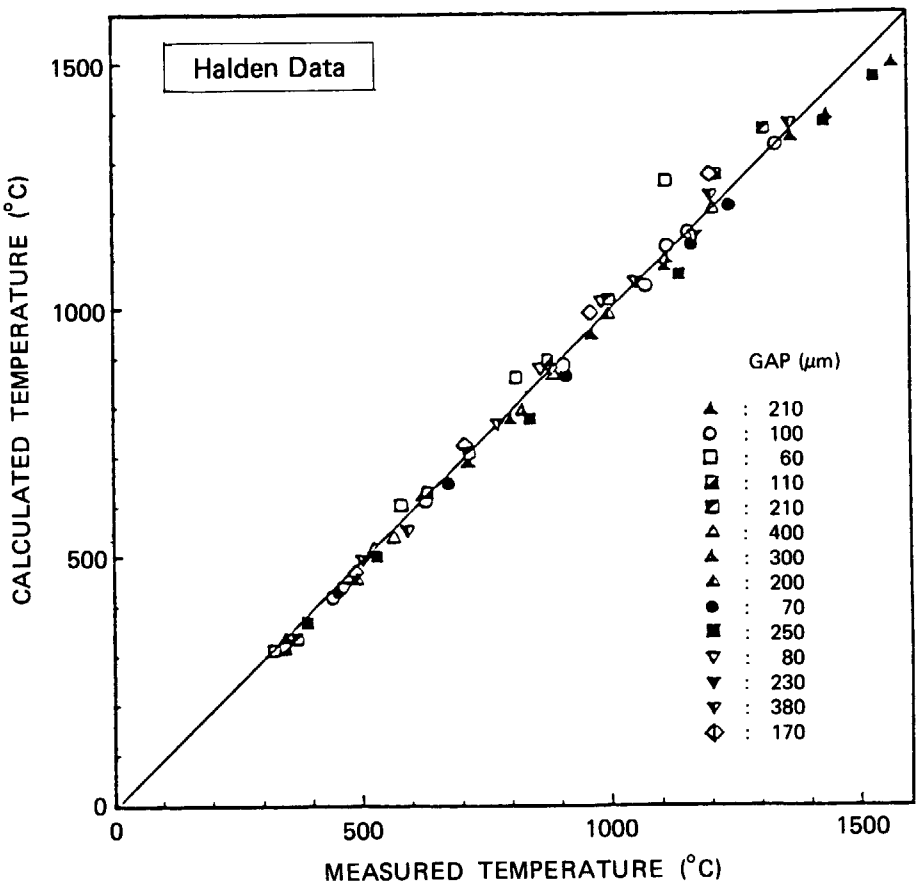

Fig. 14 Comparison between Measured and Calculated Fuel Center Temperatures of Various Experimental Fuel Rods during the First Power Operations.

The calculated fuel center temperatures are compared with the measurements as shown in **Fig. 14**. The results of FEMAXI-III calculations were in good agreement with the measurements and it confirmed the capability of the FEMAXI-III code to predict the fuel center temperatures for a variety of fuel rods with different initial gap sizes.

6.2 Fission Gas Release Calculations

To assess the fission gas release model and gap closure models which depend on the burnup, the FEMAXI-III calculations have been compared with the fission gas release data obtained from the Studsvik Inter Ramp Project.

The data were obtained from the fuel rods which were irradiated to the burnup levels from 11 to 23 MWd/tUO_2 and subjected to the power ramp experiments. The whole irradiation histories including the power ramp for the test fuel rods were fully simulated by the FEMAXI-III code.

The calculated fission gas release fractions are compared with the PIE gas analysis results of eleven rods in **Fig. 15** as a function of ramp terminal power level.

The results of calculations were in reasonable agreement with the measurements and it confirmed the capability of FEMAXI-III code to predict the thermal behaviors of high exposure fuel rods.

6.3 Fuel Rod Deformation Calculations

In the Halden Project, the in-pile fuel rod diameter measurements are extensively

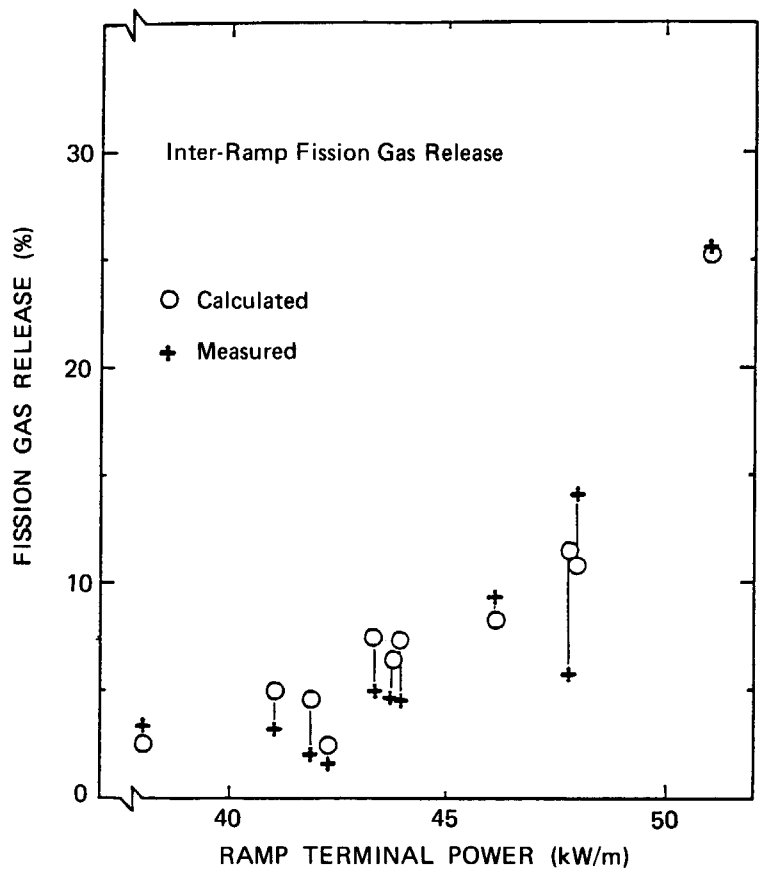

Fig. 15 Comparison between Measured and Calculated Fission Gas Release as a Function of Ramp Terminal Power Level.

performed in the experiments, and the diameter changes during the power increase have been directly observed.

To assess the FEM mechanical models, FEMAXI-III calculations have been compared with the in-pile data of diameter measurements.

Figure 16 shows the calculated and measured ridge height as a function of rod power during the first power operation. The calculation simulates the onset power at which the fuel-cladding mechanical interaction starts and the general trend of ridge growth with rod power. While the calculation without the initial relocation can not simulate the measured behavior. Therefore, the fuel relocation model plays an important role in the analysis of the fuel-cladding mechanical interacfion.

Figure 17 shows the calculated fuel rod deformation at 41 kw/m of linear heat rate during start up. This figure is a computer graphic of FEMAXI-III calculation, however the displacement is enlarged by hundred times to exaggerate the ridge shape reproduced by the code calculation.

These results of mechanical calculations confirmed the capability of FEM mechanical models incorporated in the FEMAXI-III code to analyze the local mechanical behaivor of fuel rod.

6.4 Running Time

The running time depends on the length and complexity of irradiation history. The running time (CPU time) for the thermal and mechanical analysis of the Inter-Ramp fuel rods mentioned before was on the order of 1-3 min. for the full history on the FACOM M-380 computer. This running time is acceptable for the full analysis of a problem with long-term irradiation including many power changes.

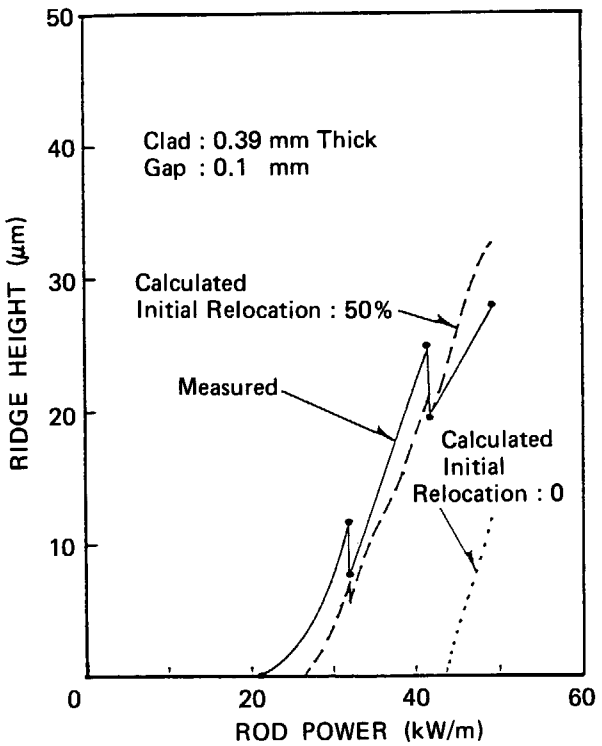

Fig. 16 Measured and Calculated Ridge Growth as a Function of Rod Power during the First Power Operation.

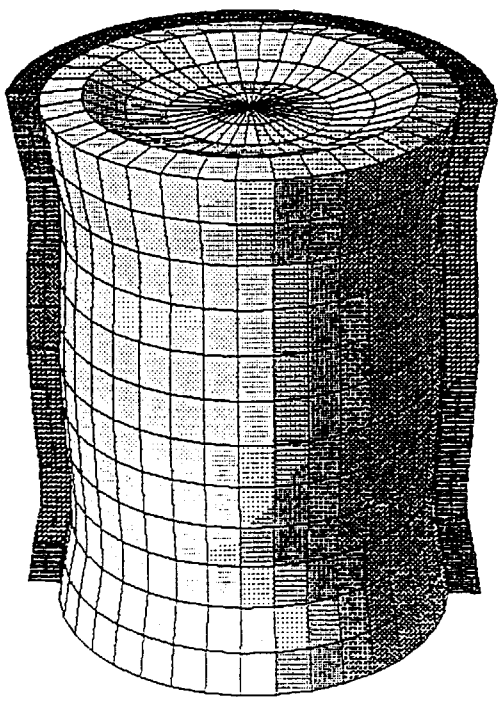

Fig. 17 Calculated Fuel Rod Deformation during Start-up.

7. Conclusions

A computer code FEMAXI-III has been developed to analyze the thermal and mechanical behavior of light water fuel rod during its irradiation life. FEMAXI-III can analyze the integral behavior of a whole fuel rod throughout its life, as well as the localized mechanical behavior at a small part of fuel rod. The localized phenomena, such as the cladding bamboo-ridge formed by the fuel pellets, is analyzed by the two-dimensional axisymmetric finite element method.

Efforts have been made to achieve the accurate and stable solution for a long irradiation problem including power ramps within reasonable running time. This work have been successfully accomplished by the several treatments such as the use of a quadratic isoparametric element, the exact treatment of contact problem between fuel and cladding by the direct method, the application of the implicit algorithm to the solution of non-linear material problems, the effective treatment of fuel cracking and healing by changing the elastic modulus, the application of the finite element analysis to a minimized region of fuel rod, and the use of an efficient sparse matrix storage scheme for the solution of global stiffness equation.

The results of applications of the FEMAXI-III code, presented here, show that the agreement is quite satisfactory.

It is expected that the FEMAXI-III code will be used to study the thermal and mechanical behavior of light water fuel rods and to improve the fuel rod design and the operating conditions.

Acknowledgement

The authors gratefelly acknowledge the considerable help received from numerous sources in the development of this code. In particular, the authors wish to thank: Mr. M. Sogame and Mr. T. Kogai of Nippon Nuclear Fuel Development Co. Ltd., and H. Tanaka of Central Research Institute of Electric Power Industries for their great help in the code assessment works; Mr. A. Ishibashi, Mr. N. Otsubo, and Mr. T. Mizushima of Century Research Center Corp. for their help in the code programming works; Mr. H. Ando, Mr. M. Uchida, Mr. Y. Harayama, Mr. A. Kikuchi, Mr. F. Izumi and Mr. M. Fujita of Japan Atomic Energy Research Institute for their useful discussions.

References

1) Duncombe E., Friedrich C.M., and Guilinger W.H. : An Analytic Model for the Prediction of In-Pile Behavior of Oxide Fuel Rods, Nucl. Tech. **12**, 194-208 (1971).
2) Godesar R., Guyette M., and Hoppe N. : COMETHE II-A Computer Code for Predicting the Mechanical and Thermal Behavior of a Fuel Pin, Nucl. App. & Tech., **9**, 205-217 (1970).
3) Jankus V.Z. and Weeks R.W. : LIFE-II-A Computer Analysis of Fast-Reactor Fuel-Element Behavior as a Function of Reactor Operating History, Nucl. Eng. and Des. **18**, 83-96 (1972).
4) Lassmann K. : URANUS-A Computer Programme for the Thermal and Mechanical Analysis of the Fuel Rods in a Nuclear Reactor, ibid **45**, 325-342 (1978).
5) Visser C., VanBuren W., Wilson W.K., and Cabrielse S.W. : Fuel Rod Deformations, A Time Dependent Finite Element Analysis of Axisymmetric Fuel Rods, Including Pellet and Effects, WERL-ELPLA-1 (1970).
6) Swanson J.A. et al. : Application of Finite Element Method for the Thermal Creep, Irradiation Induced Creep, and Swelling for LMFBR Design, 1st SMIRT, L4/3, Berlin, (1973).
7) Levy S. and Wilkinson J.P.D. : A Three-Dimensional Study of Nuclear Fuel Rod Behavior During Startup, 1st SMIRT, D1/5, Berlin, (1973).
8) Rashid Y.R. : Mathematical Modeling and Analysis of Fuel Rods, Nucl. Eng. and Des. **29**, 22-32 (1974).
9) Ichikawa M. : Analysis of Fuel Rod Deformation by an Axisymmetric Finite Element Method, Enlarged Halden Programme Group Meeting, Geilo, Norway, (1975).
10) Kinoshita M. and Ichikawa M. : Fuel Rod Deformation Code FEMAXI-II and Its Application, Nucl. Eng. and Des. **56**, 49-56 (1980).
11) Ito K., Ishida M. and Oguma M. : FEAST, A Finite Element Computer Code for Analysis of the Thermo-Mechanical Fuel Rod Behavior, EHPGM, Loen, Norway, (1978).
12) Iwano Y. : MIPAC, A Computer Code for Fuel Performance Analysis by the Finite Element Method, IAEA Specialists Meeting on Fuel Element Performance Computer Modelling, Blackpool, UK, (1978).
13) Nakajima T., Ichikawa M., Iwano Y., Ito K., Saito H., Kashima K., Kinoshita M., and Okubo T., : FEMAXI-III-An Axisymmetric Finite Element Fuel Behavior Code, JAERI-M 9251, (1981) [in Japanese].
14) Ito K., Ichikawa M., Okubo T., and Iwano Y., : FEMAXI-III, A Computer Code for Fuel Rod Performance Analysis, Nucl. Eng. and Des. **76**, 3-11 (1983).
15) Ito K., Ichikawa M., Nakajima T., Sogame M., Okubo T., and Saito H : A Comparison of FEMAXI-III Code Calculations with Irradiation Experiments, Res Mechanica **2**, 109-121 (1981).
16) Ichikawa M., Nakajima T., Kinoshita M., Ito K., Kogai T., Saito H., and Okubo T. : Analysis of PCI by FEMAXI-III, IAEA Specialist's Meeting, Risø, Denmark, (1980).
17) Okubo T., Ichikawa M., Ito K., Sogame M., Kinoshita M., and Saito H. : Verification of FEMAXI-III Code, IAEA Specialist's Meeting, Preston, UK, (1982).
18) Zienkiewicz O.C. : "The Finite Element Method", Third Edition, McGraw-Hill, New York, (1977).
19) Felippa C.A. : Solution of Linear Equations with Skyline-Stored Symmetric Matrix, Comp. & Struct. **5**, 13-29 (1975).
20) Mondkar D.P. and Powell G.H. : Towards Optimal In-Core Equation Solving, Comp. & Struct. **4**, 531-548 (1974).
21) Jens W.H. and Lottes P.A. : Analysis of Heat Transfer, Burnout, Pressure Drop and Density Data for High-Pressure Water, ANL-4627, (1951).
22) Dittus F.W. and Boelter L.M.K., Univ. Calif. Pubs. Eng. **2**, 443 (1930).
23) MATPRO-09, A Handbook of Materials Properties for Use in the Analysis of Light Water Reactor Fuel Rod Behavior, TREE-NUREG-1005, (1976).
24) Ross A.M. and Stoute R.L. : Heat Transfer Coefficient between UO_2 and Zircaloy-2, CRFD-1075, (1962).
25) Robertson J.A.L : $\int k\, d\theta$ in Fuel Irradiation, CRFD-835, (1959).
26) Chubb W., Storhok V.W., and Keller D.L. : Factors Affectiong the Swelling of Nuclear Fuel at High Temperatures, Nucl. Technol. **18**, 231-255 (1973).
27) Zimmermann H : Investigation on Swelling and Fission Gas behavior in Uranium Dioxide, J. Nucl. Mater. **75**, 154-161 (1978).
28) Vitanza C., Kolstad E., and Graziani V. : Fission Gas Release from UO_2 Pellet Fuel at High Burnup, ANS Topical Meeting, Portland, USA, (1979).
29) Hill R. : The Mathematical Theory of Plasticity, Clarendon Press, Oxford, (1950).
30) Rashid Y.R., Tang H.R., and Johansson E.B. : Mathematical Treatrment of Hot Pressing of Reactor Fuel,

Nucl. Eng. Des. **29**, 1-6 (1974).

31) Fisher E.S. and Renken C.T. : Single-Crystal Elastic Moduli and Hop-Bcc Transformation in T_i, Z_r, and H_f, Physical Review, PA482-A494 (1954).

32) Rodford K.C. and Terwilliger G.R. : Compressive Deformation of Polycrystalline UO_2, J. Am. Ceram. Soc. **58**, (1975).

33) Private communication.

List of Symbols

Chapter Paragraph	Symbol	Description
3.2	T_{co}	temperature of the outside of the cladding [K]
	T_w	coolant temperature [K]
	q'	linear heat rate [W/cm]
	r_{co}	outer radius of the cladding
	h_c	heat transfer coefficient between the coolant and the cladding [W/(cm^2·K)]
	$h_{c,NB}$	heat transfer coefficient between the coolant and the cladding for nucleate boiling condition [W/(cm^2·K)]
	P_w	coolant pressure [Pa]
	q''	heat flux [W/cm^2]
	$h_{c,FC}$	heat transfer coefficient between the conlant and the cladding for forced convection condition [Btu/(hr·ft^2·°F)]
	k_w	coolant thermal conductivity [Btu/(hr·ft·°F)]
	D_e	equivalent hydraulic diameter [in]
	v	coolant velocity [ft/s]
	ρ	coolant density [lb/ft^3]
	μ	viscosity of coolant water [lb/(ft·s)]
	Pr	Prandtl number
	c_p	specific heat [Btu/(lb·°F)]
	T	cladding temperature at the radius r [K]
	k_c	thermal conductivity of the cladding [W/(cm·K)]
	r	radial coordinate [cm]
	h_{gap}	heat transfer coefficient between fuel and cladding [W/(cm^2·K)]
	h_g	heat transfer coefficient through gap gas [W/(cm^2·K)]
	h_s	heat transfer coefficient through solid to solid contact spots [W/(cm^2·K)]
	h_r	heat transfer coefficient by radiation [W/(cm^2·K)]
	k_{gas}	thermal conductivity of gas mixture in the gap [W/(cm·K)]
	C	a dimensionless constant near unity
	R_{eff}	effective surface roughness of the fuel [cm]
	R_2	surface roughness of the cladding [cm]
	g_1	average temperature-jump distance for a gas at the fuel surface [cm]
	g_2	average temperature-jump distance for a gas at the cladding surface [cm]
	δ	radial gap [cm]
	n	number of components in gas mixture
	i & j	gas species
	M_i	molecular weight of gas species i
	x_i	mole fraction of gas species i
	k_i	thermal conductivity of gas species i [W/(cm·K)]

Chapter Paragraph	Symbol	Description
3.2	T	temperature of the gas [K]
	P_c	contact pressure [Pa]
	$(g_1+g_2)_i$	temperature-jump distance for gas species i [cm]
	P_{gas}	inner gas pressure [Pa]
	k_m	mean of fuel and cladding thermal conductivities [W/(cm·K)]
	R	square mean of fuel and cladding roughness
	H	Mayer hardness of the cladding [Pa]
	k_1	thermal conductivity of the fuel [W/(cm·K)]
	k_2	thermal conductivity of the cladding [W/(cm·K)]
	σ	Stephan-Boltzman constant = 5.67×10^{-12} [W/(cm^2·K^4)]
	T_1	temperature of the outer fuel surface [K]
	T_2	temperature of the inner cladding surface [K]
	e_1	emissivity of the outer fuel surface
	e_2	emissivity of the inner cladding surface
	ψ	thermal neutron flux [n/(s·cm^2)]
	r	radial coordinate [cm]
	I_0, K_0	modified Bessell functions of zero order
	I_1, K_1	modified Bessell functions of first order
	κ	inverse diffusion length for neutrons in the fuel [cm^{-1}]
	r_{fi}	inner radius of the fuel [cm]
	e	enrichment of U^{235} [%]
	f_d	fraction of theoretical density
	r_{fo}	outer radius of the fuel [cm]
	a	fraction of inner and outer surface heat generation rate
	b	degree of heat generation distribution function = 2
	$\bar{r}_1$	normalized radius of fuel inner surface = r_{fi}/r_{fo}
	$\bar{r}$	normalized radius of the fuel = r/r_{fo}
	q'''	heat generation rate per unit volume of fuel [W/cm^3]
	T_{fo}	temperature of the outside of the fuel [K]
	T_{ci}	temperature of the inside of the cladding [K]
	k_f	thermal conductivity of the fuel [W/(cm·K)]
	β	porosity coefficient
	K_1, K_2, K_3, K_4 & K_5	constants
3.3	u^{rel}	radial displacement of the fuel by relocation [cm]
	α	relocation parameter
	δ_0	as-fabricated radial gap [cm]
	$\left(\frac{\Delta V}{V_0}\right)^d$	volume change by densification
	V_0	initial free volume
	ΔV_{max}	maximum volume change of porosity
	BU	burnup [MWd/tUO_2]
	SBU	burnup constant for densification
	$\left(\frac{\Delta V}{V_0}\right)^{ss}$	volume change by solid fission product swelling

Chapter Paragraph	Symbol	Description
3.3	$\left(\frac{\Delta V}{V_0}\right)^{gs}$	volume change by gaseous fission product swelling
	$\left(\frac{\Delta l}{l_0}\right)_f^{th}$	linear thermal expansion of the fuel
	l_0	initial length
	u_f	fuel radial displacement [cm]
	m	number of concentric ring
	Δr	width of concentric ring [cm]
	$\left(\frac{\Delta l}{l_0}\right)_c^{th}$	cladding axial thermal expansion
	$\left(\frac{\Delta D}{D_0}\right)_c^{th}$	cladding diametral thermal expansion
	D_0	initial diameter
	u_c^{creep}	radial displacement of the cladding by creep [cm]
	u_c	cladding radial displacement [cm]
	E_c	Young's modulus for cladding [Pa],
	ν_c	poisson's ratio for cladding
	δ	radial gap between fuel and cladding [cm]
	δ_0	as-fabricated radial gap [cm]
	δ_{fc}	cladding radial displacement after contact [cm]
	P_{fc}	contact pressure between fuel and cladding [Pa]
	Δr_c	initial thickness of cladding [cm]
3.4	β	fission gas production rate per unit length of fuel [mole/(cm·s)]
	i	concentric ring number
	j	axial segment number
	q'	heat generation rate per unit length of fuel [W/cm]
	Y	yielding ratio of (Kr + Xe) = 0.3
	E_f	fission energy = 200 MeV
	N_A	Avogadoro constant = 6.02×10^{23}
	BU^*	incubation burnup [MWd/tUO_2]
	T_{fc}	fuel centerline temperature [°C]
	f^{ij}	release fraction of fission gas in the concentric ring i at the axial segment j
	T^{ij}	fuel temperature in the concentric ring i at the axial segment j [°C]
	BU^j	burnup at the axial segment j [MWd/tUO_2]
	n_r	number of released gas moles from the fuel [mol]
	m	number of axial segments considered
	l	length of axial segment [cm]
	t	irradiation time [s]
	x_{He}	mole fraction of helium
	x_{Kr}	mole fraction of krypton
	x_{Xe}	mole fraction of xenon
	n_o	number of gas moles initially in the fuel rod [mol]
	n_t	total number of gas moles in the fuel rod [mol]

Chapter Paragraph	Symbol	Description
3.4	$x_{o,He}$	initial mole fraction of helium
	$x_{o,Kr}$	initial mole fraction of krypton
	$x_{o,Xe}$	initial mole fraction of xenon
	P_{gas}	inner gas pressure [Pa]
	T_{av}	volume average temperature [K]
	R	universal gas conetant = 8.314 [J/(K·mol)]
	V_{pl}	volume of the plenum [m^3]
	V^j_{gap}	volume of the gap between fuel and cladding in axial segment j [m^3]
	V^j_h	volume of the central hole in axial segment j [m^3]
	V^j_{int}	volume of the internal void in the fuel in axial segment j [m^3]
	T_{pl}	plenum temperature [K]
	T^j_{gap}	gap temperature between fuel and cladding in axial segment j [K]
	$\bar{T}_f$	volume average temperature of the fuel [K]
4.2	B	strain-displacement matrix
	$\{\sigma\}$	stress vector
	$\{\varepsilon\}$	strain vector
	$\{\Delta\varepsilon^{ne}\}$	incremental non-elastic strain vector
	β	non-elastic strain rate vector
	D	stress-strain matrix
	$\{F\}$	external force vector
	ψ	non-linear descrete eguation operator
	n	time step number
	$\{\Delta\varepsilon^e_{n+1}\}$	incremental elastic strain vector during the time interval Δt_{n+1}
	$\{\Delta\sigma_{n+1}\}$	incremental stress vector during the time interval Δt_{n+1}
	$C_{n+\theta}$	strain-stress matrix expressed as an intermediate between C_n and C_{n+1}
	$n+\theta$	intermediate point between t_n and t_{n+1}
	Δt_{n+1}	time interval between the time t_n and t_{n+1}
	$\{\Delta\varepsilon_{n+1}\}$	incremental total strain vector druing the time interval Δt_{n+1}
	$\{\Delta\varepsilon^c_{n+1}\}$	incremental creep strain vector during the time interval Δt_{n+1}
	$\{\Delta\varepsilon^p_{n+1}\}$	incremental plastic strain vector during the time interval Δt_{n+1}
	$\{\Delta\varepsilon^0_{n+1}\}$	incremental free expansion strain vector during the time interval Δt_{n+1}
	$\{\Delta u_{n+1}\}$	incremental nodal displacement vector during the time interval Δt_{n+1}
	ψ	non-linear descrete equation operator
	i	iteration number
	$\{du^{i+1}_{n+1}\}$	increments of nodal displacements during the iteration i and $i+1$
	$\{d\sigma^{i+1}_{n+1}\}$	increments of stresses during the iteration i and $i+1$
	$\dot{\bar{\varepsilon}}^c$	uniaxial creep strain rate
	f	creep function
	$\bar{\sigma}$	equivalent stress
	$\bar{\varepsilon}^c$	total creep strain (equivalent creep strain)

Chapter Paragraph	Symbol	Description
4.2	T	temperature
	ϕ	fast neutron flux
	$\{\dot{\varepsilon}^c\}$	creep strain rate vector
	$\{\sigma'\}$	deviatoric stress vector
	F, G, H and N	anisotropic coefficients
	α	hot pressing parameter
	σ_r	radial stress
	σ_z	axial stress
	σ_θ	circumferential stress
	τ_{rz}	shear stress
	$\hat{D}^i_{n+\theta}$	elastic and creep matrix computed by intermediate values between t_n and t_{n+1}
	h	yield function
	Q	plastic potential function
	$\bar{\varepsilon}_p$	equivalent plastic strain
	$\Delta\lambda_{n+1}$	proportionality constant during the time interval Δt_{n+1}
	$\hat{D}^{p,i}_{n+\theta}$	elasto-plastic and creep matrix computed by intermediate values between t_n and t_{n+1}
	E_r, E_z and E_θ	elastic moduluses during cracking in radial, axial, and circumferential directions respectively
	E	elastic modulus in uncracked condition
	ν	poisson's ratio
	E_c	elastic modulus in completely cracked condition
	j	principal direction
	ε^{rel}_j	initial relocation strain in the j direction
	$\Delta\varepsilon^p_{h,n+1}$	incremental volumetric strain due to plastic hot pressing during the time interval Δt_{n+1}
	$\Delta\varepsilon^c_{h,n+1}$	incremental volumetric strain due to creep hot pressing during the time interval Δt_{n+1}
	$\Delta\varepsilon_{h,n+1}$	incremental volumetric strain due to plastic and creep hot pressing during the time interval Δt_{n+1}
	$K^i_{n+\theta}$	finite element stiffness matrix
	$\{\Delta F^i_{n+1}\}$	force vector
	$\{\delta_i\}$	displacement vector of node i
	u_i	radial displacement of node i
	v_i	axial displacement of node i
	$\{\delta\}^e$	element nodal displacement vector
	$\{\delta\}$	displacements at arbitrary point within the element
	N	displacement (shape) function
	I	2 × 2 indentity matrix
	ξ, η	normalized co-ordinates
	r_i, z_i	actual co-ordinates of node i
	ε_r, ε_z, ε_θ, and γ_{rz}	radial, axial, circumferential, and shear strains respectively
	J	Jacobian matrix

Chapter paragraph	Symbol	Description
4.2	n	number of integrating points in the ξ direction
	m	number of integrating points in the η direction
	ξ_i, η_i	integrating positions
	H_i, H_j	quadrature weighting coefficients
4.3	$\{v\}$	axial displacement vector
	$\{u\}$	radial diaplacement vector
	v_c	cladding axial dixplacement
	$\{I\}$	unit vector
	P_w	coolant pressure
	P_{gas}	inner gas pressure
	U_f, U_c	radial contact forces. Subscripts refer to fuel and cladding respectively.
	V_f, V_c	axial contact forces
	V^{pp}	axial reaction force between pellet and pellet
	δ	radial gap between fuel and cladding
	n	time step number
	t	time
	$\Delta u_f, \Delta u_c$	increments of radial displacements of fuel and cladding respectively after contact
	$\Delta v_f, \Delta v_c$	increments of axial displscements of fuel and cladding respectively after contact
	μ	friction coefficient between fuel and cladding
	δ^{pp}	gap between pellet and pellet
	$t_{n+\alpha}$	intermediate time between t_n and t_{n+1}
	$\{\Delta v\}^{pp}$	increments of axial displacement vector of all nodes on the pellet-pellet interface
	$\Delta\bar{v}^{pp}$	increment of axial displacement of contact nodes on the pellet-pellet interface
	$K_{n+\theta}$	global stiffness matrix computed by intermediate values between t_n and t_{n+1}
	i, j	row positions corresponding to radial and axial components of fuel contact node
	k, l	row positions corresponding to radial and axial components of cladding contact node
	U_{n+1}, V_{n+1}	radial and axial contact forces between fuel and cladding at the time t_{n+1}
	$K_{n+\theta}^{(i)}$	ith row of matrix $K_{n+\theta}$
	$\Delta\bar{F}_{n+1}^{(i)}$	radial component of nodal forces of fuel contact node
	$\Delta\bar{F}_{n+1}^{(j)}$	axial component of nodal forces of fuel contact node
	$\Delta\bar{v}_{f,n+1}$	incremental axial displacement of contact nodes on the pellet-pellet interface
	$\Delta\bar{v}_{c,n+1}$	incremental axial displacement of nodes on the top of cladding
	$\bar{V}$	axial force induced by the axial restraint condition
	E_f	Young's modulus for fuel
	E_c	Young's modulus for cladding

Chapter paragraph	Symbol	Description
5.2	ν_f	poisson's ratio for fuel
	ν_c	poisson's ratio for cladding
	σ_Y	yield stress
	σ_{Y0}	0.2% yield stress
	n	strain hardening exponent
	σ_{Y0}^{t}	out-of-pile 0.2% yield stress
	$\Delta\sigma_{Y0}^{irr}$	increment of 0.2% yield stress due to irradiation induced hardening
	F	fission rate
	R	gas constant = 1.987 [cal/(mol·K)]
	Q	activation energy for diffusion
	G	grain size

Appendix A : Code Construction

The code consists of the MAIN program and many subroutines. The MAIN program deceides the necessary memory size and sets the address of variables. The real calculation is done in the subroutine FEMAX3 which is called by MAIN program.

The tree structure of the FEMAXI-III subroutines is shown in **Fig. A1**, which shows how they are called and the flow of them, together with the brief description of their functions.

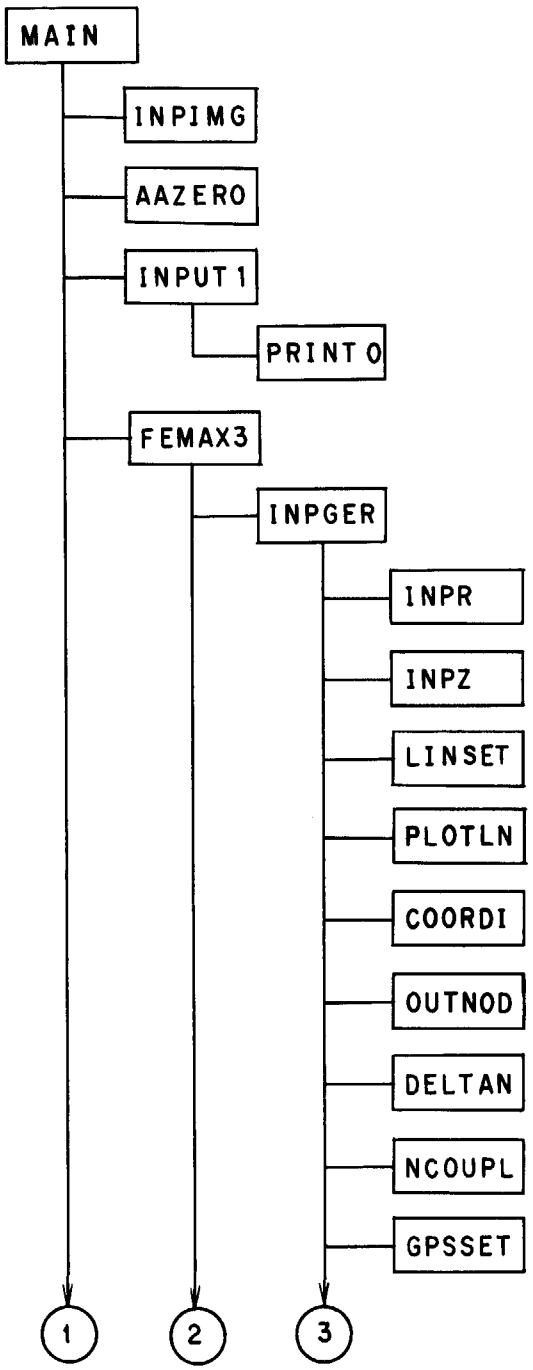

Set the address of variable dimension.

Print the list of input data.

Zero-set of variables in labelled common.

Parameters input except operating conditions.

Print the input parameters.

Control the whole calculation procedure.

Generate the finite element meshes.

Set the radial coordinates of meshes.

Set the axial coordinates of meshes.

Set the connection table between boundary nodes and related elements.

Print the map of finite element meshes.

Set the coordinates of nodal points.

Print the coordinates of nodal points.

Set the connection table between nodal points and elements.

Set the node couples between fuel and cladding during contact conditions.

Determine the total number of freedoms of nodal points.

Fig. A1 Structure of FEMAXI-III Code.

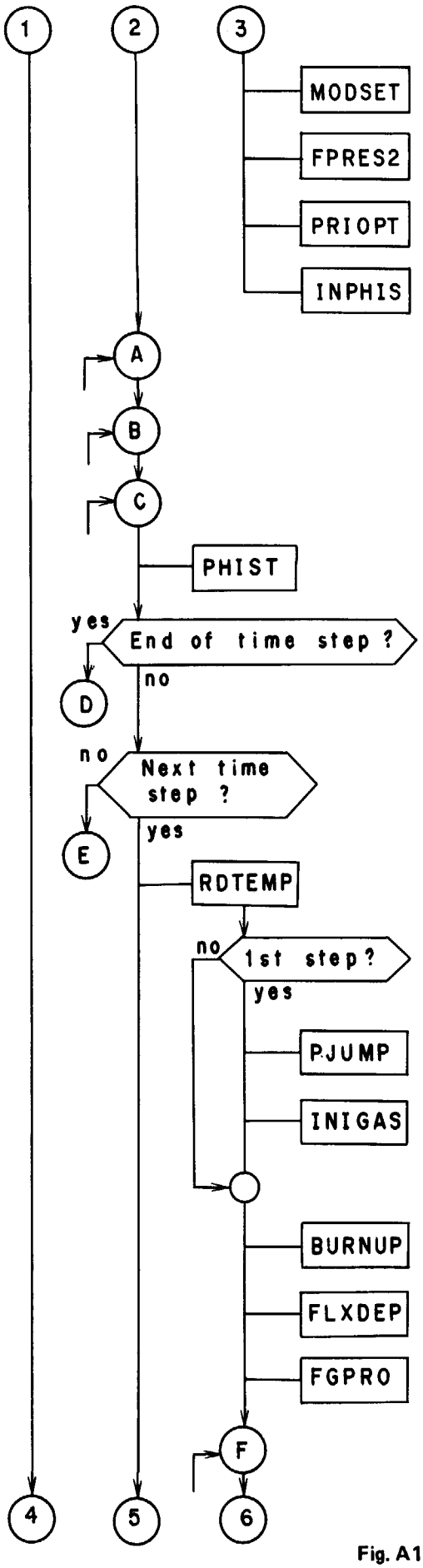

Determine the total memory size for global stiffness matrix.

Calculate the covering area of boundary nodal points.

Print the optional parameters.

Input the operating conditions.

Beginning of time step loop.

Beginning of time step cut iterations.

Beginning of sliding/bonding iteration.

Control the time step.

End of time step ?

Next time step ?

Thermal analysis part.

1st time step ?

Calculate the gap size after initial relocation.

Calculate the free volume and initial gas content.

Calculate the burnup.

Calculate the flux depression in the fuel.

Calculate the produced gaseous fission product.

Beginning of gas release iteration loop.

Fig. A1 Continued.

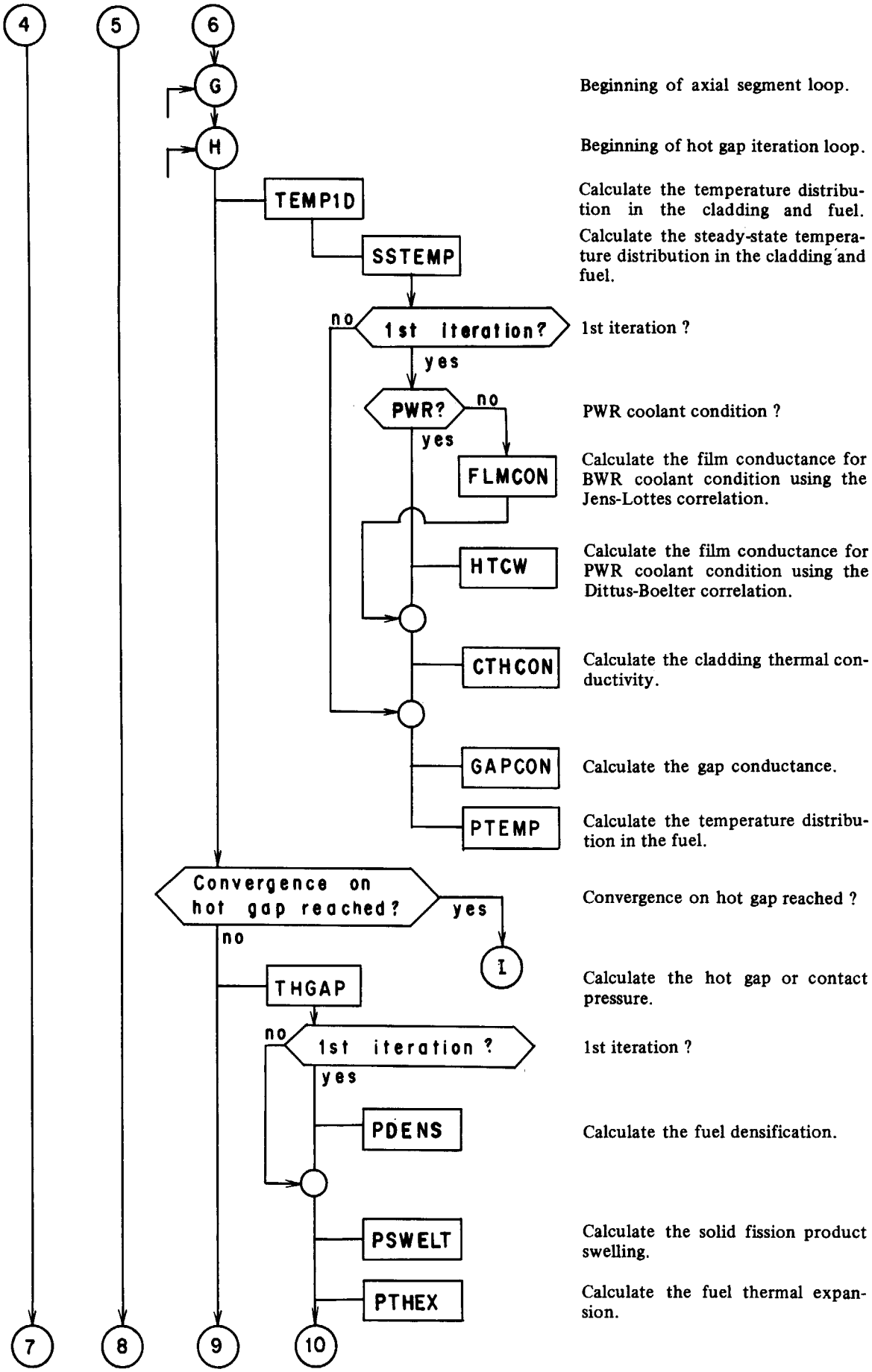

Fig. A1 Continued.

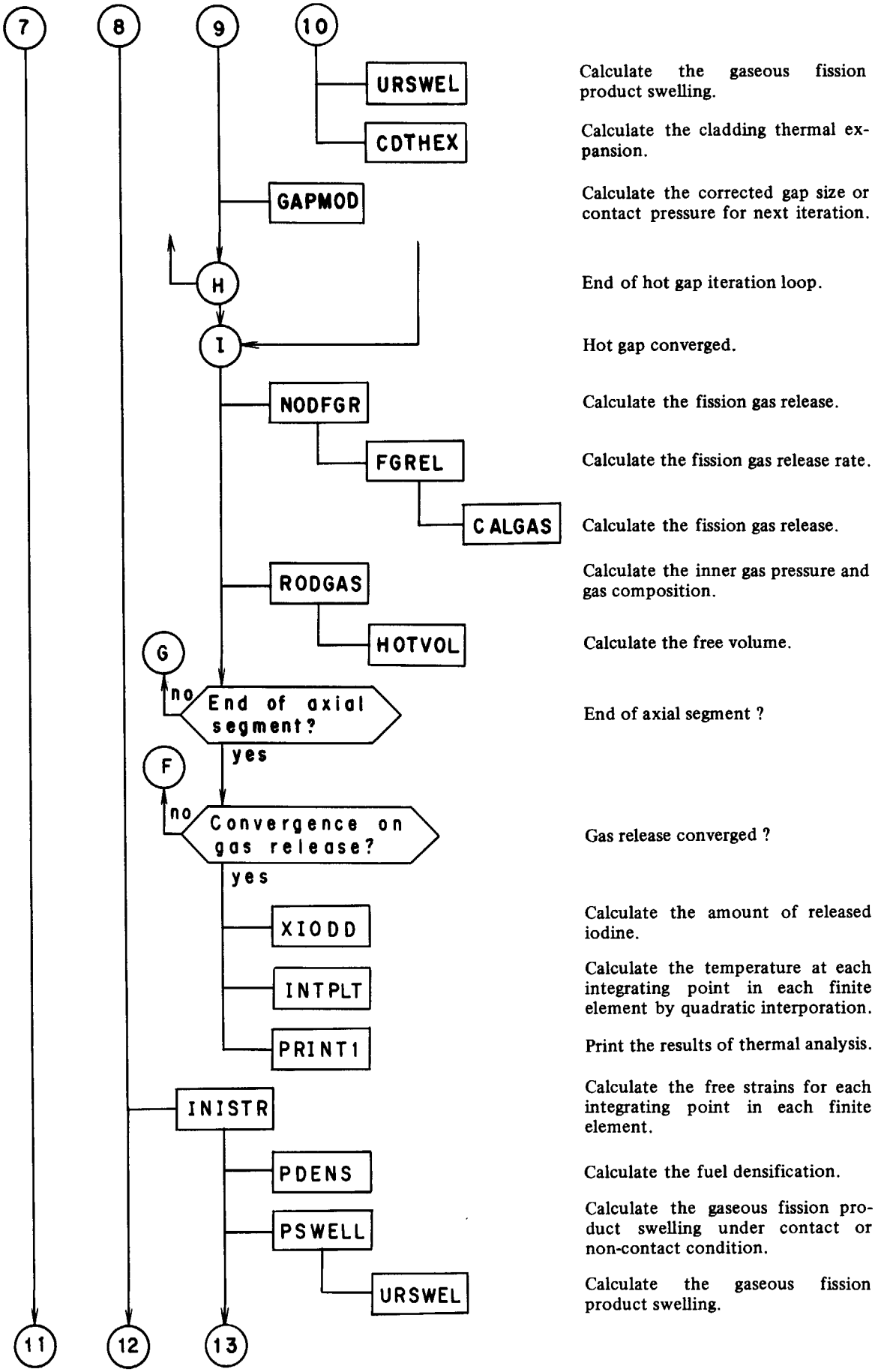

Fig. A1 Continued.

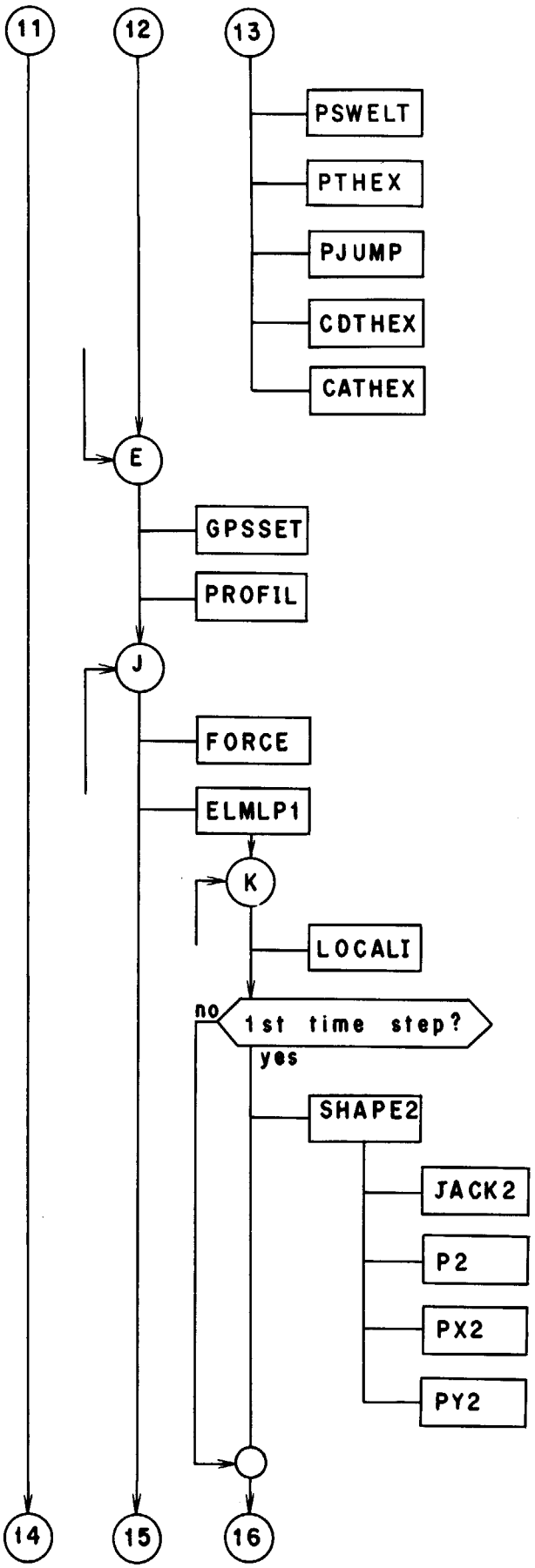

Calculate the solid fission product swelling.

Calculate the fuel thermal expansion.

Calculate the gap size after initial relocation.

Calculate the cladding diametral thermal expansion.

Calculate the cladding axial thermal expansion.

Start the time step cut iteration for mechanical analysis.

Set the connection table between nodal points and vector numbers in global matrix.
Set the connection table between vector numbers and coefficient numbers in global matrix.

Beginning of the Newton-Raphson iteration loop.

Calculate the nodal force vectors.

Set the stiffness matrix and force vectors.

Beginning of the finite element loop.

Read the all mechanical imformations at each integrating point, such as stress, strain, etc.

1st time step ?

Set the shape function.

Set the Jacobian matrix.

Calculate the N_i values.

Calculate the $\partial N_i / \partial \xi$ values.

Calculate the $\partial N_i / \partial \eta$ values.

Fig. A1 Continued.

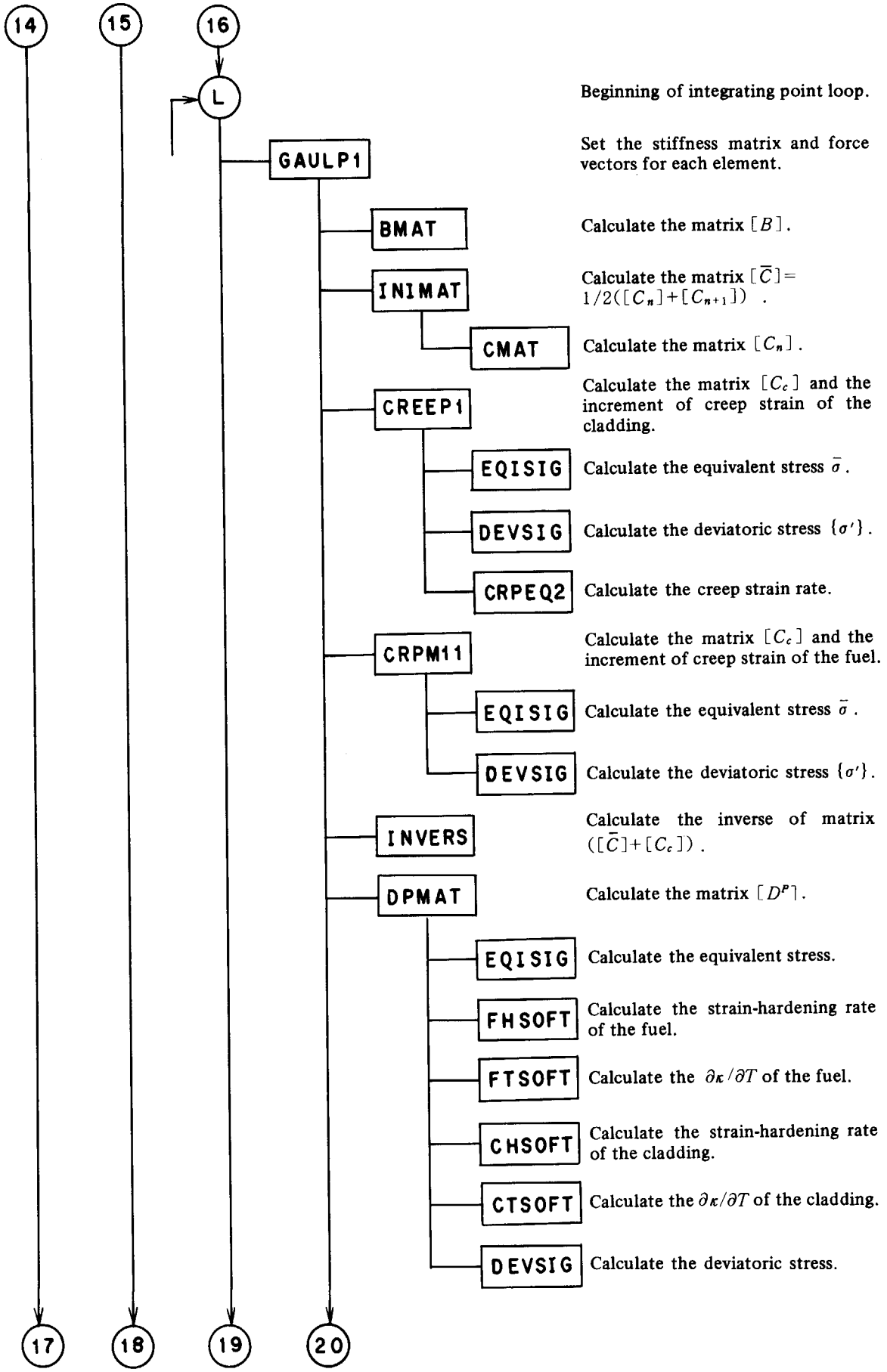

Fig. A1 Continued.

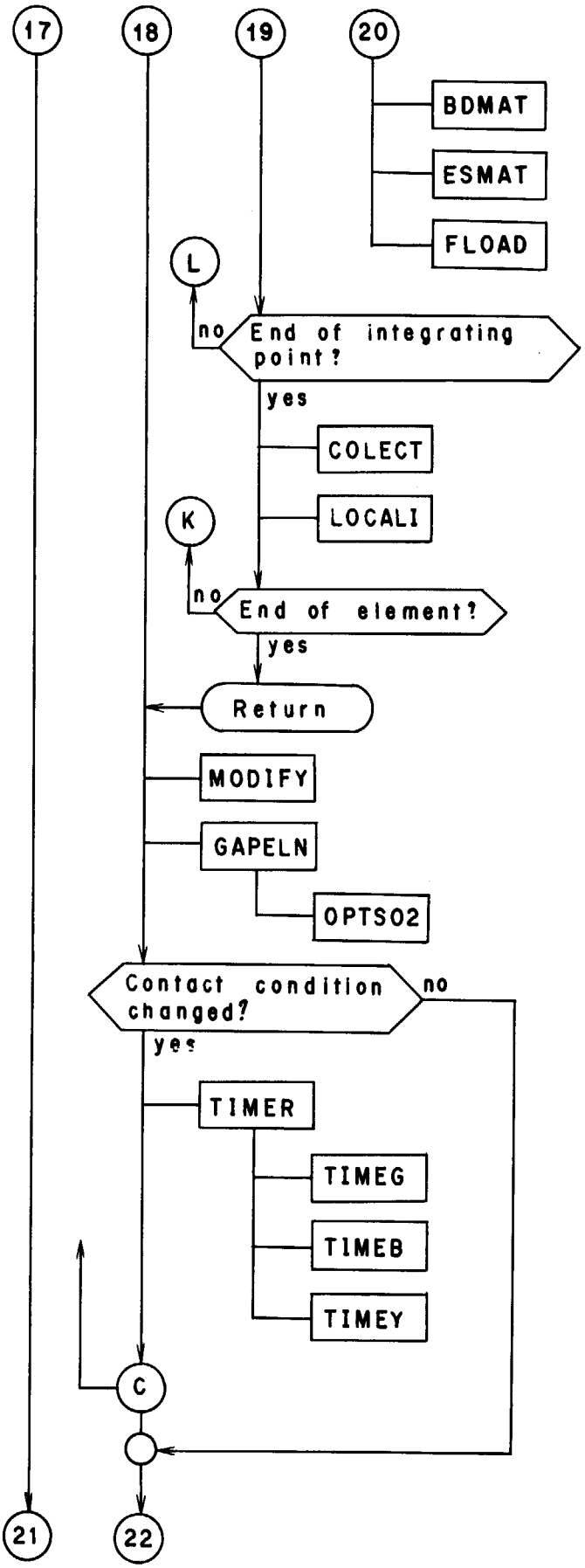

Calculate the matrix $[B^T][D^P]$.

Calculate the stiffness martix $[K_e]$.

Calculate the nodal force vectors $\{F_e\}$.

End of integrating point loop ?

Store the element stiffness matrix and nodal force vectors into the global matrix and force vector.
Store the all mechanical informations at each integrating point, such as stress, strain, etc.

End of element loop ?

Set the boundary conditions.

Set the boundary conditions in the next step.

Solve the linear equations.

Contact condition changed ?

Set only the boundary condition in the next sliding/bonding iteration, here.
Set the next boundary condition between fuel and cladding in the next time step.
Set the next boundary condition at upper surface of fuel in the next time step.

Set the material condition, elastic or yielding, in the next time step.

Fig. A1 Continued.

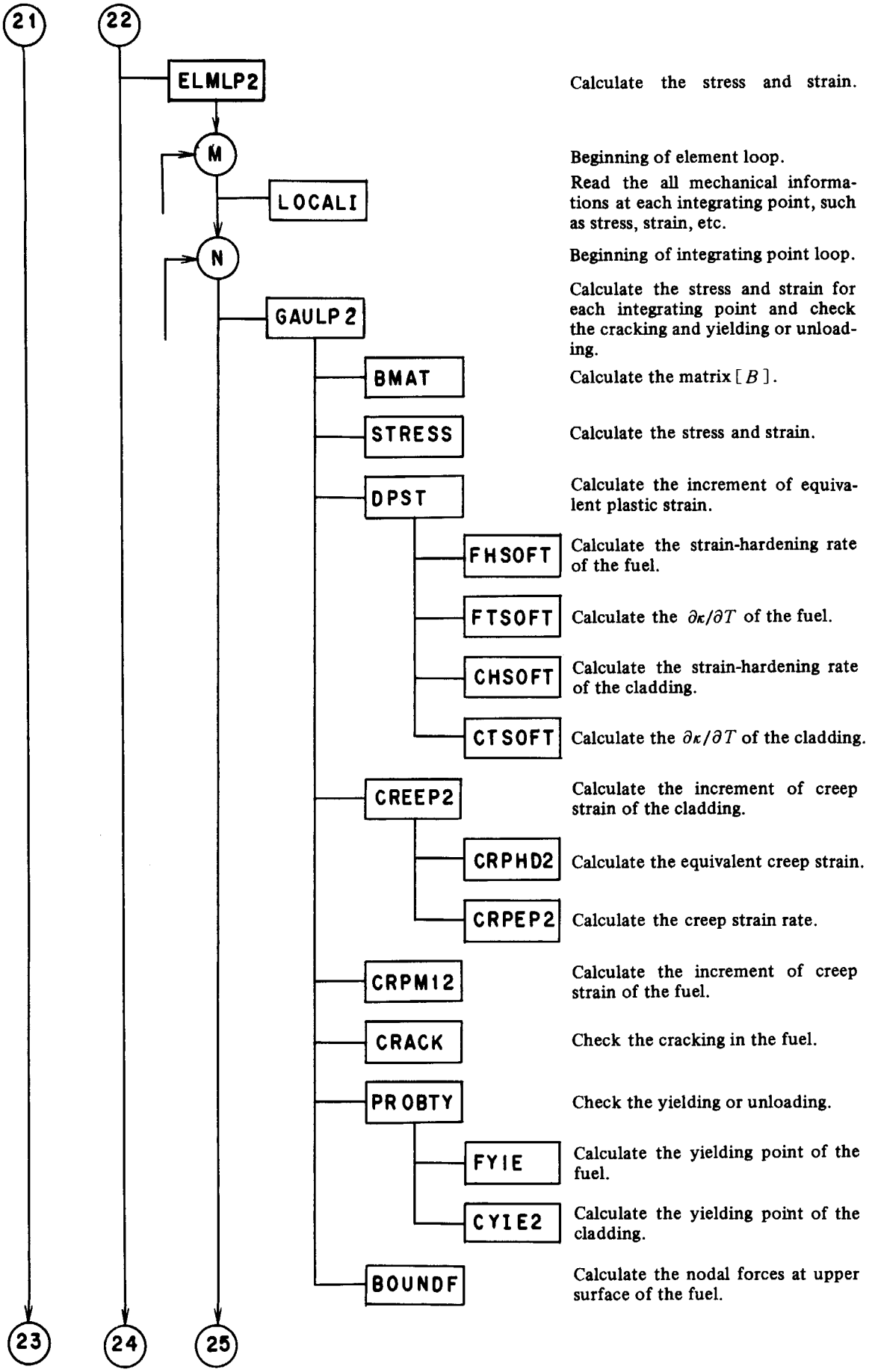

Fig. A1 Continued.

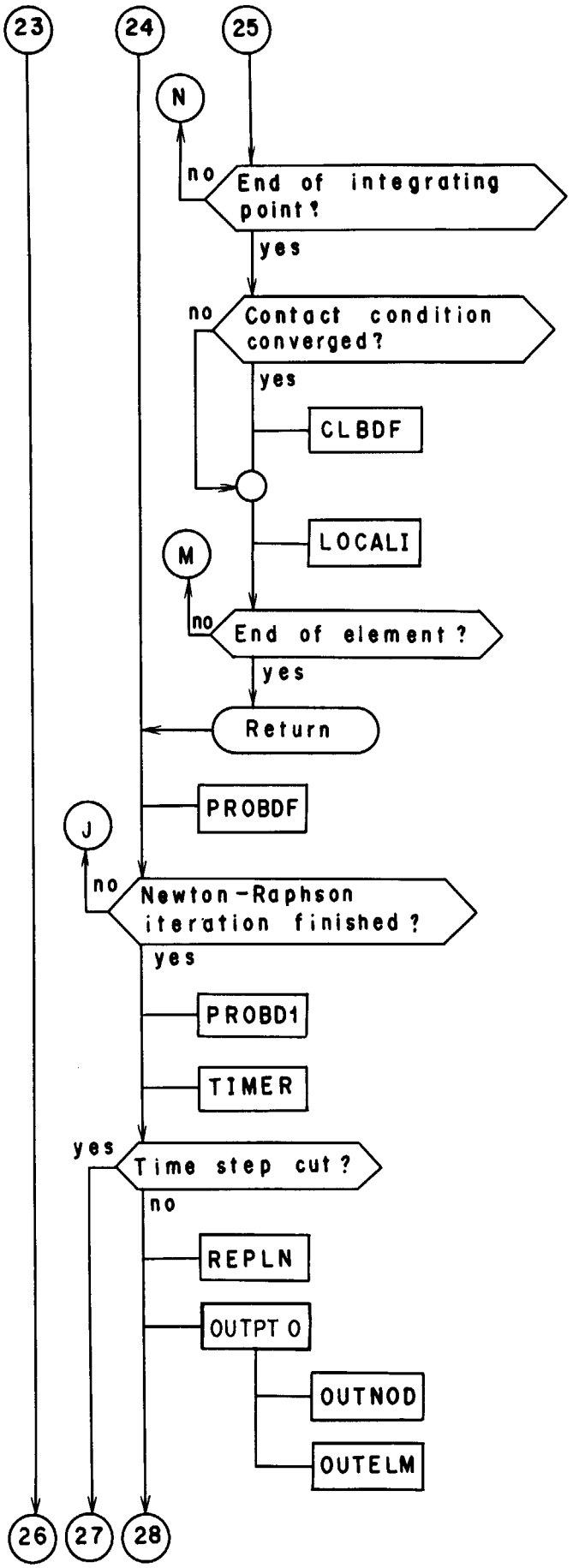

End of integrating point loop ?

Contact condition converged ?

Calculate the nodal forces on the fuel boundary surfaces.

Store the all mechanical informations at each integrating point.

End of element loop ?

Set the boundary conditions of fuel and cladding.

Newton-Raphson iteration finished ?

Calculate the factors of time step for pellet-pellet interaction.

Set the minimum factor of time step cut and the boundary conditions and material conditions in the next time step.

Time step cut ?

Linear interporation of temperatures, free strains, etc.

Print the results of mechanical calculations.

Print the nodal displacement.

Print the stresses and strains in the elements.

Fig. A1 Continued.

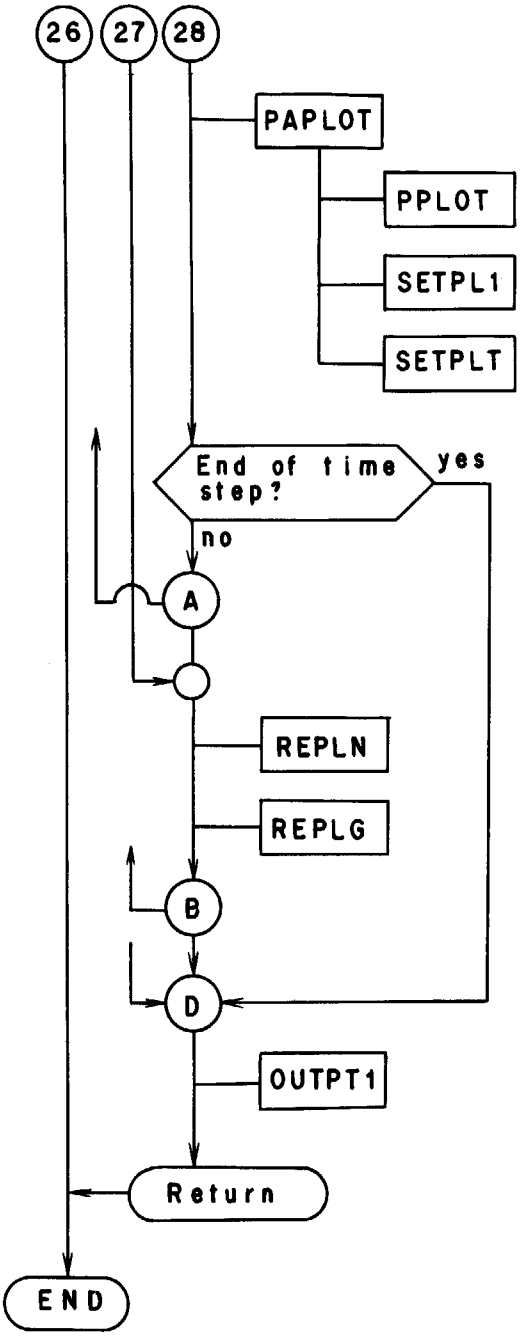

Plot the radial deformations of fuel and cladding and plot the cracking and yielding map.

Plot the radial deformations of fuel and cladding.

Plot the frame of the map.

Plot the symbols of yielding and cracking for each integrating point in each element.

End of time step ?

Linear interporation of temperatures, free strains, etc. at each node.

Linear interporation of temperatures, free strains, etc. at each integrating point.

End of time step cut iteration loop.

End of time step loop.

Print the calculational results.

End of calculation.

Fig. A1 Continued.

Appendix B : FEMAXI-III Input

The input deck of the FEMAXI-III code consists of

1) A title card,
2) A namelist card,
3) Data cards,
4) History cards,
5) A stop card at the end.

The parameters in the namelist card include constants peculiar to the specific models, variable storage sizes, and optional parameters for restart and output.

The parameters in the data cards include the geometrical description of the fuel element and several material parameters.

The history cards include the operational history of the reactor. The variation of power and related coolant temperature between input history is assumed linear by the code.

The input parameters are listed in **Table A1** in the order required by the code. A short description of the parameters is also given in **Table A1**. The parameters in the namelist are described in **Table A2**. A sample input of FEMAXI-III is shown in **Table A3**.

(1) Restart Option

The restart option in FEMAXI-III is used for a problem with long-term irradiation that is difficult to finish the calculation within a limited running time at one time. **Fig. A2** shows that the use of restart option provides the user with the ability to run a problem dividing into a several parts. A restrart run follows a previous run whose results of calculations are stored on some permanent device such as the disk file. These run differs from a usual run in the following:

- control cards;
- setting the namelist variables for restart.

The control cards must indicate to the computer system that the disk files are needed to read and write the results of calculations.

The namelist variables INTST, IREST, NREC1, and NERC5 must be set according to the case. As described in **Table A1**, if INTST is set to 1, calculational results are written on the disk file. This disk file number must be set by the variable NREC5. The initial stored value of NREC5 is 12.

If IREST is set to 1, calculational results stored on the disk file are read to execute a restart run. For the restart run, the disk file number, on which the results of calculations obtained in the previous run are stored is defined by the variable NREC1. The initial stored value of NREC1 is 11. If the previous results are stored on the disk file 12, the value NREC1 must be changed to 12.

The history data for the restart run is needed to set from the 1st time step to the specified time step at which the restart run is stopped. The other inputs such as the geometrical data must be also set as same as the previous run. Therefore, a complete set of input including the full history data must be set for the final restart run.

Table A1 Input Parameters for FEMAXI-III

Card No.	Format	Symbol	Description
1	20A4	MTITL(I), I = 1, 20	Title of the calculation
2			Namelist card. See **Table A2**.
3	3I10	NAX	Number of axial segments ($1 \leq NAX \leq 12$).
		IFEM	Axial segment number at which FEM mechanical analysis is performed ($1 \leq IFEM \leq 12$).
		IPLANT	Option number for reactor type. 1 = HBWR, 2 = BWR, 3 = PWR. Currently uniform heat generation is assumed in the case that IPLANT is selected as 3 (PWR).
4	I10, 2F10.0	MRASA	Option number for cladding type. 0 = recrystallized cladding tube, 1 = stress-relieved cladding tube.
		CDIN	Cladding inner diameter (cm).
		CDOUT	Cladding outer diameter (cm).
5	2I10, 6F10.0	IDISH(I)	Option number for dishing type. 0 = non-dished, 1 = dished at one end, 10 = all pellets are dished at one end, and you can omit the input of this variable after the 2nd card, 2 = dished at both ends, 20 = all pellest are dished at both ends, and you can omit the input of this variable after the 2nd card.
		ICHAM(I)	Option number for chamfering type. 0 = non-chamfered, 1 = chamfered, 10 = all pellets are chamfered, and you can omit the input of this variable after the 2nd card.
		PDIN(I)	Fuel inner diameter (cm). If all pellets have a same inner diameter, you shoud set this variable as a minus value. Then you can omit the input of this variable after the 2nd card.
		PDOUT(I)*	Fuel outer diameter (cm).
		PLENG(I)*	Fuel length (cm).
		ENR(I)*	Enrichment of U^{235} (fraction).
		FDEN(I)*	Fraction of theoretical density.
		DZ(I)*	Length of axial segment (cm).
			You must set this card repeatedly "NAX" times (NAX is defined in Card 3). You can omit the input of variables with * after the 2nd card, if the value is same as previous one.
	For non-dished pellet, you must omit the card 6.		

Table A1 Continued

Card No.	Format	Symbol	Description
6	3F10.0	DISH	Dishing diameter (cm).
		DEPTH	Dishing depth (cm).
		DISHB	Diameter of dish bottom (cm).
For non-chamfered pellet, you must omit the card 7.			
7	2F10.0	CHAMR	Chamfer width (cm).
		CHAMZ	Chamfer height (cm).
8	7F10.0	PLENUM	Plenum volume (cm^3).
		GPIN	Initial inner gas pressure (MPa).
		GMIXO(1)	Initial fraction of helium gas.
		GMIXO(2)	Initial fraction of nitrogen gas.
		GMIXO(3)	Initial fraction of krypton gas.
		GMIXO(4)	Initial fraction of xenon gas.
		PWEIT	Total weight of fuel stack (gram).
9	I10	NHIST	Number of time step
10**	6F10.0, 2I5	A1	Time (hr).
		B1	Burnup. Unit of variable B1 is defined by the parameter IBUNP in the namelist. MWd/tUO_2, if IBUNP = 0, MWd/tU , if IBUNP = 1, GJ/kgU , if IBUNP = 2. You must set either A1 or B1.
		A2	Linear heat rate (W/cm).
		A5*	Fast neutron flux ($n/cm^2/sec$).
		A3*	Coolant temperature (K).
		A4*	Coolant pressure (MPa).
		IT	Optional number for the input of history data. If IT is set as 0, the time A1 (or burnup B1) is regarded as the time (or burnup) from the 1st time step or the last time step after which IT is set as −100. If IT is set as −100, the time A1 (or burnup B1) is regarded as the time increment (or burnup increment) from the previous time step. If IT is set as 100, the time A1 (or burnup B1) is regarded as the time (or burnup) from the 1st time step.
		IP	Option number for the output. 0 = detailed output is not made, $\geqq$1= detailed output is made for this time step. You can omit the input of variables with * after the 2nd card if the value is same as previous one. However you can not omit the input at the final time step for the power A2 and the fast neutron flux A5. For the input of power, it is not allowed to set 0. You must set 0.001 instead of 0.

Table A1 Continued

Card No.	Format	Symbol	Description
11**	12F5.0, I5	RH(I), I = 1, 12	Relative axial power distribution.
		II	Number of time steps which have the same axial power distribution. If the power distribution does not change for the next "II" steps (including this step), you can omit this card "II-1" times.
Caption ** : You must set a couple of cards (Card 10 & 11) "NHIST" times. But you can omit Card 11 if "II" is specified at the previous time step.			
12	A4	IEND	This is the termination card. You must write "STOP" from the 1st to 4th columns.

Table A2 Namelist parameters for FEMAXI-III

Parameter	Description	Stored value
IREST	Option number for restart run. 0 = restart run is not done, 1 = restart run is done.	0
INTST	Option number for writing of results on the disk file. 0 = results is not stored on the disk file, 1 = results is stored on the disk file.	0
NREC5	Disk file number for writing the results.	12
NREC1	Disk file number for reading the results.	11
ICK1	Option number for the analysis. 0 = thermal and FEM mechanical analysis is done, 1 = FEM mechanical analysis is not done (only thermal analysis is done).	0
IBUNP	Option number for defining the unit of burnup in the input. 0 = MWd/tUO_2, 1 = MWd/tU, 2 = GJ/kgU.	0
INPCK	Option number for checking the input. 0 = usual run is made, 1 = only input is checked (calculation is not done).	0
NGR2	Memory size to store the values of produced gases and release fractions at each time step.	5000
NGR3	Table size storing the address of values of produced gases and release fractions.	300
CRFAC	Acceleration factor for the creep strain rate of cladding in the PWR fuel rods.	1.3
DMAX	Increased density in the resintering test (1700 °C X 24 hr), (%).	1.0
DE	Equivalent hydraulic diameter of the coolant channel (cm).	1.18
V	Innlet velocity of coolant (cm/sec).	500

Table A2 Continued

Parameter	Description	Stored value
IPH	Option number to determine the increment of power during the time interval.	0
	0 = power increment is determined at the segment where FEM analysis is performed.	0
	1 = power increment is determined at the segment where the power is the highest.	
IOPT1	Option number to define the presence of bottom plenum.	0
	0 = there is not the bottom plenum,	
	1 = there is the bottom plenum.	
SBU	Burnup at which densification terminates (MWd/tUO_2).	2500
IWREL(I),	Option number for the output of stresses and strains at each integration point in each finite element at the specified time step.	
	0 = output is not made,	
	1 = output is made.	
IWREL(1)	radial stresses (σ_r).	0
IWREL(2)	axial stresses (σ_z).	1
IWREL(3)	circumferential stresses (σ_θ).	1
IWREL(4)	shear stresses (τ_{rz}).	0
IWREL(5)	equivalent stresses ($\bar{\sigma}$).	1
IWREL(6)	yield stresses (σ_Y).	0
IWREL(7)	radial strains (ε_r).	0
IWREL(8)	axial strains (ε_z).	0
IWREL(9)	circumferential strains (ε_θ).	0
IWREL(10)	shear strains (γ_{rz}).	0
IWREL(11)	equivalent plastic strains ($\bar{\varepsilon}^p$).	1
IWREL(12)	radial creep strains (ε_r^c).	0
IWREL(13)	axial creep strains (ε_z^c).	0
IWREL(14)	circumferential creep strains (ε_θ^c).	1
IWREL(15)	radial elastic strains (ε_r^e).	0
IWREL(16)	axial elastic strains (ε_z^e).	0
IWREL(17)	circumferential elastic strains (ε_θ^e).	0
IWREL(18)	radial thermal strains (ε_r^{th}).	0
IWREL(19)	axial thermal strains (ε_z^{th}).	0
IWREL(20)	strains by densification (ε^{den}).	0
IWREL(21)	strains by swelling (ε^{sw}).	0
IWREL(22)	Young's modulus in the radial direction.	0
IWREL(23)	Young's modulus in the axial direction.	0
IWREL(24)	Young's modulus in the circumferential direction.	0

Table A3 Sample Input for FEMAXI-III

```
                                  I N P U T    D A T A    L I S T
                                  -------------------------------
                    1         2         3         4         5         6         7         8
CARD NO. ....5....0....5....0....5....0....5....0....5....0....5....0....5....0....5....0
      1. *** FEMAXI-III SAMPLE CALCULATION ***
      2.  ¥INPUT ICK1=0 ¥END
      3.          10         5         3
      4.           1    0.8360    0.9511
      5.           2         0       0.0     0.819     1.344    0.0826    0.9516     9.828
      6.           2         0       0.0     0.819     1.344    0.0826    0.9516     9.828
      7.           2         0       0.0     0.819     1.344    0.0826    0.9516     9.828
      8.           2         0       0.0     0.819     1.344    0.0826    0.9516     9.828
      9.           2         0       0.0     0.819     1.344    0.0826    0.9516     9.828
     10.           2         0       0.0     0.819     1.344    0.0826    0.9516     9.828
     11.           2         0       0.0     0.819     1.344    0.0826    0.9516     9.828
     12.           2         0       0.0     0.819     1.344    0.0826    0.9516     9.828
     13.           2         0       0.0     0.819     1.344    0.0826    0.9516     9.828
     14.           2         0       0.0     0.819     1.344    0.0826    0.9516     9.828
     15.       0.595      0.03       0.0
     16.         5.2      1.38       1.0       0.0       0.0       0.0     531.1
     17.          14
     18.         0.0                0.001  0.33E+14     534.1     13.73
     19.  0.56 0.76 0.92 0.99 1.00 0.99 0.99 0.92 0.78 0.61                 6
     20.         1.0               200.0                                        1
     21.                1000.0      200.0
     22.         0.5               150.0                                  -100
     23.                5000.0      150.0
     24.         1.0                0.001  0.33E+14     534.1     13.73 -100     1
     25.         0.5                0.001  0.80E+14     577.1     14.60 -100
     26.  0.22 0.57 0.85 0.99 1.00 0.75 0.52 0.35 0.11 0.05                 8
     27.         1.0               200.0                                        0
     28.        25.0               200.0                                        1
     29.        25.5               350.0                                        0
     30.        26.0               500.0                                        1
     31.        30.0               500.0                                        0
     32.        50.0               500.0                                        1
     33.        51.0                0.001  0.80E+14     577.1     14.60         1
     34. STOP
         ....5....0....5....0....5....0....5....0....5....0....5....0....5....0....5....0
```

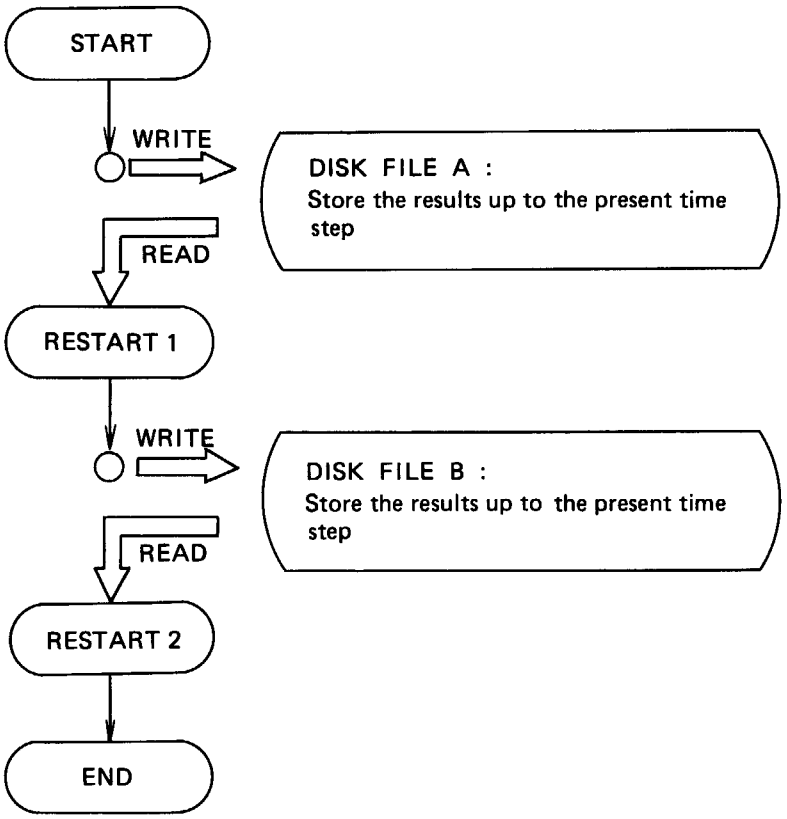

Fig. A2 Restart Option in FEMAXI-III.

Appendix C : Sample Output

```
                                   I N P U T    D A T A    L I S T
                                   -------------------------------
                        1         2         3         4         5         6         7         8
CARD NO. ....5....0....5....0....5....0....5....0....5....0....5....0....5....0....5....0....5....0
      1. *** FEMAXI-III SAMPLE CALCULATION ***
      2.  *INPUT ICK1=0 *END
      3.          5         3         3
      4.          1    0.8360    0.9511
      5.          2         0       0.0     0.819     1.344    0.0826    0.9516    19.656
      6.          2         0       0.0     0.819     1.344    0.0826    0.9516    19.656
      7.          2         0       0.0     0.819     1.344    0.0826    0.9516    19.656
      8.          2         0       0.0     0.819     1.344    0.0826    0.9516    19.656
      9.          2         0       0.0     0.819     1.344    0.0826    0.9516    19.656
     10.      0.595      0.03       0.0
     11.        5.2      1.38       1.0       0.0       0.0       0.0     531.1
     12.         14
     13.        0.0               0.001  0.33E+14     534.1     13.73
     14.  0.76 0.90 1.00 0.90 0.78                                         6
     15.        1.0               200.0                                         0
     16.               1000.0     200.0
     17.        0.5               150.0                                    -100
     18.               2000.0     150.0
     19.        1.0               0.001  0.33E+14     534.1     13.73 -100    0
     20.        0.5               0.001  0.80E+14     577.1     14.60 -100
     21.  0.57 0.90 1.00 0.75 0.52                                         8
     22.        1.0               200.0                                         0
     23.       25.0               200.0                                         1
     24.       25.5               350.0                                         0
     25.       26.0               500.0                                         1
     26.       30.0               500.0                                         0
     27.       50.0               500.0                                         0
     28.       51.0               0.001  0.80E+14     577.1     14.60         0
     29. STOP
         ....5....0....5....0....5....0....5....0....5....0....5....0....5....0....5....0
&INPUT
IREST=0,INTST=0,NGR2=5000,NGR3=300,INPCK=0,IBUNP=0,ICK1=0,DMAX=1.0000000000000000,SBU=2500.00000000000000,CRFAC=1.3000000000000004,DE=
1.17999999999999994,V=500.000000000000000,IPH=0,IWREL=0,1,1,0,1,0,0,0,0,0,1,0,0,1,0,0,0,0,0,0,0,0,0,0,0,IOPT1=0,NREC1=11,NREC5=12,
&END
```

```
-----------------------------------------------------------------------------
 *** FEMAXI-III SAMPLE CALCULATION ***
-----------------------------------------------------------------------------


P.W.R. FUEL ROD.

*INPUT DATA

(1) PELLET SPECIFICATIONS ----

 NODE      DIAMETER (CM)        SHAPE       U-235     FRACTIONAL    ONE PELLET      NODE
         INSIDE  OUTSIDE    CHAMF  DISH    ENRICH.     DENSITY     LENGTH (CM)     LENGTH (CM)
   1      0.0      0.819            **       0.083      0.952          1.344          19.656
   2      0.0      0.819            **       0.083      0.952          1.344          19.656
 * 3      0.0      0.819            **       0.083      0.952          1.344          19.656
   4      0.0      0.819            **       0.083      0.952          1.344          19.656
   5      0.0      0.819            **       0.083      0.952          1.344          19.656

 DISH DIAMETER (CM) =     0.595          DISH DEPTH    (CM) =     0.030          DISH BOTTOM   (CM) =     0.0
 PELLET TOTAL WEIGHT (GRAM)        =   531.100
 GRAIN SIZE (MICRON)               =    15.000
 MAXIMUM FRACTIONAL DENSITY        =     0.962
 SATURATE BURNUP (MWD/TUO2)        =  2500.000

(2) OTHERS

 CLAD. MATERIAL IS STRESS RELIEVED ZIRCALOY
 CLAD. INSIDE DIAMETER (CM)        =       0.836
 CLAD. OUTSIDE DIAMETER (CM)       =       0.951

 THERMAL RELOCATION (-)            =       0.300
 PLENUM VOLUME (CM**3)             =       5.200
 INITIAL GAS PRESSURE (MPA)        =       1.380

 INITIAL GAS COMPOSITION (PERCENT)
                         HELIUM  = 100.0
                         NITROGEN=   0.0
                         KRYPTON =   0.0
                         XENON   =   0.0
 PELLET SURFACE ROUGHNESS (CM)     =      0.0005
 CLADDING SURFACE ROUGHNESS (CM)   =      0.0001
 ROOM TEMPERATURE (DEG.K)          =    291.15
```

```
*********************************************************************************************************************************
*                                                                                                                               *
*    *** FEMAXI-III SAMPLE CALCULATION ***                                                    -- FEMAXI-III ( MOD-03 ) --       *
*                                                                                                                               *
*********************************************************************************************************************************


                             NODAL POINT AND ELEMENT CONNECTION MAP
                             ---------------------------------------

                            *** PELLET ***                  GAP     *** CLADDING ***

           7+ 11+ 18+ 22+ 29+ 33+ 40+ 44+ 51+ 55+ 62         I  69+ 73+ 80
          +       +       +       +       +       +            +       +
           6   3  17   6  28   9  39  12  50  15  61         I  68  18  79
          +       +       +       +       +       +            +       +
           5+ 10+ 16+ 21+ 27+ 32+ 38+ 43+ 49+ 54+ 60         I  67+ 72+ 78
          +       +       +       +       +       +            +       +
           4   2  15   5  26   8  37  11  48  14  59         I  66  17  77
          +       +       +       +       +       +            +       +
           3+  9+ 14+ 20+ 25+ 31+ 36+ 42+ 47+ 53+ 58         I  65+ 71+ 76
          +       +       +       +       +       +            +       +
           2   1  13   4  24   7  35  10  46  13  57         I  64  16  75
          +       +       +       +       +       +            +       +
           1+  8+ 12+ 19+ 23+ 30+ 34+ 41+ 45+ 52+ 56         I  63+ 70+ 74


                                                ***** NODAL COORDINATE (MICRON) *****


    (R-DIRECTION)                                                           GAP
    0.0  425.0  850.0 1275.0 1700.0 2125.0 2550.0 2975.0 3348.3 3721.7 4095.0I 4180.0 4467.7 4755.5
    0.0         850.0        1700.0        2550.0        3348.3        4095.0I 4180.0        4755.5
    0.0  425.0  850.0 1275.0 1700.0 2125.0 2550.0 2975.0 3348.3 3721.7 4095.0I 4180.0 4467.7 4755.5
    0.0         850.0        1700.0        2550.0        3348.3        4095.0I 4180.0        4755.5
    0.0  425.0  850.0 1275.0 1700.0 2125.0 2550.0 2975.0 3348.3 3721.7 4095.0I 4180.0 4467.7 4755.5
    0.0         850.0        1700.0        2550.0        3348.3        4095.0I 4180.0        4755.5
    0.0  425.0  850.0 1275.0 1700.0 2125.0 2550.0 2975.0 3348.3 3721.7 4095.0I 4180.0 4467.7 4755.5


    (Z-DIRECTION)                                                           GAP
 6420.0 6426.1 6444.3 6474.6 6517.3 6572.3 6639.8 6720.0 6720.0 6720.0 6720.0I 6720.0 6720.0 6720.0
 5350.0        5370.2        5431.1        5533.2        5600.0        5600.0I 5600.0        5600.0
 4280.0 4284.0 4296.2 4316.4 4344.9 4381.5 4426.5 4480.0 4480.0 4480.0 4480.0I 4480.0 4480.0 4480.0
 3210.0        3222.1        3258.6        3319.9        3360.0        3360.0I 3360.0        3360.0
 2140.0 2142.0 2148.1 2158.2 2172.4 2190.8 2213.3 2240.0 2240.0 2240.0 2240.0I 2240.0 2240.0 2240.0
 1070.0        1074.0        1086.2        1106.6        1120.0        1120.0I 1120.0        1120.0
    0.0    0.0    0.0    0.0    0.0    0.0    0.0    0.0    0.0    0.0    0.0I    0.0    0.0    0.0


                                       CALCULATIONAL VARIABLE TABLE (1)
                                      ----------------------------------
         CALCULATION OPTION
        --------------------
    NAME                                DESCRIPTION                                                 DIMENSION           VALUE
    ------                             -------------                                               -----------         -------
    IREST          RESTART OPTION (=0;NORESTART, =1;RESTART)                                            -                  0
    INTST          DRAW UP RESTART TAPE OPTION (=0;NO, =1;YES)                                          -                  0
    IPLT           DRAW UP PLOTTER TAPE OPTION (=0;NO, =1;YES)                                          -                  0
    NREC1          RESTART TAPE NUMBER                                                                  -                 11
    NREC2          PLOTTER TAPE NUMBER                                                                  -                  1
    DPXX           POWER INCREMENTAL WIDTH                                                             W/CM               10.0
    EFCOEF         TIME INCREMENTAL WIDTH PARAMETER (BE RESTRICTED FROM CREEP)                          -                 10.0
    ITEND          NEWTON-RAPHSON ITERATION COUNT                                                       -                  1
    KUMAX          BOUNDARY CONDITION ITERATION COUNT                                                   -                 10
    THETC          CREEP PARAMETER                                                                      -                  1.0
    THETP          YIELD PARAMETER                                                                      -                  0.5
    AY             TILTING VALUE                                                                        CM                 0.0
    AMU            PELLET/CLADDIND FRICTION COEF.                                                       -                  0.40
    ILOCK          LOCKING OPTION (=0;P/C GAP SIZE, =1;AXIAL COORDINATE)                                -                  0
    TROOM          ROOM TEMPERATURE                                                                    DEG.K             291.15
    IBUNP          BURNUP DIMENSION FLAG (=0;MWD/TUO2, =1;MWD/TU, =2;GJ/KGU)                            -                  0
    INPCK          INPUT DATA CHECK OPTION (=0;CALCULATION, =1;INPUT DATA CHECK)                        -                  0
    CRTM           OUTPUT DATA OPTION (FINAL INFORMATION GIVES AFTER CRTM)                              HR                 0.0
    ITIMG          BOUNDARY CONDITION TIME STEP CONTROL OPTION (=0;NO, =1;YES)                          -                  1
    ITIMY          ELASTIC/PLASTIC CONDITION TIME STEP CONTROL OPTION (=0;NO, =1;YES)                   -                  1
    IPH            POWER INCREMENTAL WIDTH ATTENTION NODE (=0;IFEM NODE,=1,MAXIMUM VARIABLE NODE)       -                  0
    ICK1           MECHANICAL CALCULATION OPTION (=0;CALCULATE, =1;NO CALCULATE)                        -                  0
    ICHI           ELASTIC CALCULATION OPTION (=0;NO, =1;YES)                                           -                  0
    IWREL          ELEMENT INFORMATION OUTPUT CONTROL TABLE (=0;OFF, =1;ON)                             -
      1   SIG(R)      0       2   SIG(Z)      1       3   SIG(T)      1       4   SIG(RZ)     0       5   EQ.SIG      1
      6   SIGY        0       7   EPS(R)      0       8   EPS(Z)      0       9   EPS(T)      0      10   EPS(RZ)     0
     11   EPSP        1      12   EPSC(R)     0      13   EPSC(Z)     0      14   EPSC(T)     1      15   EPSE(R)     0
     16   EPSE(Z)     0      17   EPSE(T)     0      18   EPSTH(R)    0      19   EPSTH(Z)    0      20   EPSDEN      0
     21   EPSSWL      0      22   ELAST(R)    0      23   ELAST(Z)    0      24   ELAST(T)    0

         DIMENSION INFORMATION
        -----------------------
    NAME                                DESCRIPTION                                                 DIMENSION           VALUE
    ------                             -------------                                               -----------         -------
    LASR           RIAL DIMENSION AREA (USED)                                                           -              23263
    LD             RIAL DIMENSION AREA (DEFINED)                                                        -              46600
    LASI           INTEGER DIMENSION AREA (USED)                                                        -               7607
    LDI            INTEGER DIMENSION AREA (DEFINED)                                                     -              10000
    NODE           NODAL POINT NUMBER                                                                   -                 80
    NOD2           NODAL POINT FREEDUM NUMBER                                                           -                160
    NELM           ELEMENT NUMBER                                                                       -                 18
    NPAR           GAP PAIR NUMBER                                                                      -                  7
    NMAX           SYMMETRIC MATRIX FREEDUM NUMBER                                                      -                137
    NMY            NON-SYMMETRIC MATRIX FREEDUM NUMBER                                                  -                 14
    NMK            BOUNDARY PAIR NUMBER                                                                 -                  6
    MAX            SYMMETRIC MATRIX AREA                                                                -               2806
```

NCR	NON-SYMMETRIC MATRIX AREA	-	291
MM	CLADDING LAYER NUMBER	-	1
NN	PELLET LAYER NUMBER	-	5
KK	AXIAL LAYER NUMBER	-	3
NAX	AXIAL NODE NUMBER	-	5
NHIST	TIME HISTORY POINT NUMBER	-	14

CALCULATIONAL VARIABLE TABLE (2)

PELLET OPTION

NAME	DESCRIPTION	DIMENSION	VALUE
HO,FO,GO,EO	PARAMETER OF ANISOTROPY	-	1.0 1.0 1.0 3.0
GAMR,GAMZ,GAMT	CRACK PARAMETER	-	0.0 0.0 0.0
BETA	HOTPRESS PARAMETER	-	0.002
YEC	PELLET CRACK ELASTIC VALUE (YEC(R),YEC(Z),YEC(T))	PA	2.0D+09 2.0D+09 2.0D+09
FRELOC	MECHANICAL RELOCATION PARAMETER	-	0.50
EPSRLZ	AXIAL RELOCATION PARAMETER	-	3.000D-03
DCHG	RE-RELOCATOIN PARAMETER	-	0.50
SPCON	UNRESTRAINT SWELLING BOUNDARY STRESS	PA	-1.000D+06
XN	UNRESTRAINT SWELLING BOUNDARY STRESS COEF.	-	1.00

CLADDING OPTION

NAME	DESCRIPTION	DIMENSION	VALUE
HO,FO,GO,EO	PARAMETER OF ANISOTROPY	-	1.0 1.0 1.0 3.0

FILM CONDUCTANCE OPTION

NAME	DESCRIPTION	DIMENSION	VALUE
V	COOLANT VELOSITY	CM/SEC	500.00
DE	EQUIVALENT HYDRAURIC DIAMETER	CM	1.180

HISTORY DATA (1)

NHIST	TIME H: M: S	BURNUP MWD/TUO2	BURNUP MWD/TU	BURNUP GJ/KGU	L.H.R. W/CM	COOLANT TEMP. DEG.K	COOLANT PRESS. MPA	FAST NEUTRON FLUX N/CM2.S	HISTRY OPTION	PRINT OPTION
1	0: 0: 0	0.0	0.0	0.0	0.00	534.10	13.73	3.300D+13	0	0
2	1: 0: 0	0.8	0.9	0.08	200.00	534.10	13.73	3.300D+13	0	0
3	648:12:53	1000.0	1134.5	97.90	200.00	534.10	13.73	3.300D+13	0	0
4	648:42:53	1000.7	1135.3	97.97	150.00	534.10	13.73	3.300D+13	-100	0
5	2375:22:16	3000.0	3403.5	293.70	150.00	534.10	13.73	3.300D+13	0	0
6	2376:22:16	3000.6	3404.2	293.76	0.00	534.10	13.73	3.300D+13	-100	0
7	2376:52:16	3000.6	3404.2	293.76	0.00	577.10	14.60	8.000D+13	-100	0
8	2377:22:16	3001.0	3404.6	293.79	200.00	577.10	14.60	8.000D+13	0	0
9	2401:22:16	3038.0	3446.6	297.42	200.00	577.10	14.60	8.000D+13	0	1
10	2401:52:16	3039.1	3447.8	297.53	350.00	577.10	14.60	8.000D+13	0	0
11	2402:22:16	3040.7	3449.7	297.69	500.00	577.10	14.60	8.000D+13	0	1
12	2406:22:16	3056.2	3467.2	299.20	500.00	577.10	14.60	8.000D+13	0	0
13	2426:22:16	3133.4	3554.8	306.76	500.00	577.10	14.60	8.000D+13	0	0
14	2427:22:16	3135.3	3557.0	306.94	0.00	577.10	14.60	8.000D+13	0	0

RELATIVE POWER FACTOR = 0.0

HISTORY DATA (2)

NHIST	TIME H: M: S	L.H.R. W/CM	AXIAL NODE PEAKING FACTOR 1	2	3	4	5
1	0: 0: 0	0.00	0.760	0.900	1.000	0.900	0.780
2	1: 0: 0	200.00	0.760	0.900	1.000	0.900	0.780
3	648:12:53	200.00	0.760	0.900	1.000	0.900	0.780
4	648:42:53	150.00	0.760	0.900	1.000	0.900	0.780
5	2375:22:16	150.00	0.760	0.900	1.000	0.900	0.780
6	2376:22:16	0.00	0.760	0.900	1.000	0.900	0.780
7	2376:52:16	0.00	0.570	0.900	1.000	0.750	0.520
8	2377:22:16	200.00	0.570	0.900	1.000	0.750	0.520
9	2401:22:16	200.00	0.570	0.900	1.000	0.750	0.520
10	2401:52:16	350.00	0.570	0.900	1.000	0.750	0.520
11	2402:22:16	500.00	0.570	0.900	1.000	0.750	0.520
12	2406:22:16	500.00	0.570	0.900	1.000	0.750	0.520
13	2426:22:16	500.00	0.570	0.900	1.000	0.750	0.520
14	2427:22:16	0.00	0.570	0.900	1.000	0.750	0.520

MECHANICAL ATTENTION NODE NUMBER = 3

NST	CAL	DCAL	T.C.	TIME	LHR	BURNUP
1	2	2	0	0.00	0.00	0.00
2	4	2	0	0.05	10.00	0.00
3	6	2	0	0.10	20.00	0.01
4	8	2	0	0.15	30.00	0.02
5	10	2	0	0.20	40.00	0.03
6	12	2	0	0.25	50.00	0.05
7	14	2	0	0.30	60.00	0.07
8	16	2	0	0.35	70.00	0.09
9	18	2	0	0.40	80.00	0.12
10	20	2	0	0.45	90.00	0.16
11	22	2	0	0.50	100.00	0.19
12	24	2	0	0.55	110.00	0.23
13	26	2	0	0.60	120.00	0.28
14	28	2	0	0.65	130.00	0.33
15	30	2	0	0.70	140.00	0.38
16	32	2	0	0.75	150.00	0.43
17	34	2	0	0.80	160.00	0.49
18	36	2	0	0.85	170.00	0.56
19	38	2	0	0.90	180.00	0.63
20	40	2	0	0.95	190.00	0.70
21	42	2	0	1.00	200.00	0.77
22	44	2	0	46.55	200.00	71.09
23	46	2	0	546.55	200.00	843.04
24	48	2	0	648.21	200.00	1000.00
25	50	2	0	648.31	190.00	1000.15
26	52	2	0	648.41	180.00	1000.29
27	54	2	0	648.51	170.00	1000.43
28	56	2	0	648.61	160.00	1000.56
29	58	2	0	648.71	150.00	1000.68
30	60	2	0	698.71	150.00	1058.57
31	62	2	0	1198.71	150.00	1637.53
32	64	2	0	1698.71	150.00	2216.49
33	66	2	0	2198.71	150.00	2795.45
34	68	2	0	2375.37	150.00	3000.00
35	70	2	0	2375.44	140.00	3000.07
36	72	2	0	2375.50	130.00	3000.14
37	74	2	0	2375.57	120.00	3000.21
38	76	2	0	2375.64	110.00	3000.27
39	78	2	0	2375.70	100.00	3000.32
40	80	2	0	2375.77	90.00	3000.37
41	82	2	0	2375.84	80.00	3000.41
42	84	2	0	2375.90	70.00	3000.45
43	86	2	0	2375.97	60.00	3000.49
44	88	2	0	2376.04	50.00	3000.51
45	90	2	0	2376.10	40.00	3000.54
46	92	2	0	2376.17	30.00	3000.56
47	94	2	0	2376.24	20.00	3000.57
48	96	2	0	2376.30	10.00	3000.58
49	98	2	0	2376.37	0.00	3000.58
50	100	2	0	2376.87	0.00	3000.58
51	102	2	0	2376.90	10.00	3000.58
52	104	2	0	2376.92	20.00	3000.58
53	106	2	0	2376.95	30.00	3000.59
54	108	2	0	2376.97	40.00	3000.59
55	110	2	0	2377.00	50.00	3000.60
56	112	2	0	2377.02	60.00	3000.61
57	114	2	0	2377.05	70.00	3000.63
58	116	2	0	2377.07	80.00	3000.64
59	118	2	0	2377.10	90.00	3000.66
60	120	2	0	2377.12	100.00	3000.68
61	122	2	0	2377.15	110.00	3000.70
62	124	2	0	2377.17	120.00	3000.72
63	126	2	0	2377.20	130.00	3000.74
64	128	2	0	2377.22	140.00	3000.77
65	130	2	0	2377.25	150.00	3000.80
66	132	2	0	2377.27	160.00	3000.83
67	134	2	0	2377.30	170.00	3000.86
68	136	2	0	2377.32	180.00	3000.89
69	138	2	0	2377.35	190.00	3000.93
70	140	2	0	2377.37	200.00	3000.96

```
    *** FEMAXI-III SAMPLE CALCULATION ***

STAGE NO. =   71      TIME (HRS) = 2401.3712      COOLANT TEMP.(K) =577.100      COOLANT PRESS.(MPA) = 14.600

        L.H.R.    BURN UP      GAP CONDUCTANCE (W/CM**2 K)              TEMPERATURE (K)            CLEARANCE    CONTACT
NODE    (W/CM)   (MWD/TUO2)    TOTAL    GAS    SOLID    RAD.        PC      PS      CI      CO     (MICRONS)   FORCE(MPA)   NODE
  1    114.000     2301.8     0.4001  0.3958  0.0     0.0043     915.6   712.5   602.9   588.7     47.458       0.0         1
  2    180.000     2734.2     0.4652  0.4601  0.0     0.0051    1126.4   766.5   617.7   595.3     40.385       0.0         2
* 3    200.000     3038.0     0.4904  0.4851  0.0     0.0053    1191.2   779.0   622.1   597.4     37.872       0.0         3
  4    150.000     2728.6     0.4352  0.4304  0.0     0.0047    1028.8   743.5   611.0   592.3     43.452       0.0         4
  5    104.000     2359.9     0.3923  0.3881  0.0     0.0042     884.3   702.6   600.6   587.6     48.340       0.0         5

                          BURN UP            PELLET DISP. (MICRONS)                    CLADDING DISP. (MICRONS)
                          (FISS/CC     THRMAL,    IRRAD.     DENSIFI    RELOC
NODE    CSFR*    PFAC*    *10**20)     EXPANS     SWELL      CATION     ATION        CREEP
  1    0.7597   2.0000      0.65       10.469     2.115     -12.010     23.687       -7.707
  2    0.7597   2.0000      0.77       17.308     2.513     -12.549     23.687       -8.400
* 3    0.7597   2.0000      0.86       19.452     2.792     -12.817     23.687       -8.854
  4    0.7597   2.0000      0.77       14.105     2.508     -12.543     23.687       -8.391
  5    0.7597   2.0000      0.67        9.473     2.169     -12.095     23.687       -7.804

  INITIAL GAS (MOL)                  =   4.53D-03

FISSION GAS RESULT

  LOCAL FISSION GAS RELEASE FRACTION (AXIAL NODE)
1 0.00500  2 0.00500  3 0.00500  4 0.00500  5 0.00500

  ROD AVERAGE FISSION GAS RELEASE FRACTION =  0.00500            FRACTIONS OF GAS MIXTURE (PERCENT)
                                                                   HE     N2     KR     XE
  ROD GAS PRESSURE ( MPA )          =    3.204                    99.8    0.0    0.0    0.2

  TOTAL GAS (MOL)                    =   4.53D-03

  RELEASED IODINE ( GRAM/CM**2 )     = 2.01D-07     (AVERAGE)          2.32D-07     (PEAK)

              (MOL)      HE          N2          KR          XE                  TOTAL
 PRODUCED GAS . . . .  0.0         0.0         2.44D-04    1.63D-03  . . . .   1.88D-03
 RELEASED GAS . . . .  0.0         0.0         1.22D-06    8.16D-06  . . . .   9.38D-06
 ROD      GAS . . . .  4.53D-03    0.0         1.22D-06    8.16D-06  . . . .   4.53D-03

RADIAL TEMPERATURE DISTRIBUTION AT AXIAL NODE OF  3
                                PELLET                                  / GAP /    CLAD.
...1.....2.....3.....4.....5.....6.....7.....8.....9....10....11          ...1.....2.....3
1191  1187  1173  1151  1120  1081  1034   979   918   851   779          622   609   597
```

```
*****************************************************************************************************************
********* OUTPUT  ---STAGE---  71 ***************************************************************************
*****************************************************************************************************************

    TIME                          2401.37  HR
    LINEAR HEAT RATING             200.00  W/CM
    FAST NEUTRON FLUX            8.00D+13  N/CM**2.S
    FISSION RATE                 1.18D+13  FISSIONS/CM**3.S
    BURNUP                       3.04D+03  MWD/TUO2


********* TEMPERATURE DISTRIBUTION ******************************************************************************
        N   TEMP(K)        N   TEMP(K)        N   TEMP(K)        N   TEMP(K)        N   TEMP(K)
        1   1190.37        2   1179.21        3   1162.90        4   1129.85        5   1097.89
        6   1044.34        7    998.17        8    931.34        9    880.94       10    807.30
       11    616.64       12    602.36

********* PELLET/CLADDING MECHANICAL INTERACTION STATUS *********************************************************

----------- -------  ----------------------------------------  ----------------------------------------  ----------
   NODAL    CONTACT                  P E L L E T                              C L A D D I N G                RADIAL GAP
COMBINATION SURFACE  INCREMENTAL STRESS(PA)    TOTAL STRESS(PA)   INCREMENTAL STRESS(PA)    TOTAL STRESS(PA)
 FUEL-CLAD   STATUS  RADIAL      AXIAL       RADIAL      AXIAL    RADIAL      AXIAL       RADIAL      AXIAL       (MICRONS)
----------- -------  ----------------------------------------  ----------------------------------------  ----------
   62- 69    OPEN    0.0         0.0         0.0         0.0      0.0         0.0         0.0         0.0         2.5287D+01
   61- 68    OPEN    0.0         0.0         0.0         0.0      0.0         0.0         0.0         0.0         2.8246D+01
   60- 67    OPEN    0.0         0.0         0.0         0.0      0.0         0.0         0.0         0.0         2.9152D+01
   59- 66    OPEN    0.0         0.0         0.0         0.0      0.0         0.0         0.0         0.0         2.9143D+01
   58- 65    OPEN    0.0         0.0         0.0         0.0      0.0         0.0         0.0         0.0         2.8975D+01
   57- 64    OPEN    0.0         0.0         0.0         0.0      0.0         0.0         0.0         0.0         2.8817D+01
   56- 63    OPEN    0.0         0.0         0.0         0.0      0.0         0.0         0.0         0.0         2.8776D+01

********* PELLET/PELLET MECHANICAL INTERACTION STATUS ***********************************************************

----------- -------  ---------------------  ------------------------------  ---------------------
   NODAL    CONTACT   AXIAL STRESS (PA)        AXIAL DISPLACEMENT (CM)        RADIAL GAP (MICRONS)
   POINT     STATUS  INCREMENTAL    TOTAL     DISP.      CONTACT   DISTANCE    MINMUM     BOUNDARY
----------- -------  ---------------------  ------------------------------  ---------------------
      7      OPEN    0.0         0.0         6.4736D-01  0.0       0.0       2.5287D+01  3.0000D+00
     11      OPEN    0.0         0.0         6.4794D-01  0.0       0.0       2.5287D+01  3.0000D+00
     18      OPEN    0.0         0.0         6.4971D-01  0.0       0.0       2.5287D+01  3.0000D+00
     22      OPEN    0.0         0.0         6.5266D-01  0.0       0.0       2.5287D+01  3.0000D+00
     29      OPEN    0.0         0.0         6.5682D-01  0.0       0.0       2.5287D+01  3.0000D+00
     33      OPEN    0.0         0.0         6.6220D-01  0.0       0.0       2.5287D+01  3.0000D+00
     40      OPEN    0.0         0.0         6.6882D-01  0.0       0.0       2.5287D+01  3.0000D+00
     44      OPEN    0.0         0.0         6.7671D-01  0.0       0.0       2.5287D+01  3.0000D+00
     51      OPEN    0.0         0.0         6.7655D-01  0.0       0.0       2.5287D+01  3.0000D+00
     55      OPEN    0.0         0.0         6.7639D-01  0.0       0.0       2.5287D+01  3.0000D+00
     62      OPEN    0.0         0.0         6.7625D-01  0.0       0.0       2.5287D+01  3.0000D+00
```

```
                                         ***** NODAL DISPLACEMENT (MICRON) *****

(R-DIRECTION)                                                 GAP
   0.0   7.2  14.2  21.1  27.8  34.1  40.3  46.2  50.8  55.3  59.5I  -0.2   0.9   1.9
   0.0        13.0        25.6        37.5        47.8        56.5I  -0.2         1.9
   0.0   6.4  12.8  19.1  25.2  31.1  36.9  42.3  47.0  51.4  55.6I  -0.2   0.9   1.9
   0.0        12.9        25.3        36.9        47.0        55.6I  -0.2         1.9
   0.0   6.5  13.0  19.3  25.5  31.4  37.1  42.6  47.2  51.6  55.8I  -0.2   0.9   1.9
   0.0        13.1        25.6        37.3        47.3        55.9I  -0.2         1.9
   0.0   6.6  13.1  19.5  25.7  31.6  37.3  42.8  47.4  51.8  56.0I  -0.2   0.9   1.9

(Z-DIRECTION)                                                 GAP
  53.6  53.4  52.8  52.0  50.9  49.7  48.4  47.1  45.5  43.9  42.5I   8.8   8.8   8.8
  44.0        43.4        42.1        40.5        38.8        37.2I   7.3         7.3
  34.4  34.3  34.1  33.7  33.3  32.9  32.5  32.2  31.7  31.3  31.1I   5.9   5.9   5.9
  25.3        25.1        24.8        24.4        24.1        23.9I   4.4         4.4
  16.6  16.6  16.5  16.5  16.4  16.3  16.3  16.3  16.2  16.2  16.2I   2.9   2.9   2.9
   8.2         8.2         8.2         8.2         8.2         8.2I   1.5         1.5
   0.0   0.0   0.0   0.0   0.0   0.0   0.0   0.0   0.0   0.0   0.0I   0.0   0.0   0.0


                                 ***** ELEMENT INFORMATION   STRESS (MN/M**2) *****                 PLOT NUMBER =  2

SIG(Z)                                                        GAP
  -0.4  -0.4  -0.4  -0.4  -0.4  -0.2  -0.1   0.1   0.2   0.2        I  -50.4  -49.9
  -3.3  -3.1  -2.7  -2.0  -1.3  -0.4   0.1   0.6   1.0   1.5        I  -50.4  -49.9
  -6.5  -5.8  -5.0  -3.3  -1.9  -0.3   0.3   1.1   1.7   2.7        I  -50.4  -49.9
  -9.7  -8.6  -7.0  -4.3  -2.3  -0.2   0.5   1.5   2.4   3.7        I  -50.4  -49.9
 -11.1  -9.8  -7.9  -4.8  -2.4  -0.2   0.6   1.7   2.7   4.1        I  -50.4  -49.9
 -12.0 -10.6  -8.5  -5.0  -2.5  -0.1   0.6   1.9   2.8   4.3        I  -50.4  -49.9


                                 ***** ELEMENT INFORMATION   STRESS (MN/M**2) *****                 PLOT NUMBER =  3

SIG(T)                                                        GAP
   0.4   0.5   0.6   0.9   1.2   1.8   2.4   3.2   3.8   4.7        I  -98.5  -96.2
  -3.5  -3.2  -2.5  -1.4  -0.5   0.4   1.1   2.0   2.7   3.8        I  -98.5  -96.2
  -4.6  -4.0  -3.2  -1.8  -0.7   0.4   1.0   2.0   2.7   3.8        I  -98.5  -96.2
  -4.9  -4.3  -3.4  -1.8  -0.7   0.4   1.1   2.1   2.8   3.9        I  -98.5  -96.2
  -4.6  -4.1  -3.1  -1.6  -0.5   0.5   1.3   2.2   3.0   4.0        I  -98.5  -96.2
  -4.5  -3.9  -3.0  -1.5  -0.4   0.6   1.3   2.3   3.0   4.0        I  -98.5  -96.2


                                 ***** ELEMENT INFORMATION   STRESS (MN/M**2) *****                 PLOT NUMBER =  5

EQ.SIG                                                        GAP
   0.8   1.1   1.4   1.9   2.3   2.7   3.1   3.6   4.0   4.6        I   80.2   72.7
   0.7   1.9   2.8   3.5   3.6   3.5   3.1   3.2   3.2   3.4        I   80.2   72.7
   2.0   2.4   2.8   3.0   3.2   3.0   3.1   3.0   3.2   3.6        I   80.2   72.7
   4.8   4.3   3.6   2.7   2.6   2.7   2.7   3.0   3.3   4.0        I   80.2   72.7
   6.5   5.6   4.5   2.9   2.3   2.5   2.6   3.1   3.5   4.2        I   80.2   72.7
   7.5   6.5   5.1   3.0   2.2   2.4   2.6   3.1   3.6   4.3        I   80.2   72.7


                                 ***** ELEMENT INFORMATION   STRAIN (0.01 PERCENT) *****            PLOT NUMBER = 11

EPSP                                                          GAP
   0.0   0.0   0.0   0.0   0.0   0.0   0.0   0.0   0.0   0.0        I    0.0    0.0
   0.0   0.0   0.0   0.0   0.0   0.0   0.0   0.0   0.0   0.0        I    0.0    0.0
   0.0   0.0   0.0   0.0   0.0   0.0   0.0   0.0   0.0   0.0        I    0.0    0.0
   0.0   0.0   0.0   0.0   0.0   0.0   0.0   0.0   0.0   0.0        I    0.0    0.0
   0.0   0.0   0.0   0.0   0.0   0.0   0.0   0.0   0.0   0.0        I    0.0    0.0
   0.0   0.0   0.0   0.0   0.0   0.0   0.0   0.0   0.0   0.0        I    0.0    0.0


                                 ***** ELEMENT INFORMATION   STRAIN (0.01 PERCENT) *****            PLOT NUMBER = 14

EPSC(T)                                                       GAP
   0.7   0.9   1.3   1.9   2.4   3.1   3.4   3.6   3.5   3.2        I  -13.5  -10.0
  -0.6  -0.3   0.3   1.2   1.7   2.1   2.1   2.3   2.3   2.2        I  -13.5  -10.0
   1.0   1.2   1.7   2.2   2.5   2.3   2.2   2.1   2.0   1.8        I  -13.5  -10.0
   2.7   2.7   3.1   3.3   3.3   2.6   2.2   2.0   1.8   1.5        I  -13.5  -10.0
   3.7   3.7   3.9   4.0   3.7   2.8   2.3   2.0   1.8   1.5        I  -13.5  -10.0
   4.3   4.2   4.4   4.4   4.0   2.9   2.4   2.0   1.8   1.4        I  -13.5  -10.0
***STAGE***  71     TIME     2401.37 (HR)     POWER     200.00(W/CM)
    PCMI PLOT(MM)
      Z       0.0               0.020             0.040             0.060             0.080             0.100
              I-----------------I-----------------I-----------------I-----------------I-----------------I
7      6.72   I                     G                              P                      C
6      5.60   I                        G                         P                        C
5      4.48   I                         G                       P                         C
4      3.36   I                         G                       P                         C
3      2.24   I                         G                       P                         C
2      1.12   I                         G                       P                         C
1      0.0    I                         G                       P                         C

***** CRACK AND YIELD MAP  (*=YES) *****

   CRACK(R)                  CRACK(Z)                   CRACK(T)                  YIELD
   PELLET         CLADDING   PELLET          CLADDING   PELLET          CLADDING  PELLET          CLADDING
```

```
  +--+--+--+--+--+ +--+        +--+--+--+--+--+ +--+        +--+--+--+--+--+ +--+        +--+--+--+--+--+ +--+
  I**I* I  I  I  I I  I        I  I  I  I *I**I I  I        I**I**I**I**I**I I  I        I  I  I  I  I  I I  I
  I  I  I  I  I  I I  I        I  I  I  I**I**I I  I        I  I  I *I**I**I I  I        I  I  I  I  I  I I  I
  +--+--+--+--+--+ +--+        +--+--+--+--+--+ +--+        +--+--+--+--+--+ +--+        +--+--+--+--+--+ +--+
  I  I  I  I  I  I I  I        I  I  I  I**I**I I  I        I  I  I *I**I**I I  I        I  I  I  I  I  I I  I
  I  I  I  I  I  I I  I        I  I  I  I**I**I I  I        I  I  I *I**I**I I  I        I  I  I  I  I  I I  I
  +--+--+--+--+--+ +--+        +--+--+--+--+--+ +--+        +--+--+--+--+--+ +--+        +--+--+--+--+--+ +--+
  I  I  I  I  I  I I  I        I  I  I  I**I**I I  I        I  I  I *I**I**I I  I        I  I  I  I  I  I I  I
  I  I  I  I  I  I I  I        I  I  I  I**I**I I  I        I  I  I *I**I**I I  I        I  I  I  I  I  I I  I
  +--+--+--+--+--+ +--+        +--+--+--+--+--+ +--+        +--+--+--+--+--+ +--+        +--+--+--+--+--+ +--+
NST =   71   CAL =   142   DCAL =    2   T.C. =   0   TIME =  2401.37   LHR = 200.00   BURNUP =  3038.02
NST =   72   CAL =   144   DCAL =    2   T.C. =   0   TIME =  2401.40   LHR = 210.00   BURNUP =  3038.07
NST =   73   CAL =   146   DCAL =    2   T.C. =   0   TIME =  2401.44   LHR = 220.00   BURNUP =  3038.13
NST =   74   CAL =   148   DCAL =    2   T.C. =   0   TIME =  2401.47   LHR = 230.00   BURNUP =  3038.18
NST =   75   CAL =   150   DCAL =    2   T.C. =   0   TIME =  2401.50   LHR = 240.00   BURNUP =  3038.24
NST =   76   CAL =   152   DCAL =    2   T.C. =   0   TIME =  2401.54   LHR = 250.00   BURNUP =  3038.31
NST =   77   CAL =   154   DCAL =    2   T.C. =   0   TIME =  2401.57   LHR = 260.00   BURNUP =  3038.37
NST =   78   CAL =   156   DCAL =    2   T.C. =   0   TIME =  2401.60   LHR = 270.00   BURNUP =  3038.44
NST =   79   CAL =   158   DCAL =    2   T.C. =   0   TIME =  2401.64   LHR = 280.00   BURNUP =  3038.51
NST =   80   CAL =   160   DCAL =    2   T.C. =   0   TIME =  2401.67   LHR = 290.00   BURNUP =  3038.59
NST =   81   CAL =   162   DCAL =    2   T.C. =   0   TIME =  2401.70   LHR = 300.00   BURNUP =  3038.66
NST =   82   CAL =   164   DCAL =    2   T.C. =   0   TIME =  2401.74   LHR = 310.00   BURNUP =  3038.74
NST =   83   CAL =   166   DCAL =    2   T.C. =   0   TIME =  2401.77   LHR = 320.00   BURNUP =  3038.82
NST =   84   CAL =   168   DCAL =    2   T.C. =   0   TIME =  2401.80   LHR = 330.00   BURNUP =  3038.90
NST =   85   CAL =   170   DCAL =    2   T.C. =   0   TIME =  2401.84   LHR = 340.00   BURNUP =  3038.99
NST =   86   CAL =   172   DCAL =    2   T.C. =   0   TIME =  2401.87   LHR = 350.00   BURNUP =  3039.08
NST =   87   CAL =   180   DCAL =    8   T.C. =   3   TIME =  2401.90   LHR = 360.00   BURNUP =  3039.17
NST =   88   CAL =   188   DCAL =    8   T.C. =   2   TIME =  2401.94   LHR = 370.00   BURNUP =  3039.26
NST =   89   CAL =   196   DCAL =    8   T.C. =   2   TIME =  2401.97   LHR = 380.00   BURNUP =  3039.36
NST =   90   CAL =   202   DCAL =    6   T.C. =   1   TIME =  2402.00   LHR = 390.00   BURNUP =  3039.46
NST =   91   CAL =   204   DCAL =    2   T.C. =   0   TIME =  2402.04   LHR = 400.00   BURNUP =  3039.56
NST =   92   CAL =   206   DCAL =    2   T.C. =   0   TIME =  2402.07   LHR = 410.00   BURNUP =  3039.67
NST =   93   CAL =   214   DCAL =    8   T.C. =   3   TIME =  2402.10   LHR = 420.00   BURNUP =  3039.77
NST =   94   CAL =   218   DCAL =    4   T.C. =   1   TIME =  2402.14   LHR = 430.00   BURNUP =  3039.88
NST =   95   CAL =   220   DCAL =    2   T.C. =   0   TIME =  2402.17   LHR = 440.00   BURNUP =  3039.99
NST =   96   CAL =   228   DCAL =    8   T.C. =   3   TIME =  2402.20   LHR = 450.00   BURNUP =  3040.11
NST =   97   CAL =   234   DCAL =    6   T.C. =   2   TIME =  2402.24   LHR = 460.00   BURNUP =  3040.23
NST =   98   CAL =   250   DCAL =   16   T.C. =   7   TIME =  2402.27   LHR = 470.00   BURNUP =  3040.35
NST =   99   CAL =   254   DCAL =    4   T.C. =   1   TIME =  2402.30   LHR = 480.00   BURNUP =  3040.47
NST =  100   CAL =   258   DCAL =    4   T.C. =   1   TIME =  2402.34   LHR = 490.00   BURNUP =  3040.59
```

```
   *** FEMAXI-III SAMPLE CALCULATION ***

STAGE NO. =  101      TIME (HRS) = 2402.3712      COOLANT TEMP.(K) =577.100      COOLANT PRESS.(MPA) = 14.600

        L.H.R.    BURN UP      GAP CONDUCTANCE (W/CM**2 K)              TEMPERATURE (K)              CLEARANCE    CONTACT
NODE    (W/CM)   (MWD/TUO2)    TOTAL    GAS    SOLID    RAD.        PC      PS      CI      CO      (MICRONS)   FORCE(MPA)   NODE
  1    285.000     2303.3     0.5727  0.5665  0.0      0.0061    1497.8   832.3   640.9   606.0     28.856       0.0         1
  2    450.000     2736.6     1.6070  1.5664  0.0348   0.0059    1967.9   784.5   676.8   622.7      0.0         2.783       2
* 3    500.000     3040.7     2.1012  1.8493  0.2459   0.0060    2123.6   779.1   687.6   627.8      0.0        18.997       3
  4    375.000     2730.6     0.8568  0.8505  0.0      0.0063    1778.2   828.9   660.6   615.1     13.820       0.0         4
  5    260.000     2361.3     0.5353  0.5293  0.0      0.0059    1411.0   822.2   635.4   603.4     31.729       0.0         5

                          BURN UP            PELLET DISP. (MICRONS)                    CLADDING DISP. (MICRONS)
                          (FISS/CC     THRMAL,     IRRAD.     DENSIFI     RELOC
NODE    CSFR*    PFAC*    *10**20)     EXPANS      SWELL      CATION      ATION       CREEP
  1    0.7597   2.0000      0.65       30.162      2.117     -12.012     23.687      -7.709
  2    0.7597   2.0000      0.77       46.102     16.777     -12.551     23.687      -8.403
* 3    0.7597   2.0000      0.86       52.396     17.050     -12.819     23.687      -8.858
  4    0.7597   2.0000      0.77       39.917      7.677     -12.545     23.687      -8.394
  5    0.7597   2.0000      0.67       27.103      2.170     -12.097     23.687      -7.806

  INITIAL GAS (MOL)                  =   4.53D-03

FISSION GAS RESULT

  LOCAL FISSION GAS RELEASE FRACTION (AXIAL NODE)
1 0.00500  2 0.05727  3 0.13904  4 0.00500  5 0.00500

  ROD AVERAGE FISSION GAS RELEASE FRACTION =  0.04680            FRACTIONS OF GAS MIXTURE (PERCENT)
                                                                   HE     N2     KR     XE
  ROD GAS PRESSURE ( MPA )          =    3.821                     98.1    0.0    0.2    1.7

  TOTAL GAS (MOL)                    =   4.61D-03

  RELEASED IODINE ( GRAM/CM**2 )     = 1.88D-06     (AVERAGE)           6.45D-06     (PEAK)

                (MOL)      HE          N2          KR          XE                  TOTAL
 PRODUCED GAS . . . .  0.0          0.0         2.44D-04    1.63D-03   . . . .   1.88D-03
 RELEASED GAS . . . .  0.0          0.0         1.14D-05    7.65D-05   . . . .   8.79D-05
 ROD      GAS . . . .  4.53D-03     0.0         1.14D-05    7.65D-05   . . . .   4.61D-03


RADIAL TEMPERATURE DISTRIBUTION AT AXIAL NODE OF  3
                                PELLET                                  / GAP /    CLAD.
...1.....2.....3.....4.....5.....6.....7.....8.....9....10....11                  ...1.....2.....3
2124  2109  2063  1985  1872  1729  1561  1374  1175   975   779                   688   657   628
```

```
*********************************************************************************************************************
********* OUTPUT  ---STAGE--- 101 ***************************************************************************************
*********************************************************************************************************************

     TIME                          2402.37  HR
     LINEAR HEAT RATING             500.00  W/CM
     FAST NEUTRON FLUX            8.00D+13  N/CM**2.S
     FISSION RATE                 2.93D+13  FISSIONS/CM**3.S
     BURNUP                       3.04D+03  MWD/TU02
```

********* TEMPERATURE DISTRIBUTION *********

N	TEMP(K)	N	TEMP(K)	N	TEMP(K)	N	TEMP(K)	N	TEMP(K)
1	2120.80	2	2082.99	3	2027.01	4	1908.15	5	1791.08
6	1598.81	7	1437.57	8	1217.71	9	1061.88	10	853.77
11	674.49	12	639.97						

********* PELLET/CLADDING MECHANICAL INTERACTION STATUS *********

NODAL COMBINATION FUEL-CLAD	CONTACT SURFACE STATUS	PELLET INCREMENTAL STRESS(PA) RADIAL	PELLET INCREMENTAL STRESS(PA) AXIAL	PELLET TOTAL STRESS(PA) RADIAL	PELLET TOTAL STRESS(PA) AXIAL	CLADDING INCREMENTAL STRESS(PA) RADIAL	CLADDING INCREMENTAL STRESS(PA) AXIAL	CLADDING TOTAL STRESS(PA) RADIAL	CLADDING TOTAL STRESS(PA) AXIAL	RADIAL GAP (MICRONS)
62- 69	FIXD	-2.7359D+06	3.1703D+04	-3.1426D+07	-4.6264D+06	2.7359D+06	-3.1703D+04	3.1426D+07	4.6264D+06	2.6021D-14
61- 68	FIXD	-1.1994D+06	7.0290D+04	-8.0291D+06	3.1790D+05	1.1994D+06	-7.0290D+04	8.0291D+06	-3.1790D+05	6.0715D-14
60- 67	OPEN	0.0	0.0	0.0	0.0	0.0	0.0	0.0	0.0	2.0908D+00
59- 66	FIXD	-2.0409D+06	-1.2842D+05	-6.8448D+06	-1.6733D+05	2.0409D+06	1.2842D+05	6.8448D+06	1.6733D+05	4.3368D-14
58- 65	FIXD	-2.2843D+06	-2.0257D+05	-8.6715D+06	-5.4973D+05	2.2843D+06	2.0257D+05	8.6715D+06	5.4973D+05	2.6021D-14
57- 64	FIXD	-2.0057D+06	3.0797D+04	-1.1852D+07	5.1038D+05	2.0057D+06	-3.0797D+04	1.1852D+07	-5.1038D+05	8.6736D-15
56- 63	FIXD	-2.2081D+06	0.0	-1.1647D+07	0.0	2.2081D+06	0.0	1.1647D+07	0.0	3.4694D-14

********* PELLET/PELLET MECHANICAL INTERACTION STATUS *********

NODAL POINT	CONTACT STATUS	AXIAL STRESS (PA) INCREMENTAL	AXIAL STRESS (PA) TOTAL	AXIAL DISPLACEMENT (CM) DISP.	AXIAL DISPLACEMENT (CM) CONTACT	AXIAL DISPLACEMENT (CM) DISTANCE	RADIAL GAP (MICRONS) MINMUM	RADIAL GAP (MICRONS) BOUNDARY
7	OPEN	0.0	0.0	6.5434D-01	6.8060D-01	2.6260D-02	8.6736D-15	3.0000D+00
11	OPEN	0.0	0.0	6.5485D-01	6.8060D-01	2.5751D-02	8.6736D-15	3.0000D+00
18	OPEN	0.0	0.0	6.5621D-01	6.8060D-01	2.4394D-02	8.6736D-15	3.0000D+00
22	OPEN	0.0	0.0	6.5866D-01	6.8060D-01	2.1944D-02	8.6736D-15	3.0000D+00
29	OPEN	0.0	0.0	6.6236D-01	6.8060D-01	1.8243D-02	8.6736D-15	3.0000D+00
33	OPEN	0.0	0.0	6.6721D-01	6.8060D-01	1.3393D-02	8.6736D-15	3.0000D+00
40	OPEN	0.0	0.0	6.7326D-01	6.8060D-01	7.3391D-03	8.6736D-15	3.0000D+00
44	FIXD	-9.0113D+06	-8.1201D+07	6.8060D-01	6.8060D-01	0.0	8.6736D-15	3.0000D+00
51	OPEN	0.0	0.0	6.8015D-01	6.8060D-01	4.4521D-04	8.6736D-15	3.0000D+00
55	OPEN	0.0	0.0	6.7979D-01	6.8060D-01	8.1036D-04	8.6736D-15	3.0000D+00
62	OPEN	0.0	0.0	6.7955D-01	6.8060D-01	1.0526D-03	8.6736D-15	3.0000D+00

***** NODAL DISPLACEMENT (MICRON) *****

(R-DIRECTION)

										GAP			
0.0	14.9	29.2	41.6	53.4	64.3	74.2	81.8	86.5	89.6	91.9I	6.9	7.9	8.6
0.0		22.8		44.6		63.4		78.3		90.0I	5.0		6.9
0.0	11.5	23.2	34.2	44.6	54.2	63.0	70.6	76.6	81.5	85.7I	2.8	3.8	4.7
0.0		24.4		46.3		64.4		77.9		87.9I	2.9		4.9
0.0	13.1	25.9	37.7	48.3	57.8	66.4	74.0	79.9	84.8	89.1I	4.1	5.1	6.0
0.0		26.8		49.5		67.5		80.7		90.2I	5.2		7.1
0.0	13.8	27.0	39.1	49.8	59.3	68.0	75.6	81.4	86.4	90.7I	5.7	6.7	7.5

(Z-DIRECTION)

										GAP			
123.4	122.4	117.8	111.9	106.3	99.8	92.8	86.0	81.5	77.9	75.5I	12.9	12.9	12.9
100.6		94.2		85.3		78.0		71.4		68.4I	11.5		10.3
72.1	71.1	69.1	67.1	65.9	64.2	62.8	61.9	60.5	59.5	59.0I	9.0	8.7	8.5
48.4		47.9		47.5		47.4		47.0		47.3I	6.2		6.6
29.4	29.6	29.9	30.3	30.8	31.3	31.5	31.9	32.1	32.0	32.1I	3.9	4.2	4.5
13.8		14.4		15.2		15.7		16.1		16.7I	1.8		2.3
0.0	0.0	0.0	0.0	0.0	0.0	0.0	0.0	0.0	0.0	0.0I	0.0	0.0	0.0

***** ELEMENT INFORMATION STRESS (MN/M**2) ***** PLOT NUMBER = 2

SIG(Z)

										GAP		
-8.9	-7.0	-8.3	-6.2	-5.6	-22.4	-47.4	-34.1	-9.3	-0.1	I	-35.2	42.1
-30.7	-36.4	-34.2	-37.6	-32.6	-27.5	-28.8	-8.3	0.9	3.9	I	18.7	-9.2
-49.8	-48.1	-55.9	-58.3	-46.5	-36.8	-2.2	2.9	4.9	7.3	I	19.3	-9.8
-55.3	-55.8	-61.4	-69.6	-53.6	-37.3	0.6	5.2	8.6	13.6	I	1.6	7.3
-54.3	-57.0	-61.0	-68.3	-51.7	-43.9	0.9	6.4	9.8	13.6	I	-6.5	16.0
-55.1	-55.4	-60.7	-67.0	-50.9	-47.7	0.9	6.7	10.6	15.8	I	-13.2	20.2

***** ELEMENT INFORMATION STRESS (MN/M**2) ***** PLOT NUMBER = 3

SIG(T)

										GAP		
-7.0	-6.0	-3.6	1.7	4.6	8.3	11.0	14.1	15.9	17.9	I	-17.1	18.5
-42.5	-46.4	-43.9	-33.5	-9.5	3.3	6.7	10.8	13.3	16.2	I	-31.9	-36.1
-53.5	-49.4	-52.7	-24.2	-2.8	4.6	7.7	11.3	13.5	15.9	I	-53.6	-54.2
-53.2	-52.2	-51.5	-28.1	-2.3	6.2	9.1	12.5	14.6	17.0	I	-46.2	-35.3
-49.3	-51.1	-48.9	-26.6	-1.2	7.4	10.1	13.3	15.3	17.5	I	-29.2	-13.9
-49.9	-49.3	-48.4	-25.2	-0.7	8.1	10.8	13.9	15.8	18.0	I	-16.4	2.6

***** ELEMENT INFORMATION STRESS (MN/M**2) ***** PLOT NUMBER = 5

```
EQ.SIG                                                                                  GAP
  3.2   11.1   17.6   26.3   33.3   46.1   69.6   46.6   37.4   35.3      I   26.1   53.0
 15.4   19.1   25.2   37.8   46.5   56.7   44.8   20.8   12.8   13.8      I   44.4   26.8
 12.7   12.4   14.9   34.1   46.5   40.2   27.6   22.7   23.4   21.9      I   63.3   42.8
 12.7   13.0   16.1   37.8   46.4   40.2   26.9   25.2   23.0   22.8      I   43.0   36.9
 12.8   13.6   16.9   37.8   46.3   46.5   32.1   30.5   30.2   29.0      I   20.0   31.2
 13.1   13.4   16.8   37.7   46.3   49.9   32.5   30.7   30.2   30.0      I    3.0   30.3


                                  ***** ELEMENT INFORMATION   STRAIN (0.01 PERCENT) *****          PLOT NUMBER = 11

EPSP                                                                                    GAP
  0.0    0.0    0.0    0.0    0.0    0.0    0.0    0.0    0.0    0.0      I    0.0    0.0
  0.0    0.0    0.0    6.9   11.9    0.0    0.0    0.0    0.0    0.0      I    0.0    0.0
  0.0    0.0    0.0    2.1    9.2    0.0    0.0    0.0    0.0    0.0      I    0.0    0.0
  0.0    0.0    5.0   18.0   18.7    0.0    0.0    0.0    0.0    0.0      I    0.0    0.0
 11.0   13.6   18.0   27.4   25.5    0.0    0.0    0.0    0.0    0.0      I    0.0    0.0
 27.3   27.6   28.2   32.8   28.9    0.0    0.0    0.0    0.0    0.0      I    0.0    0.0


                                  ***** ELEMENT INFORMATION   STRAIN (0.01 PERCENT) *****          PLOT NUMBER = 14

EPSC(T)                                                                                 GAP
 11.8   10.1   11.5    6.1    3.8    3.2    3.5    3.6    3.6    3.3      I  -13.6  -10.1
-21.0  -13.5   -4.2    6.4    4.0    2.2    2.1    2.3    2.3    2.2      I  -13.7  -10.1
 -1.7    4.2   13.5   14.2    5.6    2.4    2.2    2.1    2.0    1.8      I  -13.7  -10.1
 22.4   24.8   27.3   16.9    6.9    2.8    2.2    2.0    1.8    1.5      I  -13.7  -10.1
 31.6   31.4   30.1   18.0    7.5    3.0    2.3    2.0    1.8    1.5      I  -13.7  -10.1
 32.6   30.8   30.5   18.6    7.9    3.1    2.4    2.1    1.8    1.4      I  -13.7  -10.1

***STAGE*** 101     TIME    2402.37 (HR)    POWER     500.00(W/CM)
    PCMI PLOT(MM)
      Z        0.0                0.020               0.040               0.060               0.080               0.100
               I-------------------I-------------------I-------------------I-------------------I-------------------I
7       6.72   UFI                                                                                                  X
6       5.60   UFI                                                                                                 X
5       4.48     I G                                                                                         P C
4       3.36   UFI                                                                                              X
3       2.24   UFI                                                                                             X
2       1.12   UFI                                                                                            X
1       0.0    UFI                                                                                           X

***** CRACK AND YIELD MAP  (*=YES) *****

 CRACK(R)                          CRACK(Z)                          CRACK(T)                          YIELD
 PELLET            CLADDING        PELLET            CLADDING        PELLET            CLADDING        PELLET            CLADDING
 +--+--+--+--+--+ +--+             +--+--+--+--+--+ +--+             +--+--+--+--+--+ +--+             +--+--+--+--+--+ +--+
 I  I  I  I  I  I I  I             I  I  I  I  I  I I  I             I  I *I**I**I**I I  I             I  I  I  I  I  I I  I
 I  I  I  I  I**I I  I             I  I  I  I  I**I I  I             I  I  I *I**I**I I  I             I  I *I* I  I  I I  I
 +--+--+--+--+--+ +--+             +--+--+--+--+--+ +--+             +--+--+--+--+--+ +--+             +--+--+--+--+--+ +--+
 I  I  I  I  I  I I  I             I  I  I  I *I**I I  I             I  I  I *I**I**I I  I             I  I +I* I  I  I I  I
 I  I  I  I  I  I I  I             I  I  I  I**I**I I  I             I  I  I *I**I**I I  I             I  I++I* I  I  I I  I
 +--+--+--+--+--+ +--+             +--+--+--+--+--+ +--+             +--+--+--+--+--+ +--+             +--+--+--+--+--+ +--+
 I  I  I  I  I  I I  I             I  I  I  I**I**I I  I             I  I  I *I**I**I I  I             I++I+*I* I  I  I I  I
 I  I  I  I  I  I I  I             I  I  I  I**I**I I  I             I  I  I *I**I**I I  I             I++I+*I* I  I  I I  I
 +--+--+--+--+--+ +--+             +--+--+--+--+--+ +--+             +--+--+--+--+--+ +--+             +--+--+--+--+--+ +--+

NST =  101   CAL =   260   DCAL =    2   T.C. =   0   TIME =  2402.37   LHR = 500.00   BURNUP =  3040.72
NST =  102   CAL =   262   DCAL =    2   T.C. =   0   TIME =  2402.38   LHR = 500.00   BURNUP =  3040.77
NST =  103   CAL =   264   DCAL =    2   T.C. =   0   TIME =  2402.51   LHR = 500.00   BURNUP =  3041.25
NST =  104   CAL =   266   DCAL =    2   T.C. =   0   TIME =  2402.64   LHR = 500.00   BURNUP =  3041.77
NST =  105   CAL =   268   DCAL =    2   T.C. =   0   TIME =  2402.79   LHR = 500.00   BURNUP =  3042.34
NST =  106   CAL =   270   DCAL =    2   T.C. =   0   TIME =  2403.03   LHR = 500.00   BURNUP =  3043.27
NST =  107   CAL =   272   DCAL =    2   T.C. =   0   TIME =  2403.95   LHR = 500.00   BURNUP =  3046.83
NST =  108   CAL =   276   DCAL =    4   T.C. =   0   TIME =  2405.03   LHR = 500.00   BURNUP =  3050.97
NST =  109   CAL =   282   DCAL =    6   T.C. =   1   TIME =  2406.37   LHR = 500.00   BURNUP =  3056.16
NST =  110   CAL =   292   DCAL =   10   T.C. =   3   TIME =  2426.37   LHR = 500.00   BURNUP =  3133.35
NST =  111   CAL =   296   DCAL =    4   T.C. =   1   TIME =  2426.39   LHR = 490.00   BURNUP =  3133.43
NST =  112   CAL =   302   DCAL =    6   T.C. =   1   TIME =  2426.41   LHR = 480.00   BURNUP =  3133.50
NST =  113   CAL =   308   DCAL =    6   T.C. =   1   TIME =  2426.43   LHR = 470.00   BURNUP =  3133.58
NST =  114   CAL =   310   DCAL =    2   T.C. =   0   TIME =  2426.45   LHR = 460.00   BURNUP =  3133.65
NST =  115   CAL =   312   DCAL =    2   T.C. =   0   TIME =  2426.47   LHR = 450.00   BURNUP =  3133.72
NST =  116   CAL =   314   DCAL =    2   T.C. =   0   TIME =  2426.49   LHR = 440.00   BURNUP =  3133.79
NST =  117   CAL =   316   DCAL =    2   T.C. =   0   TIME =  2426.51   LHR = 430.00   BURNUP =  3133.86
NST =  118   CAL =   318   DCAL =    2   T.C. =   0   TIME =  2426.53   LHR = 420.00   BURNUP =  3133.92
NST =  119   CAL =   320   DCAL =    2   T.C. =   0   TIME =  2426.55   LHR = 410.00   BURNUP =  3133.99
NST =  120   CAL =   322   DCAL =    2   T.C. =   0   TIME =  2426.57   LHR = 400.00   BURNUP =  3134.05
NST =  121   CAL =   324   DCAL =    2   T.C. =   0   TIME =  2426.59   LHR = 390.00   BURNUP =  3134.11
NST =  122   CAL =   326   DCAL =    2   T.C. =   0   TIME =  2426.61   LHR = 380.00   BURNUP =  3134.17
NST =  123   CAL =   328   DCAL =    2   T.C. =   0   TIME =  2426.63   LHR = 370.00   BURNUP =  3134.23
NST =  124   CAL =   330   DCAL =    2   T.C. =   0   TIME =  2426.65   LHR = 360.00   BURNUP =  3134.28
NST =  125   CAL =   332   DCAL =    2   T.C. =   0   TIME =  2426.67   LHR = 350.00   BURNUP =  3134.34
NST =  126   CAL =   334   DCAL =    2   T.C. =   0   TIME =  2426.69   LHR = 340.00   BURNUP =  3134.39
NST =  127   CAL =   336   DCAL =    2   T.C. =   0   TIME =  2426.71   LHR = 330.00   BURNUP =  3134.44
NST =  128   CAL =   338   DCAL =    2   T.C. =   0   TIME =  2426.73   LHR = 320.00   BURNUP =  3134.49
NST =  129   CAL =   340   DCAL =    2   T.C. =   0   TIME =  2426.75   LHR = 310.00   BURNUP =  3134.54
NST =  130   CAL =   342   DCAL =    2   T.C. =   0   TIME =  2426.77   LHR = 300.00   BURNUP =  3134.59
NST =  131   CAL =   344   DCAL =    2   T.C. =   0   TIME =  2426.79   LHR = 290.00   BURNUP =  3134.63
NST =  132   CAL =   346   DCAL =    2   T.C. =   0   TIME =  2426.81   LHR = 280.00   BURNUP =  3134.68
NST =  133   CAL =   348   DCAL =    2   T.C. =   0   TIME =  2426.83   LHR = 270.00   BURNUP =  3134.72
NST =  134   CAL =   350   DCAL =    2   T.C. =   0   TIME =  2426.85   LHR = 260.00   BURNUP =  3134.76
NST =  135   CAL =   352   DCAL =    2   T.C. =   0   TIME =  2426.87   LHR = 250.00   BURNUP =  3134.80
NST =  136   CAL =   354   DCAL =    2   T.C. =   0   TIME =  2426.89   LHR = 240.00   BURNUP =  3134.84
NST =  137   CAL =   356   DCAL =    2   T.C. =   0   TIME =  2426.91   LHR = 230.00   BURNUP =  3134.87
NST =  138   CAL =   358   DCAL =    2   T.C. =   0   TIME =  2426.93   LHR = 220.00   BURNUP =  3134.91
NST =  139   CAL =   360   DCAL =    2   T.C. =   0   TIME =  2426.95   LHR = 210.00   BURNUP =  3134.94
NST =  140   CAL =   362   DCAL =    2   T.C. =   0   TIME =  2426.97   LHR = 200.00   BURNUP =  3134.97
NST =  141   CAL =   364   DCAL =    2   T.C. =   0   TIME =  2426.99   LHR = 190.00   BURNUP =  3135.00
NST =  142   CAL =   366   DCAL =    2   T.C. =   0   TIME =  2427.01   LHR = 180.00   BURNUP =  3135.03
NST =  143   CAL =   368   DCAL =    2   T.C. =   0   TIME =  2427.03   LHR = 170.00   BURNUP =  3135.06
NST =  144   CAL =   370   DCAL =    2   T.C. =   0   TIME =  2427.05   LHR = 160.00   BURNUP =  3135.09
NST =  145   CAL =   372   DCAL =    2   T.C. =   0   TIME =  2427.07   LHR = 150.00   BURNUP =  3135.11
NST =  146   CAL =   374   DCAL =    2   T.C. =   0   TIME =  2427.09   LHR = 140.00   BURNUP =  3135.13
```

```
NST =  147   CAL =   376   DCAL =    2   T.C. =   0   TIME =  2427.11   LHR = 130.00   BURNUP =  3135.15
NST =  148   CAL =   378   DCAL =    2   T.C. =   0   TIME =  2427.13   LHR = 120.00   BURNUP =  3135.17
NST =  149   CAL =   380   DCAL =    2   T.C. =   0   TIME =  2427.15   LHR = 110.00   BURNUP =  3135.19
NST =  150   CAL =   382   DCAL =    2   T.C. =   0   TIME =  2427.17   LHR = 100.00   BURNUP =  3135.21
NST =  151   CAL =   384   DCAL =    2   T.C. =   0   TIME =  2427.19   LHR =  90.00   BURNUP =  3135.22
NST =  152   CAL =   386   DCAL =    2   T.C. =   0   TIME =  2427.21   LHR =  80.00   BURNUP =  3135.23
NST =  153   CAL =   388   DCAL =    2   T.C. =   0   TIME =  2427.23   LHR =  70.00   BURNUP =  3135.25
NST =  154   CAL =   390   DCAL =    2   T.C. =   0   TIME =  2427.25   LHR =  60.00   BURNUP =  3135.26
NST =  155   CAL =   392   DCAL =    2   T.C. =   0   TIME =  2427.27   LHR =  50.00   BURNUP =  3135.26
NST =  156   CAL =   394   DCAL =    2   T.C. =   0   TIME =  2427.29   LHR =  40.00   BURNUP =  3135.27
NST =  157   CAL =   396   DCAL =    2   T.C. =   0   TIME =  2427.31   LHR =  30.00   BURNUP =  3135.28
NST =  158   CAL =   398   DCAL =    2   T.C. =   0   TIME =  2427.33   LHR =  20.00   BURNUP =  3135.28
NST =  159   CAL =   400   DCAL =    2   T.C. =   0   TIME =  2427.35   LHR =  10.00   BURNUP =  3135.28
NST =  160   CAL =   402   DCAL =    2   T.C. =   0   TIME =  2427.37   LHR =   0.00   BURNUP =  3135.28
```

*** FEMAXI-III SAMPLE CALCULATION *** PAGE 1

STAGE I P O W E R H I S T O R Y I T H E R M A L I N F O R M A T I O N (NODE NUMBER 1)

NST I	TIME (HR)	LHR (W/CM)	BURNUP (MWD/TUO2)	TEMPERATURE (C) PC	PS	CI	CO	GAP CON. (W/CM2 C) TOTAL	GAS	SOLID	CLEAR (MIC)	CONTACT (MPA)	F.G.R. (%)	IOD(10-5 G/CM2)
1	0.0	0.0	0.0	261.0	261.0	261.0	261.0	0.3113	0.3090	0.0	55.301	0.0	0.500	0.000
21	1.0	152.0	0.6	715.8	431.9	295.5	276.0	0.4287	0.4248	0.0	42.223	0.0	0.500	0.000
24	648.2	152.0	760.0	717.3	435.9	295.5	276.0	0.4165	0.4125	0.0	43.961	0.0	0.500	0.006
29	648.7	114.0	760.5	597.2	401.1	286.9	272.2	0.3842	0.3806	0.0	47.531	0.0	0.500	0.006
34	2375.4	114.0	2280.0	597.2	402.3	286.9	272.2	0.3800	0.3764	0.0	47.973	0.0	0.500	0.017
49	2376.4	0.0	2280.4	261.0	261.0	261.0	261.0	0.2999	0.2976	0.0	57.492	0.0	0.500	0.017
50	2376.9	0.0	2280.4	304.0	304.0	304.0	304.0	0.3177	0.3148	0.0	57.208	0.0	0.500	0.017
70	2377.4	114.0	2280.7	642.5	439.4	329.7	315.5	0.4001	0.3957	0.0	47.478	0.0	0.500	0.017
71	2401.4	114.0	2301.8	642.4	439.3	329.7	315.5	0.4001	0.3958	0.0	47.458	0.0	0.500	0.018
86	2401.9	199.5	2302.4	920.1	508.0	348.8	324.2	0.4820	0.4767	0.0	38.918	0.0	0.500	0.018
101	2402.4	285.0	2303.3	1224.6	559.2	367.7	332.8	0.5727	0.5665	0.0	28.856	0.0	0.500	0.018
109	2406.4	285.0	2312.1	1224.7	559.2	367.7	332.8	0.5725	0.5664	0.0	28.844	0.0	0.500	0.018
110	2426.4	285.0	2356.1	1225.0	559.4	367.7	332.8	0.5719	0.5657	0.0	28.780	0.0	0.500	0.018
160	2427.4	0.0	2357.2	304.0	304.0	304.0	304.0	0.2982	0.2953	0.0	57.146	0.0	0.500	0.018

*** FEMAXI-III SAMPLE CALCULATION *** PAGE 2

STAGE I P O W E R H I S T O R Y I T H E R M A L I N F O R M A T I O N (NODE NUMBER 2)

NST I	TIME (HR)	LHR (W/CM)	BURNUP (MWD/TUO2)	TEMPERATURE (C) PC	PS	CI	CO	GAP CON. (W/CM2 C) TOTAL	GAS	SOLID	CLEAR (MIC)	CONTACT (MPA)	F.G.R. (%)	IOD(10-5 G/CM2)
1	0.0	0.0	0.0	261.0	261.0	261.0	261.0	0.3113	0.3090	0.0	55.301	0.0	0.500	0.000
21	1.0	180.0	0.7	806.4	453.5	301.8	278.8	0.4565	0.4522	0.0	39.440	0.0	0.500	0.000
24	648.2	180.0	900.0	808.5	458.8	301.8	278.8	0.4410	0.4367	0.0	41.446	0.0	0.500	0.007
29	648.7	135.0	900.6	663.4	421.5	291.7	274.3	0.4000	0.3962	0.0	45.842	0.0	0.500	0.007
34	2375.4	135.0	2700.0	661.7	421.5	291.7	274.3	0.4001	0.3962	0.0	45.522	0.0	0.500	0.021
49	2376.4	0.0	2700.5	261.0	261.0	261.0	261.0	0.3021	0.2998	0.0	56.965	0.0	0.500	0.021
50	2376.9	0.0	2700.5	304.0	304.0	304.0	304.0	0.3199	0.3170	0.0	56.682	0.0	0.500	0.021
70	2377.4	180.0	2700.9	853.4	493.4	344.5	322.2	0.4649	0.4598	0.0	40.427	0.0	0.500	0.021
71	2401.4	180.0	2734.2	853.3	493.3	344.5	322.2	0.4652	0.4601	0.0	40.385	0.0	0.500	0.021
86	2401.9	315.0	2735.2	1311.8	558.4	374.3	335.9	0.6584	0.6521	0.0	25.363	0.0	0.500	0.021
101	2402.4	450.0	2736.6	1694.8	511.4	403.7	349.5	1.6070	1.5664	0.0348	0.0	2.783	5.727	0.239
109	2406.4	450.0	2750.5	1694.7	511.3	403.7	349.5	1.6075	1.5662	0.0354	0.0	2.835	5.765	0.242
110	2426.4	450.0	2820.0	1694.5	511.2	403.7	349.5	1.6093	1.5652	0.0382	0.0	3.057	5.955	0.256
160	2427.4	0.0	2821.8	304.0	304.0	304.0	304.0	0.3724	0.3695	0.0	42.266	0.0	5.952	0.256

*** FEMAXI-III SAMPLE CALCULATION *** PAGE 3

STAGE I POWER HISTORY I THERMAL INFORMATION (NODE NUMBER 3)

NST I	TIME (HR)	LHR (W/CM)	BURNUP (MWD/TUO2)	TEMPERATURE (C) PC	PS	CI	CO	GAP CON. (W/CM2 C) TOTAL	GAS	SOLID	CLEAR (MIC)	CONTACT (MPA)	F.G.R. (%)	IOD(10-5 G/CM2)
1	0.0	0.0	0.0	261.0	261.0	261.0	261.0	0.3113	0.3090	0.0	55.301	0.0	0.500	0.000
21	1.0	200.0	0.8	872.3	467.2	306.3	280.7	0.4781	0.4737	0.0	37.386	0.0	0.500	0.000
24	648.2	200.0	1000.0	874.7	473.4	306.3	280.7	0.4603	0.4559	0.0	39.542	0.0	0.500	0.008
29	648.7	150.0	1000.7	711.3	435.1	295.0	275.8	0.4121	0.4081	0.0	44.555	0.0	0.500	0.008
34	2375.4	150.0	3000.0	708.2	433.8	295.0	275.8	0.4157	0.4117	0.0	43.672	0.0	0.500	0.023
49	2376.4	0.0	3000.6	261.0	261.0	261.0	261.0	0.3039	0.3016	0.0	56.512	0.0	0.500	0.023
50	2376.9	0.0	3000.6	304.0	304.0	304.0	304.0	0.3219	0.3190	0.0	56.229	0.0	0.500	0.023
70	2377.4	200.0	3001.0	918.3	506.0	348.9	324.2	0.4900	0.4847	0.0	37.926	0.0	0.500	0.023
71	2401.4	200.0	3038.0	918.1	505.8	348.9	324.2	0.4904	0.4851	0.0	37.872	0.0	0.500	0.023
86	2401.9	350.0	3039.1	1419.5	556.0	382.0	339.4	0.7738	0.7675	0.0	19.096	0.0	0.500	0.023
101	2402.4	500.0	3040.7	1850.5	505.9	414.4	354.6	2.1012	1.8493	0.2459	0.0	18.997	13.904	0.645
109	2406.4	500.0	3056.2	1850.4	505.9	414.4	354.6	2.1021	1.8492	0.2468	0.0	19.065	13.934	0.649
110	2426.4	500.0	3133.4	1850.1	505.7	414.4	354.6	2.1064	1.8500	0.2505	0.0	19.342	14.082	0.673
160	2427.4	0.0	3135.3	304.0	304.0	304.0	304.0	0.3755	0.3726	0.0	41.778	0.0	14.075	0.673

*** FEMAXI-III SAMPLE CALCULATION *** PAGE 4

STAGE I POWER HISTORY I THERMAL INFORMATION (NODE NUMBER 4)

NST I	TIME (HR)	LHR (W/CM)	BURNUP (MWD/TUO2)	TEMPERATURE (C) PC	PS	CI	CO	GAP CON. (W/CM2 C) TOTAL	GAS	SOLID	CLEAR (MIC)	CONTACT (MPA)	F.G.R. (%)	IOD(10-5 G/CM2)
1	0.0	0.0	0.0	261.0	261.0	261.0	261.0	0.3113	0.3090	0.0	55.301	0.0	0.500	0.000
21	1.0	180.0	0.7	806.4	453.5	301.8	278.8	0.4565	0.4522	0.0	39.440	0.0	0.500	0.000
24	648.2	180.0	900.0	808.5	458.8	301.8	278.8	0.4410	0.4368	0.0	41.446	0.0	0.500	0.007
29	648.7	135.0	900.6	663.4	421.5	291.7	274.3	0.4000	0.3962	0.0	45.842	0.0	0.500	0.007
34	2375.4	135.0	2700.0	661.7	421.5	291.7	274.3	0.4001	0.3962	0.0	45.522	0.0	0.500	0.021
49	2376.4	0.0	2700.5	261.0	261.0	261.0	261.0	0.3021	0.2998	0.0	56.965	0.0	0.500	0.021
50	2376.9	0.0	2700.5	304.0	304.0	304.0	304.0	0.3199	0.3170	0.0	56.682	0.0	0.500	0.021
70	2377.4	150.0	2700.8	755.7	470.5	337.8	319.1	0.4350	0.4302	0.0	43.489	0.0	0.500	0.021
71	2401.4	150.0	2728.6	755.6	470.4	337.8	319.1	0.4352	0.4304	0.0	43.452	0.0	0.500	0.021
86	2401.9	262.5	2729.4	1131.5	540.6	362.8	330.5	0.5680	0.5621	0.0	31.480	0.0	0.500	0.021
101	2402.4	375.0	2730.6	1505.0	555.8	387.4	341.9	0.8568	0.8505	0.0	13.820	0.0	0.500	0.021
109	2406.4	375.0	2742.2	1505.0	555.8	387.4	341.9	0.8568	0.8505	0.0	13.798	0.0	0.500	0.021
110	2426.4	375.0	2800.1	1504.6	555.4	387.4	341.9	0.8587	0.8524	0.0	13.630	0.0	0.500	0.021
160	2427.4	0.0	2801.5	304.0	304.0	304.0	304.0	0.3236	0.3207	0.0	51.278	0.0	0.500	0.021

*** FEMAXI-III SAMPLE CALCULATION *** PAGE 5

STAGE I POWER HISTORY I THERMAL INFORMATION (NODE NUMBER 5)

NST I	TIME (HR)	LHR (W/CM)	BURNUP (MWD/TUO2)	TEMPERATURE (C) PC	PS	CI	CO	GAP CON. (W/CM2 C) TOTAL	GAS	SOLID	CLEAR (MIC)	CONTACT (MPA)	F.G.R. (%)	IOD(10-5 G/CM2)
1	0.0	0.0	0.0	261.0	261.0	261.0	261.0	0.3113	0.3090	0.0	55.301	0.0	0.500	0.000
21	1.0	156.0	0.6	728.6	435.1	296.4	276.4	0.4325	0.4285	0.0	41.833	0.0	0.500	0.000
24	648.2	156.0	780.0	730.2	439.3	296.4	276.4	0.4198	0.4158	0.0	43.612	0.0	0.500	0.006
29	648.7	117.0	780.5	606.6	404.1	287.6	272.5	0.3864	0.3828	0.0	47.298	0.0	0.500	0.006
34	2375.4	117.0	2340.0	606.4	405.2	287.6	272.5	0.3828	0.3791	0.0	47.635	0.0	0.500	0.018
49	2376.4	0.0	2340.5	261.0	261.0	261.0	261.0	0.3002	0.2979	0.0	57.426	0.0	0.500	0.018
50	2376.9	0.0	2340.5	304.0	304.0	304.0	304.0	0.3180	0.3151	0.0	57.143	0.0	0.500	0.018
70	2377.4	104.0	2340.7	611.1	429.5	327.5	314.5	0.3922	0.3880	0.0	48.361	0.0	0.500	0.018
71	2401.4	104.0	2359.9	611.1	429.5	327.5	314.5	0.3923	0.3881	0.0	48.340	0.0	0.500	0.018
86	2401.9	182.0	2360.5	861.7	496.0	344.9	322.4	0.4634	0.4583	0.0	40.718	0.0	0.500	0.018
101	2402.4	260.0	2361.3	1137.9	549.1	362.2	330.3	0.5353	0.5293	0.0	31.729	0.0	0.500	0.018
109	2406.4	260.0	2369.4	1138.0	549.1	362.2	330.3	0.5351	0.5291	0.0	31.712	0.0	0.500	0.018
110	2426.4	260.0	2409.5	1138.3	549.4	362.2	330.3	0.5345	0.5285	0.0	31.646	0.0	0.500	0.018
160	2427.4	0.0	2410.5	304.0	304.0	304.0	304.0	0.2985	0.2956	0.0	57.083	0.0	0.500	0.018

*** FEMAXI-III SAMPLE CALCULATION *** PAGE 6

STAGE I	POWER HISTORY I			THERMAL INFORMATION (ROD AVERAGE)										
NST I	TIME (HR)	LHR (W/CM)	BURNUP I (MWD/TUO2)I	GAS (MOLE) TOTAL	INITIAL	RELEASE	PRODUCE	F.G.R. (%)	PRESSURE (MPA)	IOD(10-5 G/CM2)	FRACTIONS OF GAS MIXTURE (%) HE	N2	KR	XE
1 I	0.0	0.0	0.0 I	0.00453	0.00453	0.00000	0.00000	0.500	2.607	0.000	100.0	0.0	0.0	0.0
21 I	1.0	200.0	0.8 I	0.00453	0.00453	0.00000	0.00000	0.500	3.113	0.000	100.0	0.0	0.0	0.0
24 I	648.2	200.0	1000.0 I	0.00453	0.00453	0.00000	0.00062	0.500	3.061	0.007	99.9	0.0	0.0	0.1
29 I	648.7	150.0	1000.7 I	0.00453	0.00453	0.00000	0.00062	0.500	2.949	0.007	99.9	0.0	0.0	0.1
34 I	2375.4	150.0	3000.0 I	0.00453	0.00453	0.00001	0.00186	0.500	2.938	0.020	99.8	0.0	0.0	0.2
49 I	2376.4	0.0	3000.6 I	0.00453	0.00453	0.00001	0.00186	0.500	2.559	0.020	99.8	0.0	0.0	0.2
50 I	2376.9	0.0	3000.6 I	0.00453	0.00453	0.00001	0.00186	0.500	2.762	0.020	99.8	0.0	0.0	0.2
70 I	2377.4	200.0	3001.0 I	0.00453	0.00453	0.00001	0.00186	0.500	3.204	0.020	99.8	0.0	0.0	0.2
71 I	2401.4	200.0	3038.0 I	0.00453	0.00453	0.00001	0.00188	0.500	3.204	0.020	99.8	0.0	0.0	0.2
86 I	2401.9	350.0	3039.1 I	0.00453	0.00453	0.00001	0.00188	0.500	3.497	0.020	99.8	0.0	0.0	0.2
101 I	2402.4	500.0	3040.7 I	0.00461	0.00453	0.00009	0.00188	4.680	3.821	0.188	98.1	0.0	0.2	1.7
109 I	2406.4	500.0	3056.2 I	0.00461	0.00453	0.00009	0.00189	4.698	3.822	0.190	98.1	0.0	0.2	1.7
110 I	2426.4	500.0	3133.4 I	0.00462	0.00453	0.00009	0.00193	4.786	3.826	0.197	98.0	0.0	0.3	1.7
160 I	2427.4	0.0	3135.3 I	0.00462	0.00453	0.00009	0.00193	4.784	2.813	0.197	98.0	0.0	0.3	1.7

*** FEMAXI-III SAMPLE CALCULATION *** PAGE 7

STAGE I	POWER HISTORY I				PELLET INFORMATION						
NST I	TIME (HR)	LHR (W/CM)	BURNUP (MWD/TUO2)	BURNUP (MWD/TU) I	CN.TEMP (DEG.C)	DEL.DR (MIC)	DEL.DM (MIC)	UR.SWELL (0.01%)	MAX.EPSZ (0.01%)	S.SWELL (0.01%)	EPSDEN (0.01%)
1 I	0.0	0.0	0.0	0.0 I	261.0	0.0	0.0	0.0	0.0	0.0	-0.0
21 I	1.0	200.0	0.8	0.9 I	872.3	41.2	33.5	0.0	42.6	0.0	-0.0
24 I	648.2	200.0	1000.0	1134.5 I	874.7	26.2	19.5	0.0	23.8	2.2	-20.1
29 I	648.7	150.0	1000.7	1135.3 I	711.3	14.3	10.2	0.0	11.9	2.2	-20.1
34 I	2375.4	150.0	3000.0	3403.5 I	708.2	8.5	4.5	0.0	4.5	6.7	-31.2
49 I	2376.4	0.0	3000.6	3404.2 I	261.0	-19.5	-19.6	0.0	-24.5	6.7	-31.2
50 I	2376.9	0.0	3000.6	3404.2 I	304.0	-16.5	-16.6	0.0	-20.8	6.7	-31.2
70 I	2377.4	200.0	3001.0	3404.6 I	918.3	24.4	17.4	0.0	21.0	6.7	-31.2
71 I	2401.4	200.0	3038.0	3446.6 I	918.1	24.4	17.4	0.0	20.9	6.8	-31.3
86 I	2401.9	350.0	3039.1	3447.8 I	1419.5	72.7	54.6	8.3	69.6	6.8	-31.3
101 I	2402.4	500.0	3040.7	3449.7 I	1850.5	89.3	86.8	13.5	78.6	6.8	-31.3
109 I	2406.4	500.0	3056.2	3467.2 I	1850.4	80.6	81.4	13.5	76.6	6.8	-31.3
110 I	2426.4	500.0	3133.4	3554.8 I	1850.1	76.8	73.3	13.5	75.7	7.0	-31.5
160 I	2427.4	0.0	3135.3	3557.0 I	304.0	-10.4	-5.7	13.5	-10.3	7.0	-31.5

*** FEMAXI-III SAMPLE CALCULATION *** PAGE 8

STAGE I	POWER HISTORY I			GAP INFORMATION I				CLADDING INFORMATION				
NST I	TIME (HR)	LHR (W/CM)	BURNUP I (MWD/TUO2)I	AV.GAP (MIC)	D.GAP (MIC)	F.G.R. (%)	IOD(10-5I GRAM/CM2)I	DEL.DR (MIC)	DEL.DM (MIC)	DEL.RIGDE (MIC)	EPSZ (0.01%)	EPST/EPSZ (%)
1 I	0.0	0.0	0.0 I	81.3	81.3	0.5	0.0 I	0.0	0.0	0.0	0.0	0.0
21 I	1.0	200.0	0.8 I	49.1	42.2	0.5	0.0 I	2.2	2.2	0.0	1.6	149.2
24 I	648.2	200.0	1000.0 I	59.3	52.9	0.5	0.0 I	-1.5	-1.5	0.0	1.7	-92.2
29 I	648.7	150.0	1000.7 I	68.3	64.3	0.5	0.0 I	-2.1	-2.1	0.0	1.4	-163.0
34 I	2375.4	150.0	3000.0 I	69.5	65.5	0.5	0.0 I	-6.2	-6.2	0.0	1.6	-414.9
49 I	2376.4	0.0	3000.6 I	92.1	91.8	0.5	0.0 I	-8.0	-8.0	0.0	0.4	-2044.7
50 I	2376.9	0.0	3000.6 I	91.0	90.7	0.5	0.0 I	-5.7	-5.7	0.0	2.2	-268.6
70 I	2377.4	200.0	3001.0 I	58.6	51.9	0.5	0.0 I	-3.4	-3.4	0.0	3.8	-94.6
71 I	2401.4	200.0	3038.0 I	57.2	50.6	0.5	0.0 I	-4.6	-4.6	0.0	3.8	-125.6
86 I	2401.9	350.0	3039.1 I	20.4	3.8	0.5	0.0 I	-2.9	-2.9	0.0	5.0	-61.6
101 I	2402.4	500.0	3040.7 I	0.5	0.0	13.9	0.6 I	8.8	6.7	2.1	9.9	93.1
109 I	2406.4	500.0	3056.2 I	0.9	0.0	13.9	0.6 I	0.8	1.9	-1.0	7.9	11.0
110 I	2426.4	500.0	3133.4 I	6.2	0.0	14.1	0.7 I	-2.4	-4.9	2.4	7.0	-36.6
160 I	2427.4	0.0	3135.3 I	78.0	80.7	14.1	0.7 I	-9.2	-10.0	0.7	2.7	-354.8

*** FEMAXI-III SAMPLE CALCULATION *** PAGE 9

STAGE I	POWER HISTORY I			CLADDING INFORMATION							
NST I	TIME (HR)	LHR (W/CM)	BURNUP (MWD/TUO2)	IMAX.EPSCT (0.01%)	MAX.EPSP (0.01%)	R.EQSIG (MPA)	R.SIGZ (MPA)	R.SIGT (MPA)	MAX.EQSIG (MPA)	MAX.SIGZ (MPA)	MAX.SIGT (MPA)
1	0.0	0.0	0.0	0.0	0.0	80.0	-48.9	-97.7	80.0	-48.9	-97.7
21	1.0	200.0	0.8	-0.2	0.0	81.0	-51.5	-99.4	81.0	-51.5	-99.4
24	648.2	200.0	1000.0	-6.5	0.0	77.3	-49.1	-94.9	77.3	-49.1	-94.9
29	648.7	150.0	1000.7	-6.5	0.0	76.9	-48.4	-94.4	76.9	-48.4	-94.4
34	2375.4	150.0	3000.0	-11.9	0.0	75.6	-47.2	-92.8	75.6	-47.2	-92.8
49	2376.4	0.0	3000.6	-11.9	0.0	74.8	-45.2	-91.3	74.8	-45.2	-91.3
50	2376.9	0.0	3000.6	-11.9	0.0	79.6	-48.2	-97.3	79.6	-48.2	-97.3
70	2377.4	200.0	3001.0	-11.9	0.0	80.9	-50.8	-99.3	80.9	-50.8	-99.3
71	2401.4	200.0	3038.0	-13.5	0.0	80.2	-50.4	-98.5	80.2	-50.4	-98.5
86	2401.9	350.0	3039.1	-13.6	0.0	81.2	-52.3	-100.1	81.2	-52.3	-100.1
101	2402.4	500.0	3040.7	-13.6	0.0	26.1	-35.2	-17.1	63.3	19.3	-16.4
109	2406.4	500.0	3056.2	-13.9	0.0	62.7	-49.2	-82.8	80.5	-25.7	-72.1
110	2426.4	500.0	3133.4	-17.1	0.0	70.0	-52.2	-89.0	79.6	-44.0	-88.9
160	2427.4	0.0	3135.3	-17.1	0.0	74.2	-44.9	-90.8	74.2	-44.0	-88.5

*** FEMAXI-III SAMPLE CALCULATION *** PAGE 10

FINAL INFORMATION

STAGE	MAX.TIME (HR)	MAX.LHR (W/CM)	INI.GAP (MIC)	BURNUP (MWD/TUO2)	MAX.TEMP (DEG.C)	F.G.R. (%)	IOD(10-5 GRAM/CM2)	CR.DOWN(AV.) (MIC)	CR.DOWN(MAX) (MIC)	DEL.DR (MIC)	DEL.DM (MIC)	DEL.RIGDE (MIC)
160	2427.4	500.0	170.0	3135.3	1850.5	4.8	0.2	-0.0	0.0	-9.2	-10.0	0.7

CALC. TIMES	MAX.DELDR (MIC)	MAX.DELDM (MIC)	MAX.DELR (MIC)	R.MAXEQSIG (MPA)	R.MAXSIGZ (MPA)	R.MAXSIGT (MPA)	MAX.EQSIG (MPA)	MAX.SIGZ (MPA)	MAX.SIGT (MPA)	AV.GAP (MIC)	D.GAP (MIC)	CONTACT LHR(W/CM)
402	8.8	6.7	2.1	81.3	-35.2	-17.1	90.0	19.3	-16.0	81.3	81.3	358.6